2023

GENERATION AND THERAPEUTIC EVALUATION OF RECOMBINANT IMMUNOTHERAPEUTICS ON CD64+ MONOCYTIC CELL LINES AND POLARIZED *EX VIVO* DIFFERENTIATED HUMAN MACROPHAGES

Master of Science (Medicine) Dissertation

Emmanuel Adebowale Fajemisin

Supervisor: Prof. Dr. Dr. Stefan Barth

Co-Supervisor: Dr. Olusiji Alex Akinrinmade

Medical Biotechnology and Immunotherapy Research Unit

Department of Integrative Biomedical Sciences

Faculty of Health Sciences

This dissertation is submitted to the Faculty of Health Sciences, University of Cape Town, in fulfilment of the requirements for the degree of Master of Science (Medicine) in Chemical Biology.

November 2023

|DECLARATION|

I declare that this research is my original, unaided work. It is been submitted for the degree of Master of Science (Medicine) in Chemical Biology at the University of Cape Town, Cape Town, South Africa. Neither any part nor this whole thesis has been submitted previously at any other university for any other degree.

The BMC Chemical Biology referencing style has been applied as the convention for in-text citations and referencing. Each significant contribution to, and quotation in, this thesis from the work(s) of other authors and collaborators has been attributed, cited, and referenced.

This dissertation has been submitted to the Turnitin module (or equivalent similarity and originality checking software) to check for plagiarism. I confirm that my supervisor has seen my report and that any concerns revealed by such have been resolved with my supervisor.

I give the university the authority to reproduce the content, either partly or whole, for research purposes.

Signature:

Signed by candidate

Date: |27|11|2023|

|DEDICATION|

To **God Almighty,** my source and life's sustenance;

To **my Mum, Grace Fajemisin,** who inspired my love for education, and despite enormous challenges completed her Master's program excellently while nursing my little sibling; Samuel! Such grit and grace!;

To **every 'gift of men',** I have received that shaped my life and academic journey, especially related to my MSc. expedition.

"Nothing in life is to be feared, it is to be understood. Now is the time to understand more, so that we may fear less."

-:-

~ Marie Curie (Double (Science) Nobel Laurette).

|ACKNOWLEDGEMENTS|

First, I appreciate the Almighty God; His grace and benevolence sustained me in completing this MSc. dissertation.

To my supervisor, Prof. Dr. Dr. Stefan Barth, I appreciate your patience, professional mentorship, and excellent scientific insights toward completing this research. Thanks for believing in my potential at MB&I by accepting me as your student and providing full lab/academic support.

To my co-supervisor, Dr. Olusiji Alex Akinrinmade, I appreciate your timeless sacrifices, timely guidance, and excellent scientific discussions despite the distance. Thanks for mentoring me in acquiring transferable skillsets in biomedical research at *MB&I*. Thanks so much, Dr!

To every member of *MB&I*, I appreciate your valuable insights, especially Dr. Daramola Adebukola, for training in protein purification and Dennis Makafui Dogbey (PhD in view), who held my hands (with encouragement) all through this journey. Thanks so much, my brother! Also, I am grateful for the *MB&I* scientific presentations, journal clubs, and other vital training, which have widened my horizons in this academic field.

I thank Prof. Dirk Lang and Dr. Viantha Naidoo for their assistance and training at the UCT Confocal Microscopy Unit. Also, I am grateful to Tim Reid at the Flow Cytometry Unit for training and guidance on the flow cytometer and to the Sturrock lab for their steady technical support to *MB&I*.

To my scholar friends, Adetola, Adebowale, Abiodun, Johnson, et al., thanks for motivating me. My finest gratitude goes to my MCF mentor, Njoku Kelechi (PhD in view), for encouraging and supporting me in due seasons and Mr. Ogundipe for being a worthy mentor (in Faith). Also, I appreciate my best pals; Victor A, Stephen F, Tunde A, Olabisi I, Honour A et al., for inspiring support during my MSc program.

I sincerely appreciate my angel mother, Mrs Grace Tinuola Fajemisin, for her sacrifices in my life and my siblings, Joshua, Abraham, and Samuel, for being a formidable support system despite the distance. Thank you all. May we reach the peak of our destiny.

Finally, I am grateful to the Mastercard Foundation Scholars Program (MCFSP) at the University of Cape Town, South Africa, for providing total postgraduate funding for my master's program.

|CO-AUTHORED PUBLICATIONS|

- A K Daramola, O A Akinrinmade, **E A Fajemisin**, K Naran, N Mthembu, S Hadebe, F Brombacher, A M Huysamen, O E Fadeyi, R Hunter, S Barth, A recombinant Der p 1-specific allergen-toxin demonstrates superior killing of allergen-reactive IgG+ hybridomas in comparison to its recombinant allergen-drug conjugate, Immunotherapy Advances, 2022; ltac023, https://doi.org/10.1093/immadv/ltac023
- Dennis Makafui Dogbey, Valeria Sandoval Torres, **Fajemisin E.A**., Liyabona, Takunda Ngwenya, Olusiji Alex Akinrinmade, Stefan Barth. (2023). Technological advances in viral and non-viral drug delivery systems for cancer therapy. Drug Delivery and Translation Research Journal (DDTR-D-22-00279) (Springer). https://link.springer.com/article/10.1007/s13346-023-01362-3

|MANUSCRIPT PREPARATION|

- Olusiji Alex Akinrinmade**, Emmanuel Adebowale Fajemisin,** Stefan Barth. Targeted photodynamic therapy for controlled elimination of *ex vivo* pro-inflammatory macrophages *(Manuscript in preparation).*
- Olusiji Alex Akinrinmade**, Emmanuel Adebowale Fajemisin**, Stefan Barth. Generation of an anti-CD64 scFv-SNAP-auristatin F drug conjugate for treatment of $CD64^{+}$ monocyte derived acute myeloid leukemia *(Manuscript in preparation).*

|LIST OF FIGURES AND TABLES|

|FIGURES|

|TABLES|

CONTENTS

|ABSTRACT|

Introduction: Dysfunctional monocytes/macrophages have been associated with the initiation and maintenance of several chronic diseases such as rheumatoid arthritis (RA), cancer, atopic dermatitis (AD), leishmaniasis etc. In RA for example, the imbalance between pro-inflammatory and anti-inflammatory macrophages has been linked to the chronicity and prolonged inflammation observed in RA. In other diseases like cancers, tumor-associated macrophages (TAMs) form the bulk of the tumor mass and help support tumor growth and metastasis. Also, naïve macrophages can be infiltrated by pathogens and become active reservoirs of parasites like viruses, and protozoans as observed in some diseases like cutaneous leishmaniasis. Unfortunately, there are currently no clinically approved therapeutics to selectively eliminate disease-causing macrophages. In this regard, this thesis aimed to generate and evaluate the potential of different therapeutic agents to selectively eliminate the population of dysfunctional macrophages/monocytes. Previous literature and research have identified Fc gamma receptor I (FcγRI)/CD64 as a significant therapeutic target. CD64 is a transmembrane surface receptor found exclusively in myeloid lineage cells such as monocytes and different macrophage subtypes. Hence, protein engineering and biotechnology techniques were used to develop CD64-targeting immunotherapeutics that could selectively target and deliver cytotoxic agents into the disease-causing monocytic / macrophage population.

Methods: The CD64-targeting antibody fragment (H22(scFv)) was used to generate; 1) a recombinant immunotoxin (rIT) through genetic fusion with the enzymatic domain of *Pseudomonas aeruginosa* exotoxin A (ETA`), or 2) a SNAP-tag fusion protein (FP) to allow chemical coupling of the antibody fragment to the cytostatic drug monomethyl auristatin F (AURIF) or the light-sensitive dye IR700. By so doing generating an antibody drug conjugate (ADC) or a photoimmunoconjugate (PIC) respectively.

Herewith, the therapeutics evaluated in this thesis are highlighted below:

(1) rITs: H22(scFv)-ETA`, and its deimmunized version; H22(scFv)-dETA`
(2) ADC: H22(scFv)-SNAP-AURIF
(3) PIC: H22(scFv)-SNAP-IR700

Results and Discussion: All the anti-CD64 recombinant FPs were successfully expressed and characterized. After structural validation, full-length proteins were evaluated for their functional and biological activities *in vitro*. rITs – H22(scFv)-ETA`, and H22(scFv)-dETA`(RG7787-MT2), and SNAP FP, H22(scFv)-SNAP demonstrated significant antigen-specific binding to IFN-γ stimulated CD64-positive U937 and HL60 monocytic cells but not to antigen-negative cells. The functional (binding) activity of the anti-CD64 fusion proteins demonstrated by flow cytometry

confirmed that the H22(scFv) antibody domain of each recombinant protein exhibited a properly folded conformation and maintained sufficient functional antigen-binding properties. Both H22(scFv)-ETA` and H22(scFv)-dETA`(RG7787-MT2) demonstrated dose-dependent cytotoxicity with IC_{50} values in the nanomolar range against IFN-γ stimulated antigen-positive monocytic cell lines U937 and HL60. In addition, the ADC; H22(scFv)-SNAP-AURIF showed a dose-dependent killing of both IFN-γ stimulated and unstimulated CD64+ proliferating cells but not on antigen-negative cells. This next-generation ADC offers clinical benefits over rITs due to its non-protein cytotoxic agent (AURIF) that is unaffected by endosomal proteases. Similarly, the PIC,H22(scFv)-SNAP-IR700 compromised cell viability in all *ex vivo* human monocyte-derived macrophage subtypes. Since this PIC is activated by near-infrared light, it gives more control over which tissue/area of tissue for selective targeting/elimination of the macrophage subpopulation implicated in the specified diseases. Also, IR700 is a photosensitizing dye which functions as a theranostic agent under visible light – offer the potential for dual clinical benefits in the diagnosis and therapy of topical chronic skin inflammatory diseases, skin cancers and solid cancers in a minimally invasive manner.

Conclusion: CD64-targeting immunotherapeutics showed preliminary therapeutic potential and could serve as precision therapy for monocyte and macrophage-mediated diseases in the future.

|CHAPTER 1: LITERATURE REVIEW|

1.1 Origin of macrophages

Macrophages were first described by Ilya Metchnikoff in 1882 as one of the essential cells in the innate immune system involved primarily in phagocytosis and host defense against pathogen invasion [1]. Phagocytosis is a vital cellular process which entails the recruitment of macrophages to engulf and kill invading microbes, which normally result in acute inflammation, and tissue repair; and overall provide immunity against infectious pathogens [2, 3]. Macrophages are present in human tissues as tissue-resident macrophages (TRMs). These TRMs are primarily derived from circulating blood monocytes (monocytic lineage), which are produced from cell differentiations of bone-marrow hematopoietic stem cells (HSCs) (Figure 1.1) [2, 4]. Also, studies have established that specific TRMs differentiate from embryonic lineages and are maintained by self renewal e.g microglial cells (from yolk sac) and Langerhans cells (from fetal liver) [5]. Based on their origin and anatomical location, TRMs have specific nomenclature, which includes osteoclasts (bone marrow), Kupffer cells (liver), microglial cells (brain), Langerhans cells (skin), etc. These cells have been extensively studied for their roles in critical physiological processes, including innate immunity, homeostasis, tissue repair, tissue regeneration and development (Table 1.1) [3, 6, 7].

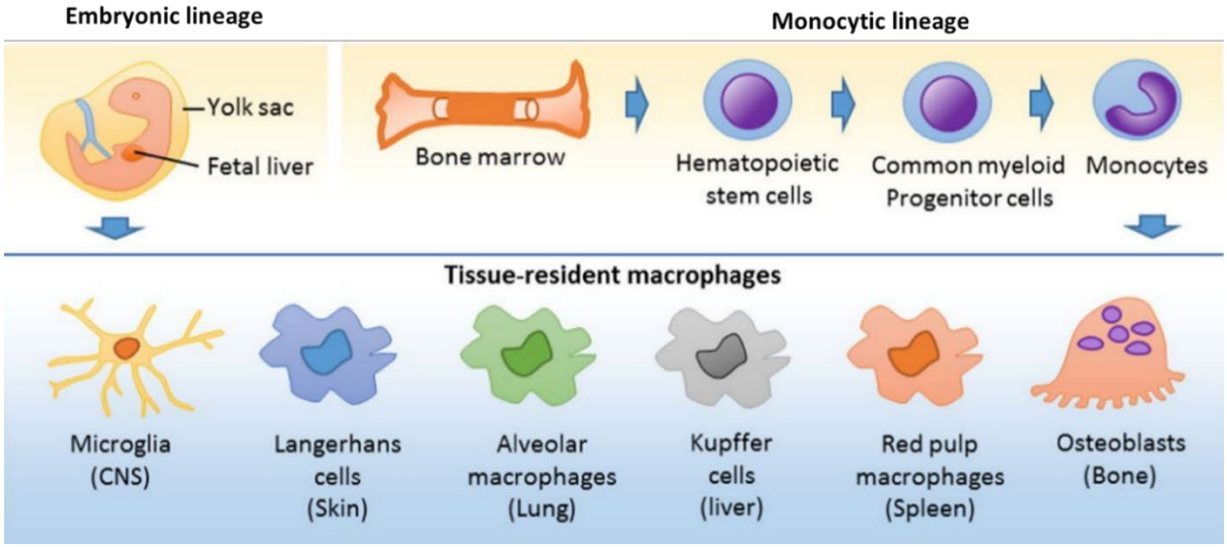

Figure 1.1. Origin of tissue-resident macrophages: Macrophages originate from the fetal yolk sac or liver, and bone marrow hematopoietic stem cells (HSCs). HSCs differentiates into circulating monocytes which infiltrates into a tissue and become tissue-resident macrophages, where they play several physiological roles such as host tissue defense from microbes. This figure was adapted with modifications from [4]

.[12].

Table 1.1: Tissue-resident macrophages and their physiological roles

Macrophage cell type	Location	Normal physiology
Microglial cells	Brain, Central Nervous system (CNS)	Regulate brain development and nervous coordination
Osteoclasts	Bone marrow	Bone resorption
Kupffer cells	Liver	Bacteria and toxin removal, lipid metabolism
Splenic cells/ Red Pulp Macrophages (RPMs)	Spleen	Activate T and B cells for antigen processing in the lymph
Langerhans cells	Epidermis of skin, mucosal	Antigen presentation and processing
Mesangial cells	Kidney	Aids ultrafiltration and regulation of blood flow in kidney capillaries; Immunomodulation
Alveolar cells	Lungs	Clears respiratory tracts of infectious or toxic particles
Cardiac macrophages	Heart and cardiac vasculature	Guide development of blood vessels

1.2 Macrophage polarization and functions

Naïve macrophages can be polarized into distinct functional subtypes based on activation by specific cytokines/stimulants present in their microenvironmental (local) milieu (Figure 1.2) [8-10]; as classically activated macrophages and alternatively activated macrophages [11].

Classically activated macrophages (CAM or M1) are involved primarily in inflammatory response and antitumor immunity [11]. They are stimulated by pro-inflammatory cytokines, especially the Th1-driven Interferon-gamma (IFN-γ), tumor necrosis factor-alpha (TNF-α), and bacterial lipopolysaccharides (LPS). They are characterized by high antigen presentation, high production of interleukins, IL-1, -6, -12, -23, and high production of reactive oxygen species (ROS) and nitric oxides (NOs) [8, 11]. Furthermore, the M1(LPS+IFN-γ) macrophages express elevated levels of the major histocompatibility complex class I and II molecules (MHC I, II) required to present tumor-associated antigens (TAAs). Conversely, alternatively activated macrophages (AAM or M2) are stimulated by interleukins, IL-4, -10, -13, often attributed to anti-inflammatory and pro-tumorigenic activities [11-13]. They are marked by several upregulated surface molecules/chemokines including dectin-1, mannose receptor (CD206), scavenger receptor A (CD204), scavenger receptors B-1, CD163, chemokine (C-C motif) receptor 2; CCR2, chemokine (C-X-C motif) receptor 1 and 2; CXCR1 and CXCR2 [14]. Other M2(IL-4) secreted chemokines includes chemokines (C-C motif) ligand CCL (1, 2, 17,18, 22, 24) and IL-1Ra. M2(IL-4) is

.[13].

characterized by downregulated pro-inflammatory cytokines (e.g., low IL-12) and upregulated anti-inflammatory cytokine (e.g., high IL-10) [15], enhanced scavenging of cellular debris, promotion of tissue remodelling and repair, and, in some cases, increased capacity to fight infection [9].

AAMs are further classified into subsets based on their induction to stimulus in their microenvironment and secretion of chemokines [14, 16]. M2a macrophages are stimulated by interleukins, IL-4 and IL-13 and produce CCL (17,18, 22, and 24), which are recognized by chemokines (C-C motif) receptors CCR (3, 4, and 8) and promote the recruitment of eosinophils, basophils, and Th2 cells. M2b results from activation with immune complexes (IC) and TLR agonists (like LPS) and produces CCL1, which recruits regulatory T cells (Tregs). IL-10 drives polarization to M2c macrophages, which produce CCL16 and 18, recruiting eosinophils and naïve T cells, respectively. M2d macrophages accumulate in the tumor microenvironment as tumor-associated macrophages (TAMs) and have high amounts of IL-10 and high vascular endothelial growth factor (VEGF), but also exhibit some M1-like characteristics such as expression of Interferon-gamma (IFN-γ) inducible chemokines including CCL5, chemokines (C-X-C motif) ligands CXCL (10, and 16) [17-19].

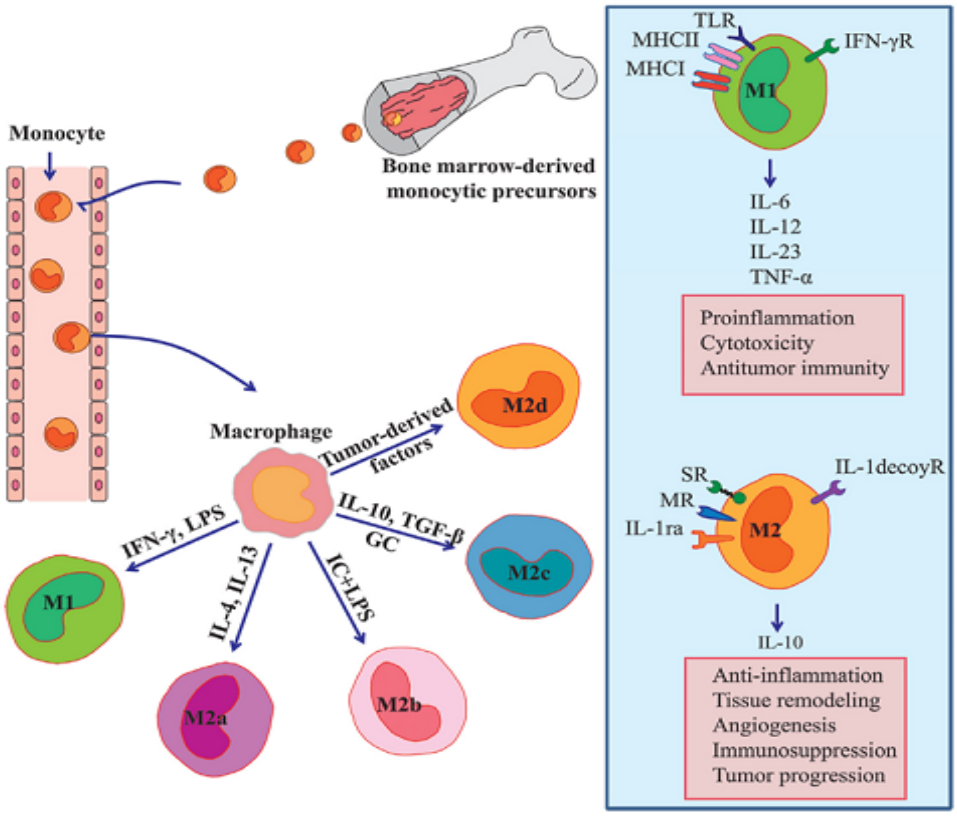

Figure 1.2. Polarization of macrophages and functionality. Circulating monocytes are precursors of tissue-resident macrophages and based on microenvironmental stimuli and secreted

chemokines, macrophages are classically activated (M1-type) or alternatively activated (M2-type). M1-type macrophages function includes proinflammation, cytotoxicity and anti-tumor responses. Contrastingly, M2-type macrophages function are angiogenesis and pro-tumor responses, anti-inflammation and tissue remodelling.

Abbreviations: LPS, lipopolysaccharide; IC, immune complex; GC, glucocorticoid; SR, scavenger receptor; MR, mannose receptor; IL-1ra, interleukin-1 receptor antagonist; TLR, Toll-like receptor; MHC, major histocompatibility complex. Figure was adapted from [11, 17].

1.3 Roles of macrophages in disease pathogenesis

Macrophages play a critical role in normal physiological processes; however, the dysregulation of macrophages has been linked to chronic inflammatory diseases in humans [20]. In several human pathologies, dysfunctional macrophages are presented in these forms: (i) Dysregulated pro-inflammatory (M1) macrophages, which play a crucial role in the pathogenesis of most chronic inflammatory diseases e.g. atopic dermatitis or rheumatoid arthritis; (ii) Tumor-associated macrophages (TAMs), mainly involved in neoplastic diseases e.g. certain solid tumors; (iii) Parasite-hosting macrophages, where they function as active reservoirs of infectious pathogens e.g. Leishmaniasis; (4) Leukemia-associated macrophages and dysfunctional monocytes, presented in certain hematological cancers especially, monocyte-derived leukemia [20, 21]. The involvement of macrophages in the pathogenesis of some examples of chronic diseases are discussed below.

1.3.1 Atopic dermatitis (AD)

Atopic dermatitis (AD) is an allergic and chronic inflammatory skin disease affecting about 190 million people globally in 2017 (Global Burden of Disease Study 2017) [22]. It is characterized by chronic itching due to increased serum levels of immunoglobulin E (IgE) and immunoglobulin G4 (IgG4) [23], eczematous skin lesions, severe dry skin, and susceptibility to cutaneous infections, specifically bacterial and viral infections [24, 25]. The dominant bacterium in AD is staphylococcus aureus (S. aureus), constituting 90% of the microflora in AD lesions, and the extent of S. aureus colonization correlates with disease activity in AD [26]. Several studies have validated the complex etiology, genetics, and activation of multiple inflammatory and immunologic pathways in AD [25]. Macrophages are established as part of immune cells present in acute and chronic AD skin inflammation (lesions) [25, 27]. Acute AD skin inflammation is characterized by overexpression of Th-2 cytokines, including interleukins IL-(4,5,13). Conversely, chronic AD skin lesions are chracterized by upregulation of Th-1 cytokines IL-5, IL-12, granulocyte macrophage colony stimulating factor (GM-CSF), and IFN-γ mRNA–expressing cells [25]. Also documented in

literature are the role of interleukin-11 (IL-11) in collagen deposition associated with the thickness of chronic lesions [28] and elevated Fc gamma receptor I (or CD64) expression levels both in chronic inflamed AD lesions due to presence of dysregulated macrophages [23]. Aside from macrophages, AD pathogenesis also involves other immune cell mechanisms, specifically T-cells (CD4+ memory cells), antigen-presenting cells (APCs), especially Langerhans cells and inflammatory dendritic epidermal cells (IDEC), and keratinocytes, which play significant roles in sustaining AD chronicity [29].

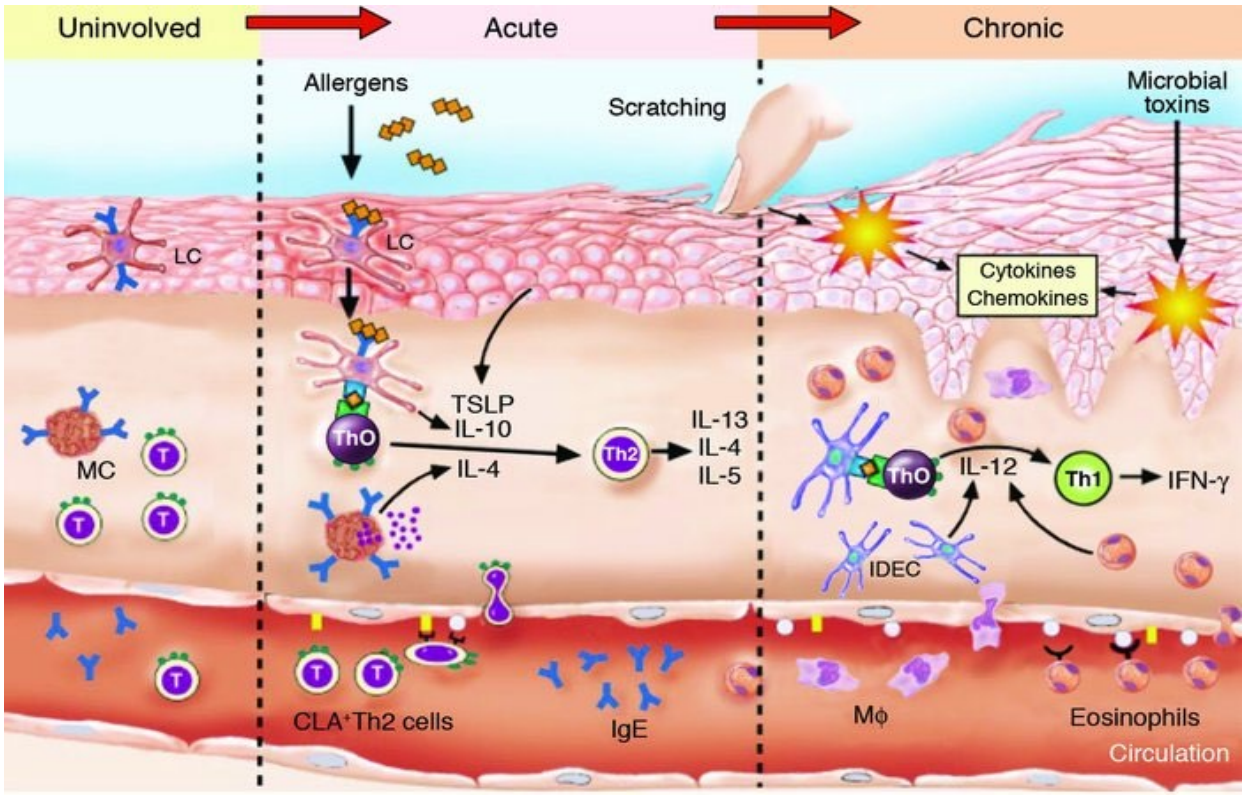

Figure 1.3. Immune cells involved in the pathogenesis of atopic dermatitis (AD).). Uninvolved (normal) skin is characterized by inactive LC, MC, normal T cells (T), normal IgE levels, and low-level expression of Th2 cytokines. However, acute skin lesions show significant infiltration of Th2 cells with increased cytokine secretion. In chronic atopic dermatitis (AD), eosinophils and macrophages infiltrate the skin, leading to increased expression of IL-12 and a switch to a T helper type 1 (Th1) cellular response. This biphasic Th2/Th1 immune response switch is clinically and histologically characterized by initial papulation and spongiosis, followed by the development of lichenification, epidermal hyperplasia, and dermal fibrosis.

Abbreviations: Langerhans cells (LC), mast cells (MC), and cutaneous lymphoid antigen (CLA) play vital immunogenic roles in AD progression. Figure was adapted from [30].

1.3.2 Monocyte-derived acute myeloid leukemia

Monocyte-derived leukemia is a malignant hematological cancer with the aberrant proliferation of immature white blood cells (specifically monocytes) in the bone marrow [31]. More specifically, acute myeloid leukemia (AML) is a common hematological cancer resulting from the repetitive proliferation of bone marrow myeloid HSCs, therefore causing an imbalance in normal blood cell production [32]. AML is associated with poor prognosis with a 5-year mean survival rate in most patients aged 60-78 [33]. Clinically, AML is characterized by a dysfunction in the monocytic-macrophage lineage; hence, the subgroups are characterized by differences in monocytic cell types and degree of maturity according to the French-American-British (FAB) classification based on microscopic analysis of routinely stained slides of AML cells are souced from leukemic bone marrow blasts from human AML patients (Table 1.2) [34, 35]. Upon monocyte activation by pro-inflammatory cytokines like IFN-γ, the CD64 receptor is upregulated and can be a significant target for immunotherapeutic agents in the treatment of AML subtypes especially M4 and M5 of the FAB classification [36, 37].

Aside from monocytes, macrophages are significant drivers of leukemia development. In leukemic blasts, specialized macrophages called leukemia-associated macrophages (LAMs) have been established as primary cells involved in cancer cell survival and drug resistance to conventional chemotherapy like cytarabine [38]. Previous studies have documented that LAMs possess organ-specific phenotypes contributing to leukemic blast proliferation in different AML models [38, 39]. In the MLL-AF9-induced mouse AML model, LAMs are found in the bone marrow and spleen at the initial stages of leukemia development. Furthermore, LAMs exhibit tissue-specific heterogenicity with more M1-like macrophages in the bone marrow, while splenic LAMs possess M2-like phenotypes [39]. Also, in AML patients and NUP98-HOXD13 mouse AML model, LAMs are present in the bone marrow and contribute to leukemia inflammation, promoting leukemia development [38]. Compared to localized, and metastatic solid tumors (e.g. breast, lung, colon, prostate, skin etc.) characterized by infiltration of tumor-associated macrophages (TAMs) or M2(IL-4) macrophages, LAMs possess both pro-inflammatory and anti-inflammatory gene expression profiles. They produce lower amounts of colony stimulating factor 1(CSF-1), tumor growth fcator-beta (TGFβ), and vascular endothelial growth factor (VEGF) than TAMs but exhibit higher amounts of interleukins: IL-1β, IL-6, and chemokines (C-X-C motif) ligand 11 , CXCL11, which contributes to its pro-tumor functions like cancer angiogenesis, immunosuppression, and metastasis [40].

.[17].

Table 1.2: AML classification based on predominating cell types developed by the French-American-British (FAB) group. The AML cells are souced from leukemic bone marrow blasts from human AML patients fixed on microscopic slides, routinely stained and viewed under microscope [34]

AML Sub-group	Morphology	Characteristics
M0	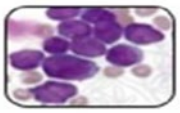	Undifferentiated acute myeloblastic leukemia (5%)
M1	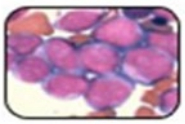	Less than 10% granulocytic differentiation, marked with a considerable number of myeloblasts
M2	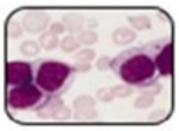	Myeloblast increment with granulocyte differentiation greater than 10%, Non-specific esterase (NSE) staining less than 20%
M3	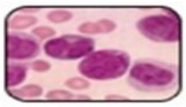	Hypergranular promyelocytes with Auer rods on Chloroacetate esterase (CAE) or Wright staining. It is also marked by primaeval, with multilobed or bibbed nuclei.
M4	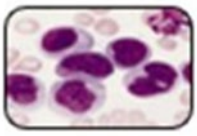	Greater than 20% but less than 80% NSE-butyrate positivity in monocytic cells
M5	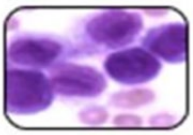	Monocytic cells with greater than 80% NSE positivity marked by monocytic differentiation
M6	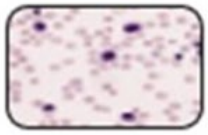	Myeloblasts composition higher than 30% and greater than 50% erythroblasts eliminating erythroid cells.

M7	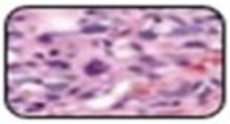	Acute megakaryoblastic leukemia (less than 5%)

1.4 Standard/conventional therapies for atopic dermatitis and monocytes-derived leukemia

Atopic dermatitis (AD) therapies: AD skin lesions are characterized by inflammation, hypersensitivity (often itchy), and infection-prone skin. Hence, treatment options recommended start with basic skincare routines in the acute state and AD topical anti-inflammatory agents in the chronic phase. The most common skincare routines for acute AD include frequent skin moisturizers to improve skin integrity, antiseptic warm baths to reduce infections, and preventing irritants or allergens that can trigger allergic skin reactions. In the chronic phase, topical pharmacological agents like topical corticosteroids (TCS) in creams and ointments are the standard therapy for the treatment of chronic eczematous lesions, lichenification and chronic pruritic inflammation on the skin. Although over 110 randomized clinical samples have proven the efficacy and safety of TCS in AD therapy, its non-targeted absorption in children's skins results in increased TCS concentration in the blood and systemic complications like hypothalamic-pituitary-adrenal (HPA)- axis suppression, which can lead to multi-organ (brain, kidneys) dysfunctions. Aside from TCS, other topical therapies include topical calcineurin inhibitors (TCI), which act on T-cells and decrease expression of inflammatory cytokines, topical phosphodiesterase 4 inhibitors, e.g., crisaborole was approved by the FDA for treatments of AD patients 2 years or older, antihistamines to prevent allergic itching, and topical antibiotics in combination with TCS could provide more efficacy in AD therapy [41].

Monocyte-derived leukemia therapies: The standard therapies used for treatment include chemotherapy, irradiation/radiotherapy, and hematopoietic stem cell transplantation (HSCT) [42]. Specifically for myeloid leukemia, remission-inducing chemotherapy using cytarabine and anthracycline with or without a purine analog were front-line treatments. The typical treatment regimens consist of a 7-day administration of standard-dose cytarabine with a 3-day anthracycline regimen ("7 + 3"), fludarabine–Ara-C– granulocyte colony-stimulating factor idarubicin, or comparable induction protocol. This is followed by consolidation chemotherapy and allogeneic stem cell transplantation (SCT) for high-risk patients. Over the past four decades, this approach has been the mainstay of therapy and has achieved complete remission (CR) in 60-80% of patients

below the age of 60 . However, it may be poorly tolerated, especially in patients with comorbidities, deficient performance status, or advanced age. Additionally, conventional chemotherapy has shown unsatisfactory response rates and survival outcomes in patients with adverse cytogenetic risk or high-risk molecular mutations, such as tumor protein 53 (TP53) alterations [42, 43].

Although standard therapies are sometimes effective in the treatment of these chronic inflammatory diseases, their non-specificity often results in systemic toxicities/complications, which limits their usability. To improve on the shortcomings of standard therapies, most research has extended to biomarker analysis, including antigens, proteins, cytokines, receptors, etc., that mediate disease progression. These biomarkers are explored in targeted approaches, especially immunotherapy and precision medicine, to generate diseased cell-specific therapeutics for effective patient treatment [44].

1.5 Human CD64 receptor

1.5.1 Structure and binding interactions to IgG

Human CD64, otherwise called the Fc gamma receptor-I (FcγRI), is a 72 kDa transmembrane glycoprotein receptor which in association with CD32 (FcγRII) and CD16 (FcγRIII) receptors comprises the large immunoglobulin (IgG) superfamily [45, 46]. Amidst other Fc receptors in humans, FcγRI has the highest binding affinity (about 10-100 times) for for the Fc part of monomeric IgG compared to FcγRII and FcγRIII and binds exclusively to IgG1, IgG3, and IgG4 but not IgG2 [45, 47].

Structurally, CD64 has three extracellular domains (EC1, EC2, EC3), a transmembrane part, and an intracellular tail (FcγR-CY) (Fig I). Both extracellular domain one (EC1) and two (EC2) are homologous to those present in other FcγRs (CD32, CD16), but extracellular domain three (EC3), which bridges EC2 with the transmembrane part is unique to CD64 [48]. It has been documented that the high binding affinity of IgG to the FcγRI lies within the EC2 domain via the hydrophobic pocket filled with leucine 235 residues [45]. Furthermore, studies have shown that the EC3 domain promotes high affinity binding by stabilizing the IgG binding conformation or extending the receptor into the extracellular space without direct contact with IgG [45, 49].

The binding interactions of IgG to CD64 involve two different mechanisms: (1) monomeric IgG binding to CD64 only leads to receptor-mediated endocytosis but not receptor activation and intracellular signaling, hence IgG recycling to the cell surface receptor occurs [48], (2) prebound IgG increases the threshold and binding affinity of CD64 for large immune complexes (ICs) especially antibody-antigen complexes to displace prebound monomeric IgG and become internalized. The internalization of ICs activates ITAM and leads to downstream effector functions

(Fig 1.4 II). Furthermore, biochemical studies investigating ICs binding in CD64+ knock-out mice have shown significant binding and internalization of ICs of various sizes to FcγRI, resulting in several effector functions [50, 51]. These effector functions include asphyxiation, inflammation, antigen presentation, and human anti-tumor responses [51].

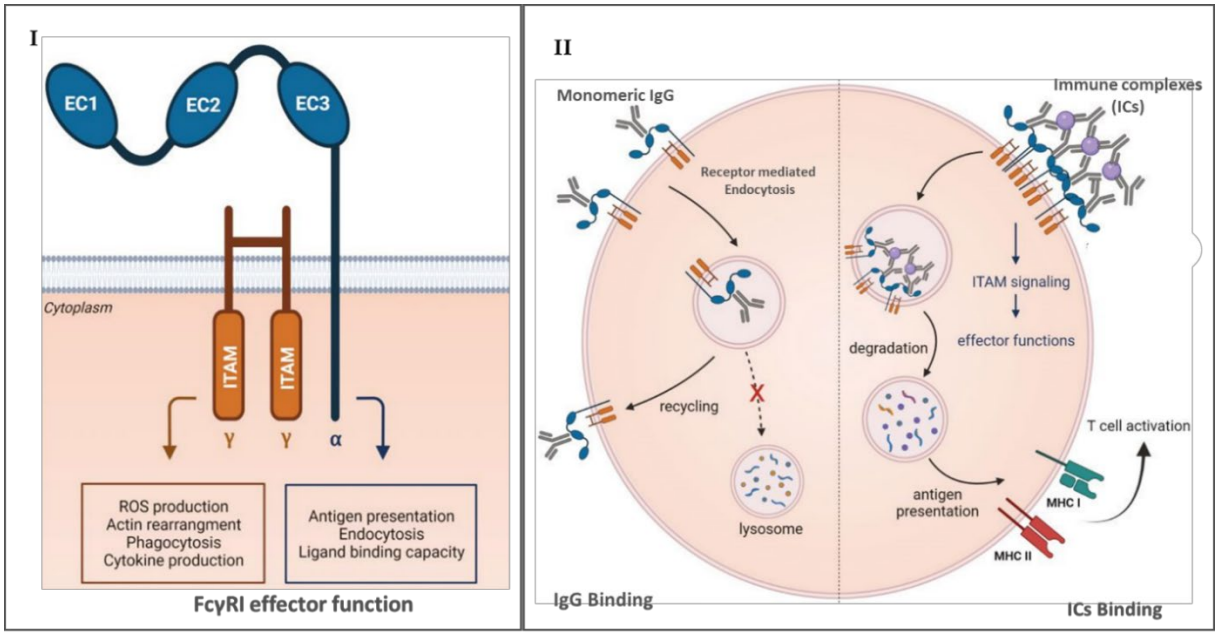

Figure 1.4. The FcγRI structure and binding interactions: (I) FcγRI has three extracellular domains: EC1, EC2, EC3; the transmembrane part; and intracellular tail (FcγRI-CY) (II) The binding of monomeric IgG to FcγRI leads to rapid internalization and recycling of the receptor-IgG complex to the plasma membrane. Prebound IgG increases the binding of ICs to FcγRI. Once ICs are internalized, ITAM signalling is induced via FcγRI, engulfing and degrading the antigen-antibody complex by lysosomal enzymes. The degraded peptides can be presented on MHCs (class 1 or 2), resulting in activation and recruiting effector T-cells functions. The figure was adapted and modified from [52].

1.5.2 CD64 expression and signalling pathways

CD64 is constitutively expressed on most myeloid cells, including monocytes, macrophages, and dendritic cells (DCs). It has also been documented that cytokines (IFN-γ and G-CSF) can induce CD64 expression on neutrophils, eosinophils, and mast cells [53]. Also, CD64 is expressed on human-derived myeloid cell lines, including U937, HL60, and THP-1 monocytic cell lines [54]. CD64 is upregulated on myeloid cells, mainly monocytes and macrophages, in the presence of pro-inflammatory cytokines such as interferon-gamma (IFN-γ) and tumor necrosis factor-alpha (TNF-α) [55, 56]. It has been documented that the IFN-γ stimulation of human monocytes and

.[21].

monocytic cell lines, U937 and HL 60, results in a ten-fold increase in CD64 receptor, and CD64 receptors on U937 could increase to 60000 receptors per cell [57, 58]. CD64 expression and upregulation by cytokines on primary macrophages and monocytes make CD64 a prime target for developing immunotherapeutics against diseases initiated by dysfunctional macrophages or monocytes [59]. Comparatively, anti-inflammatory cytokines such as IL-4, IL-10, and transforming growth factor beta (TGF-β) decrease the expression of CD64 while increasing the inhibitory CD32b expression. This alteration in CD64 expression level is pivotal in regulating CD64-mediated effector functions [52].

CD64 signalling is regulated via the immunoreceptor tyrosine-based activation motif (ITAM) on its γ-chain (Fig.3I,4). The EC2 domain interacts with monomeric IgG or immunocomplexes (ICs) such as antibody-opsonized pathogens, monoclonal antibodies, or tumor cells [51]. After crosslinking of EC2 by ICs, the tyrosine residues present in ITAM are phosphorylated by the SRC kinase family [60], which binds and activates the SYK kinases via their SH2 domains [61]. The SYK activation results in the activation of the RAP-MAPK pathway, increased intracellular calcium levels, and induction of multiple downstream targets, which activates the NF-κB transcription factors. These activation signals result in immune-mediated phagocytosis, oxidative burst, and cytokine release [62, 63]. However, the crosslinking of inhibitory CD32b causes the phosphorylation of immunoreceptor tyrosine-based inhibitory motif (ITIM), which activates the SH-2-containing phosphatases SHP1 and SHIP [62]. Subsequently, these phosphatases dephosphorylate the kinases downstream of ITAM, thereby balancing the activating signalling cascades and suppressing CD64 effector function.

Although ITIM-containing CD32b regulates immunomodulatory effects, studies have shown that activating CD64 and CD32a can generate inhibitory signals and mediate suppressive effects [64, 65]. CD64 engagement and phagocytic signalling may mediate inhibitory functions, including IL-10 secretion, reducing the production of pro-inflammatory cytokines and T-cell proliferation [66]. Also, It has been documented that IC-mediated inhibition of IFN-γ signalling pathways involving ITAM-containing CD64 and ITIM-dependent phosphatase SHP-1 on CD32b mediates effective suppression of STAT1 phosphorylation [61, 67].

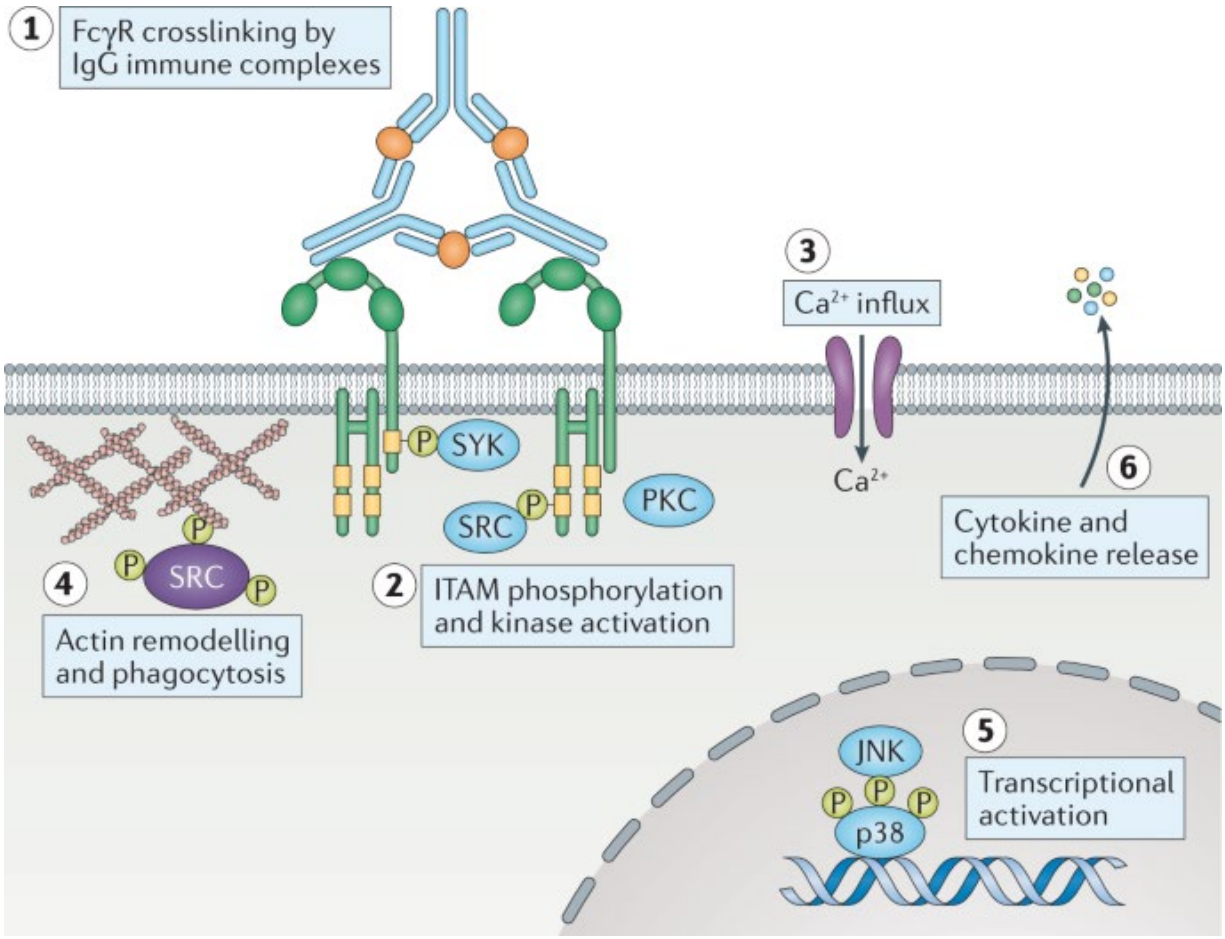

Figure 1.5. Signalling of activating FcγRs (e.g., CD64) after crosslinking with IgG immune complexes (ICs) occurs via several steps : (1) Binding of multiple ICs to Fcγ receptors (FcγRs) through low-affinity, high-avidity interactions. , (2) Crosslinking ICs with FcγRs triggers ITAM phosphorylation which subsequently activates SYK and SRC kinases, (3) Activation of protein kinase C (PKC) pathway results in the influx of intracellular Ca^{2+} levels following activation of Ca^{2+} channels, (4) As well, SRC kinase activation results in actin remodelling which are crucial for receptor-mediated internalization and phagocytosis of ICs by FcγRs, (5-6) The cellular activation of specific transcription factors such as p38 and Jun amino-terminal kinases (JNK) drives the production of pro-inflammatory cytokines and chemokines like tumor necrosis factor (TNF), IL-1β and IL-8) which mediates immune responses and alter the effector function, migration, and cells survival. Image adapted from [63].

1.6 Development of CD64-specific antibodies

The development of monoclonal antibodies (mAbs) has become a powerful clinical tool for the treatment of chronic inflammatory diseases and cancers mediated by dysfunctional macrophages and monocytes [68]. mAbs are mostly gamma immunoglobulins (IgG) made up of identical protein sequences; hence, they possess the same antigen recognition (or binding) site, affinity, and

.[23].

biological activity [69]. These antibodies work by binding specifically to overexpressed antigens (surface proteins or receptors) on target cells and mediate cell dealth mechanisms via the blockage of cell proliferation signals [70, 71]. In other words, mAbs have also been engineered to deliver cytotoxic molecules into the cytosol to induce cellular cytotoxicity [68, 69].

In a study by Guyre and colleagues, full-length anti-CD64 monoclonal antibody 197 (mAb197) produced from mice blocked phagocytosis and downregulates CD64 expression on monocytes [72]. This was possible because mAb197 recognizes and binds to two CD64 epitopes: its Fc domain binds to the Fc ligand-binding site on CD64, and its Fab domain to an epitope outside the Fc ligand-binding site. The infusion of mAb 197 in a patient with chronic immune thrombocytopenia purpura (TTP) resulted in clinical improvement as the mAb therapy prevented FcγR-mediated destruction of IgG-coated platelets in the patient's blood [72, 73].

In another study by Guyre and colleagues to overcome the potential induction of negative immune response associated with murine-derived mAb 197, CD64 specific monoclonal antibody (M22) was generated that recognizes an epitope distinct from the natural ligand-binding (Fc) site of IgG [57]. Afterwards, M22 was later humanized via grafting its complementary determining regions (CDRs) onto human IgG1 constant domains, resulting in a full-length human antibody (H22) which maintained binding specificity and high affinity for CD64 [74]. Based on the H22 format, new versions of antibody conjugates (including drug conjugates and radionuclides) targeting human CD64 were developed [75, 76]. About a decade later, De Kruif and colleagues developed a single chain variable region fragment (scFv) version of H22 called H22(scFv), which has a lower molecular weight but the same target specificity outside the normal Fc binding site [77]. This H22(scFv) has since been explored in both *in vitro* and *in vivo* studies to rapidly deliver cytotoxic molecules (effectors) to CD64+ expressing cells [78], irrespective of the saturation level of IgG on the Fc domain of CD64, resulting in improved clinical outcomes.

1.7 Recombinant immunotherapeutics targeting CD64 receptor

mAbs have been used for the production of recombinant immunotherapeutics – this novel class of drugs contain a cell-specific antibody attached via chemical conjugation or genetic fusion to an apoptosis-inducing molecule for targeted therapy [44]. Through protein engineering there has been a transition of mAb formats from full-length IgG (~ 150 kDa) to different small-sized fragments [79], especially scFvs (~ 25 – 30 kDa) (Figure 1.6). scFv possess conserved antigen-binding affinity like full-length antibodies and demonstrate improved delivery of cytotoxic molecules, clinical efficacy and systemic clearance due to its small size (Figure 1.6 - 1.7) [80]. Comparably, the renal clearance (t ½) of IgG compared to scFv is 110 hours to 2 hours, which is quite clinically

significant, when compared to the renal cut-off [79]. Furthermore, another advantage is the absence of the Fc region in scFvs which reduces immunogenicity associated with full-length mAbs [80]. The common examples of recombinant immunotherapeutics developed for targeted therapy include immunotoxins (ITs) [79], recombinant immunotoxins (rITs) [80], targeted human cytolytic fusion proteins (hCFPs) [81], and antibody-based immunoconjugates [82].

Current generation of rITs often contain a cell-specific scFv antibody fragment linked to bacteria or plant- detived toxins e.g., exotoxin A, and diphtheria toxin (from bacteria), and ricin A (from plant). However, due to the non-human origin of these cytotoxic proteins, rITs have limited clinical application due to immunogenicity [83]. Immunogenicity often results in the generation of neutralizing antibodies, which limits clinical efficacy. For this reason, the next-generation of rITs are being deimmunized [83, 84] or entirely replaced by human apoptosis-inducing enzymes e.g., granzymes, angiogenin, microtubule-associated protein tau (MAP-tau). Just like rITs, these enzymes are fused to cell-specific antibodies to generate antibody FPs called human cytolytic FPs (hCFPs). This novel class of proteins have been used successfully in (pre)clinical studies for targeted treatment of cancers [78, 81, 85-88]. Aside from hCFPs, applying protein engineering techniques has allowed the fusion of antibody to a unique self-labelling protein tags (e.g. CLIP-tag and SNAP-tag) to generate recombinant FPs [89]. These recombinant FPs are used for the development of antibody immunoconjugates [90] and are applied (pre) clinically as immunodiagnostic and immunotherapeutic agents [91].

Based on this background, the scFv targeting the CD64 receptor known as (H22(scFv)) has been used to generate recombinant therapeutics like rITs, and antibody FPs against macrophages and monocytes – driven diseaes like chronic cutaneous inflammation [79], rheumatoid arthritis [92], monocytes-derived acute myeloid leukemia [78, 93]. Specifically, H22(scFv)-based recombinant therapeutics eliminate pro-inflammatory M1(LPS+IFN-γ) macrophages responsible for chronic inflammation [92, 94] and activated CD64+ monocytic cells in leukemic blasts of AML M4 and M5 subtypes of the FAB classification [93].

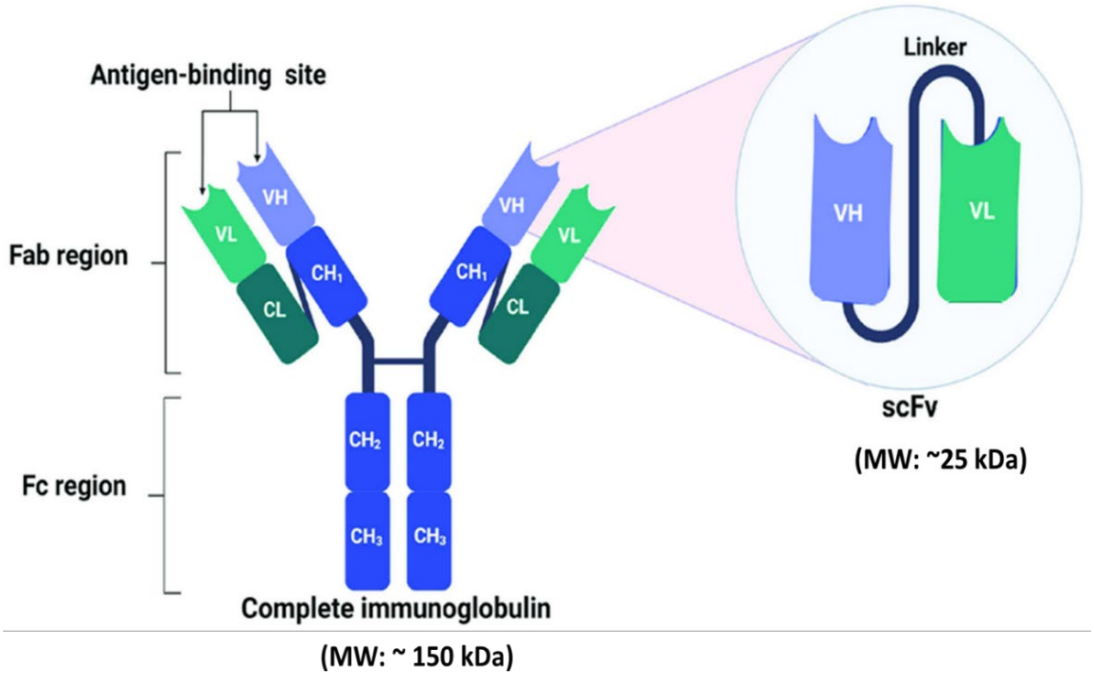

Figure 1.6. Structure of scFv: The scFv structure comprises the variable heavy (VH) and variable light (VL) chains of the complete immunoglobulin, and a linker sequence separates both VH and VL to conserve the antigen-binding affinity for the protein. This figure is adapted from [69].

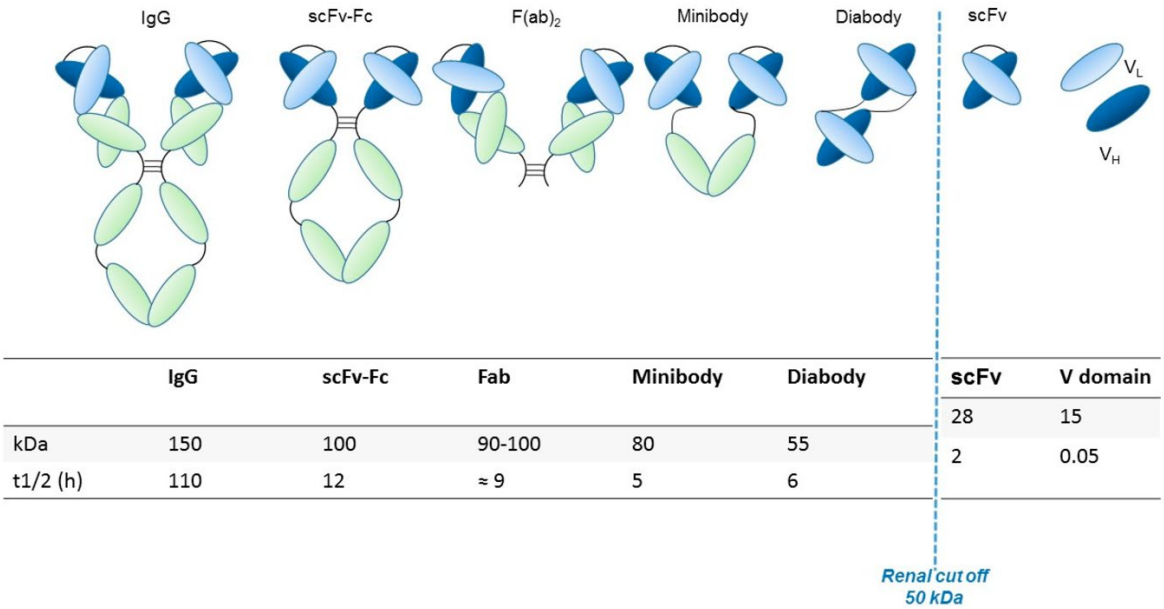

	IgG	scFv-Fc	Fab	Minibody	Diabody	scFv	V domain
						28	15
kDa	150	100	90-100	80	55	2	0.05
t1/2 (h)	110	12	≈ 9	5	6		

Figure 1.7. Different engineered antibody formats: Antibodies generated with different sizes compared to intact IgG. Ig, Immunoglobulin; scFv, single-chain variable fragment; V domain, variable domain. In the figure, the size (kDa) of each different antibody format and their half-life ($t_{1/2}$ is the clearance time for half of the molecule from circulation). This figure is accessed from [95].

1.8 CD64-targeting immunotoxins

Some immunotoxins (ITs) developed against CD64 receptor are described below with their preclinical outcomes:

1.8.1 H22(scFv)-Ricin A

Ricin A is one of the most toxic enzymes in nature, found abundantly as a protein component of castor bean seeds (*Ricinus communis*) [96]. Structurally, Ricin A is a 64 kDa protein and contains two functional domains, A and B. Domain A represents the toxic domain which inactivates eukaryotic ribosomes (approximately 1500 ribosomes per minute), resulting in inhibition of protein synthesis and induction of cell death. Domain B is the cell binding domain that binds to mammalian cell membranes, glycolipids, and glycoproteins [96, 97]. Upon translocation into the cytosol, the toxic domain A catalyzes the N-glycosidic cleavage of a specific adenine residue from 28S ribosomal RNA to form a galactose (cell)-binding lectin. This enzymatic cleavage blocks the binding of elongation factors and renders the ribosome containing depurinated 28S RNA incapable of protein synthesis [97, 98]. Also, domain A can avoid proteolytic degradation in the cytosol due to it's low lysine content. Hence, a single dose of ricin A is lethal to a cell.

Thepen and colleagues demonstrated the first therapeutic potential of anti-CD64 Ricin A for the treatment of cutaneous inflammation *in vitro* and in transgenic mice expressing human CD64. The immunotoxin contained the anti-CD64 monoclonal antibody, H22(scFv), chemically conjugated to Ricin A and was used to treat sodium lauryl sulfate (SLS)- induced chronic inflammation in human CD64+ transgenic (hCD64tg) mice. The results from intradermal injection at site of chronic inflammation showed selective elimination of activated M1 pro-inflammatory macrophages, downregulation of pro-inflammatory cytokines like IL-1 and IL-6, and subsequent resolution of chronic cutaneous inflammation after 24 hours. Also, clinical symptoms of inflammation, such as local skin temperature and capillary vasodilation, drastically decreased [79]. In another study, H22(scFv)- Ricin A was used for the selective killing of dysregulated pro-inflammatory macrophages in the synovial fluid of rheumatoid arthritis (RA) patients [99] and hCD64tg mice paws [92].

1.8.2 H22(scFv)-Exotoxin A

The most toxic virulence factor produced in the bacterium *Pseudomonas aeruginosa* is the extracellular protein Exotoxin A (PE or ETA). Structurally, PE has a molecular size of 66.99kDa and contains 613 amino acid sequences on its single polypeptide chain and 3 major functional domains (Figure 1.8) [100]. Domain Ia (aa1-252) in the N-terminus of the polypeptide chain functions as the native

PE receptor binding site. Domain II (aa 253-364) functions as the translocation domain, which supports the internalization of the toxins across intracellular vesicles, such as the endosomes and endoplasmic reticulum. Domain Ib (aa 365-404) is a domain of the unknown function, and domain III (aa 405-613) is the enzymatic domain of the toxin. The enzymatic domain, once translocated into the cytosol, acts by inactivating elongation factor 2 (EF2) through ADP-ribosylation of diphthamide on EF2. ADP-ribosylated EF2 cannot mediate polypeptide chain elongation and protein synthesis which ultimately induces cell death (Figure 1.9) [100, 101]. The current class of PE-based immunotoxins are made of a truncated version of Exotoxin A (usually PE 38 (ETA`) or PE25) genetically fused to the scFv of an antibody as compared to first generation moeties, which involved conjugation of native toxins to full-length monoclonal antibodies (Figure. 1.6) [101, 102].

In a comparative manner to H22(scFv)-Ricin A, our lab in the last decade has successfully developed a novel class of CD64-targeting ETA` - a rIT containing an H22(scFv) antibody genetically fused to ETA`, and evaluated its therapeutic potential. In a study by Hristodorov et al, H22(scFv)-ETA` demonstrated selective elimination of dysregulated pro-inflammatory (M1(LPS+IFN-γ)) macrophages and resolution of cutaneous inflammation in hCD64tg mice and patient biopsies [103, 104]. In a different study which took advantage of the ability of cross-linked CD64 to rapidly internalize IgG, bivalent H22(scFv)$_2$-ETA` was constructed and evaluated for increased uptake and cytotoxicity in CD64+ monocytic cells. The result documented shows that H22(scFv)$_2$-ETA` exert more cytotoxicity against IFN-γ stimulated CD64+ monocytic cell line (U937) at an IC_{50} value of 14 pM when compared to monovalent H22(scFv)-ETA` with an IC_{50} value of 140 pM (10X killing potential). Hence it was concluded that increased valency could remarkably improve the efficacy of anti-CD64 rIT [94].

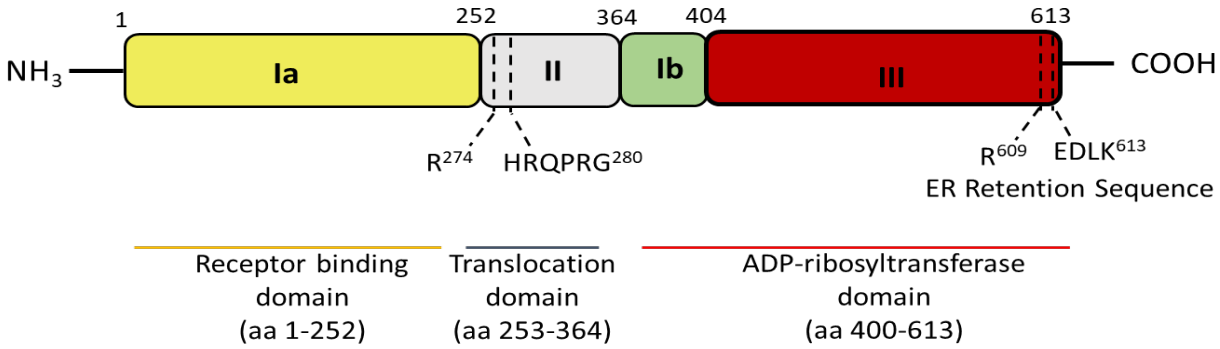

Figure 1.8. The structure and function of wild-type Pseudomonas Exotoxin A (PE or ETA, molecular Size – 66.99 kDa).). PE contains different domains with distinct functions. Domain Ia (aa 1-252) serves as the receptor-binding domain, allowing PE to bind to lipoprotein-receptor-

related protein (LRP1) or LRP1B. Domain II (aa 253-364) is responsible for facilitating the translocation of the toxin across cellular membranes. Domains Ib (aa 365-404) and III (aa 405-613) together constitute the catalytic subunit of PE, which possesses ADP-ribosyltransferase activity. The C-terminal ER retention signal (aa 609-613) is critical for retrograde routing of PE to the trans-Golgi network. These distinct domains and motifs perform essential roles in the mechanism of action of PE. Image adapted from [100].

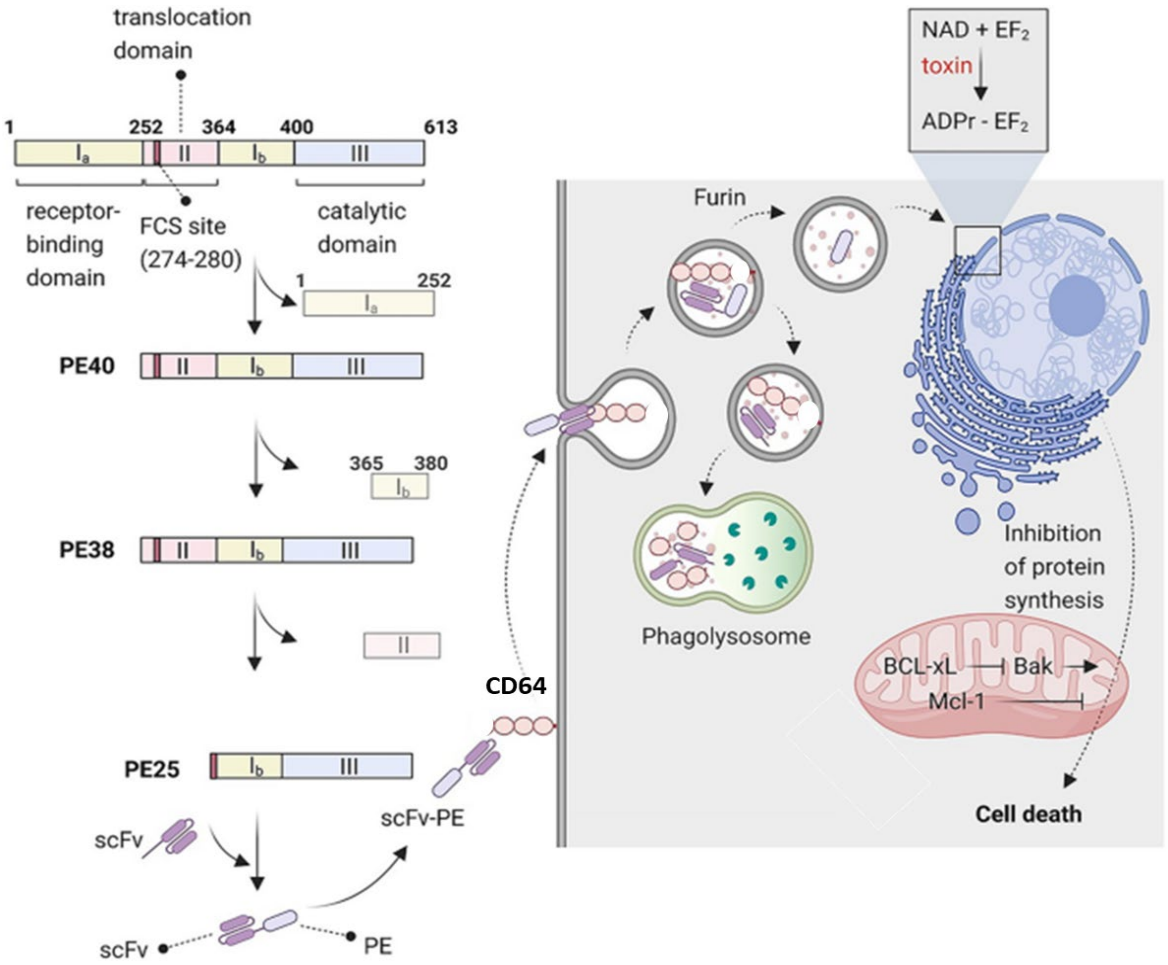

Figure 1.9. Mechanism of action of PE-based rITs: The Ia domain (aa 1–252) represents the binding domain; domain II (aa 253–364) represents the translocation/transport domain, and domain III (aa 405–613) and the last four residues of domain Ib represent the cytotoxic domain/inhibit protein biosynthesis. Domain Ia was deleted to generate PE40 (40 kDa). PE38 (38 kDa) was developed by removing domain Ia and amino acids 365–380 of domain Ib. PE25 (25 kDa) is produced by eliminating domain II from PE38 except for the furin cleavage sites (FCS). Current PE-based rITs are generated by genetic fusion of cell-specific ligand or scFv antibody to PE38 or PE25. After binding, PE-based rITs become internalized via receptor-based endocytosis and are released into the cytosol, where they induce cell death [102].

1.9 Deimmunization of ETA`-based rIT using protein engineering and computer simulations

The clinical use of rITs is limited by the immunogenicity associated with administering bacterial or plant-derived toxins. In this case, the toxin moiety due to its non-human origin induce an immune response which results in the generation of human anti-toxin neutralizing antibodies [105]. In patients, this eventually alters the pharmacokinetic profile of the administered immunotoxin, prevents the readministartion of follow-up doses and consequently reduces the overall clinical efficacy [105, 106]. For example, a single cycle administration of anti-mesothelin ETA` to patients with mesothelioma resulted in no major clinical response due to the generation of neutralizing anti-drug antibody formation (ADA), which lowers the serum half-life of the rIT and causes immune-related adverse events like allergic reactions, delayed hypersensitivity, and autoimmunity [107].

One major approach used to overcome immunogenicity is the deimmunization of rITs via protein engineering and computational simulations to identify and eliminate antigenic epitopes from rITs [108, 109]. By mapping the positions of seven major B-cell epitopes on PE38, Onda and colleagues from the Ira Pastan group eliminated B-cell epitopes by mutating amino acids (AA) with heterocyclic and large side chain (e.g. arginine, glutamine, glutamate, and lysine) to those with no side chain AA (e.g. glycine), or with small side chain (e.g. alanine and serine). Onda et al., further documented that deimmunized immunotoxin (HA22-8X) tested in mice tumor models had significantly reduced immunogenicity with retentive cytotoxic and antitumor activities [84, 110]. Another deimmunization approach was conducted by Mazor and colleaguesfrom the Ira Pastan group. This approach invloved the depletion of T-cell epitopes. Using high-resolution peptide scanning techniques, eight T cell epitopes were identified on PE38 derived from human peripheral blood mononuclear cells (PBMCs) from PE38-treated patients. The group constructed a new deimmunized rIT, LMB-T18, with 93% T-cell epitope reduction, which retained both cytotoxic and anti-tumor activity *in vitro* and *in vivo* [111, 112]. Furthermore, another study by Mazor et al., documented the depletion of both B cells and T cell epitopes to generate a new deimmunized rIT, LMB-T14. LMB-T14 contained significant domain deletion; domain II and 10 amino acid alterations on domain III of PE38. It demonstrated significantly reduced immunogenicity and improved cytotoxicity and antitumoral activity (complete remission) in A431/H9 tumor xenografts observed in mesothelioma-induced mice [112].

In collaborative research with Prof. Paolo Carloni (Institute for Advanced Simulations, Julich Germany), our lab recently identified point mutations that would improve the enzymatic activity

(cytotoxicity) of the deimmunized ETA` variant (RG7787) via super-computing molecular dynamics simulations (scMDS). RG7787 was developed by the Ira Pastan group and is composed of a humanized antibody fragment against mesothelin attached to a PE24 variant of ETA` with 7 ablated human B-cell epitopes using alanine scanning mutagenesis [113]. The resulting mutated human B-cell epitopes from RG7787 include: R490A (B cell epitope), R427A (B and T cell shared epitope), R505A (B and T cell shared epitope), R467A (B cell epitope), D463A (B cell epitope), R538A (B cell epitope), and R456A (B cell epitope) [113, 114]. Using scMDS, our lab and collaborator (Prof. Paolo Carloni) introduced point mutations on RG7787 as documented below: (1) RG7787 containing ablated B epitope, R456A changed to R456T, and (2) RG7787 containing R456T with deleted R490A. (Table 1.3). These mutations were introduced potentially to reduce the immunogenicity of RG7787 while retaining its enzymatic activity/cytotoxicity for (pre)clinical applications.

Table 1.3: Overview of Amino Acid (AA) mutations on deimmunized ETA` (dETA`) construct, RG7787 (Ira Pastan and Paolo Carloni group) (Retrieved from Daramola Adebukola PhD thesis).

dETA` construct	**AA mutations**	**Functional Characteristics**
RG7787	R427A, **R456A**, D463A, R467A, R490A, R505A, R538A	Domain II deletion (LR) + Human B-cell epitope deficient +R456A
Mutations S/N	**Point mutations identified by MDS to restore enzymatic activity**	**Point mutations from MDS added to mutations present on RG7787**
MT1	R456T	R427A, **R456T**, D463A, R467A, R490A, R505A, R538A
MT2	R456T, R490A $^{\text{deletion}}$	R427A, **R456T**, D463A, R467A, **-**, R505A, R538A

The numbers 427, 456, 463, 467, 490, 505, and 538 represent the position/site on the PE sequences where point mutations were introduced. The letters indicate the amino acid mutations at each position: **R** – Arginine, **T** – Threonine, **D** – Aspartate or Aspartic acid, **A** – Alanine. MT1 and **MT2** are referred to as Mutations 1 and 2.

1.10 Development of SNAP-tag FPs for therapeutic applications

The SNAP-tag protein is an engineered version of the human DNA repair enzyme, O^6-Alkylguanine-DNA alkyl transferase (hAGT), which catalyzes the transfer of an alkyl residue from its substrate to a cysteine residue (^{145}Cys) on AGT. Structurally, it is 20 kDa in size, and contains

182 amino acids [90, 115, 116]. A unique recombinant antibody conjugate format is created when SNAP-tag is fused to a cell-speciifc antibody fragment, allowing autocatalytic labelling of O^6-benzylguanine (BG) modified substrates in a 1:1 stoichiometry (Figure 1.10) [116, 117]. BG-modified substrates include fluorophores and small molecules like toxins, drugs, nanoparticles, or photosensitizers (Figures 1.10 -1.11) [115, 118]. Using random mutagenesis and phage display, the SNAP-tag was engineered to improve its substrate specificity and reactivity, resulting in a 52-fold reactivity than its native/wildtype AGT, increased specificity and stability under oxidizing conditions [119-121].

The SNAP-tag technology possesses unique advantages, including (i) simple reaction conditions and protein labelling at physiological pH, buffers, and room temperature, (ii) high selectivity and specificity of SNAP-tag to BG-modified substrates, which allows for labelling of complex protein mixtures, (iii) readily available and adaptable protocols that allow easy conjugation with different BG substrates [90, 117]. By combining SNAP-tag technology with antibody engineering, our lab created a unique antibody format and several SNAP-tag antibody FPs have been successfully evaluated for several pre-clinical immunotherapy applications in cancers (Figure 1.11) [122-124]. Examples include SNAP-tag antibody-drug conjugates (ADCs), with BG-modified Auristatin F and SNAP-tag Photoimmunoconjugates (PICs), with BG-modified IR700, which are discussed further in this thesis.

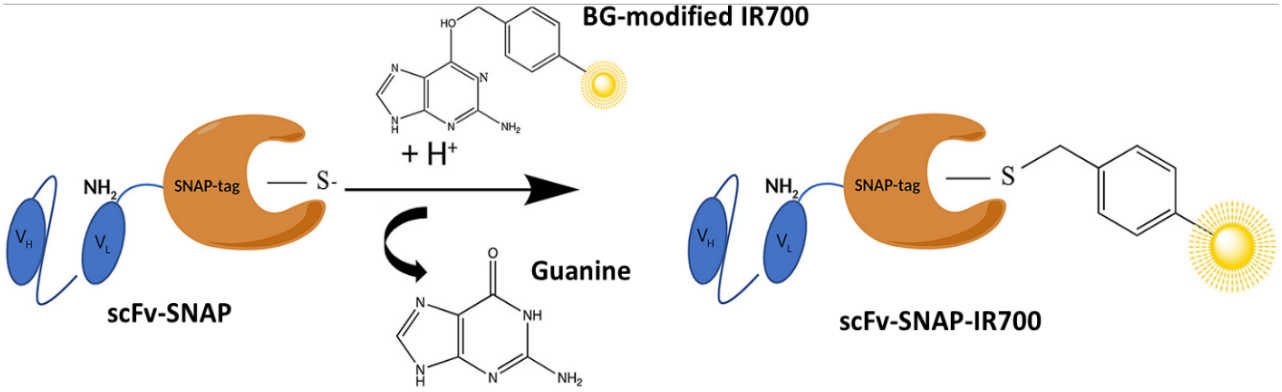

Figure 1.10. Generation of SNAP-tag immunoconjugate: The autocatalytic reaction of scFv-SNAP genetically fused to the amino terminus of a scFv and conjugated to a BG-modified photosensitizer. Images modified and adapted from [123].

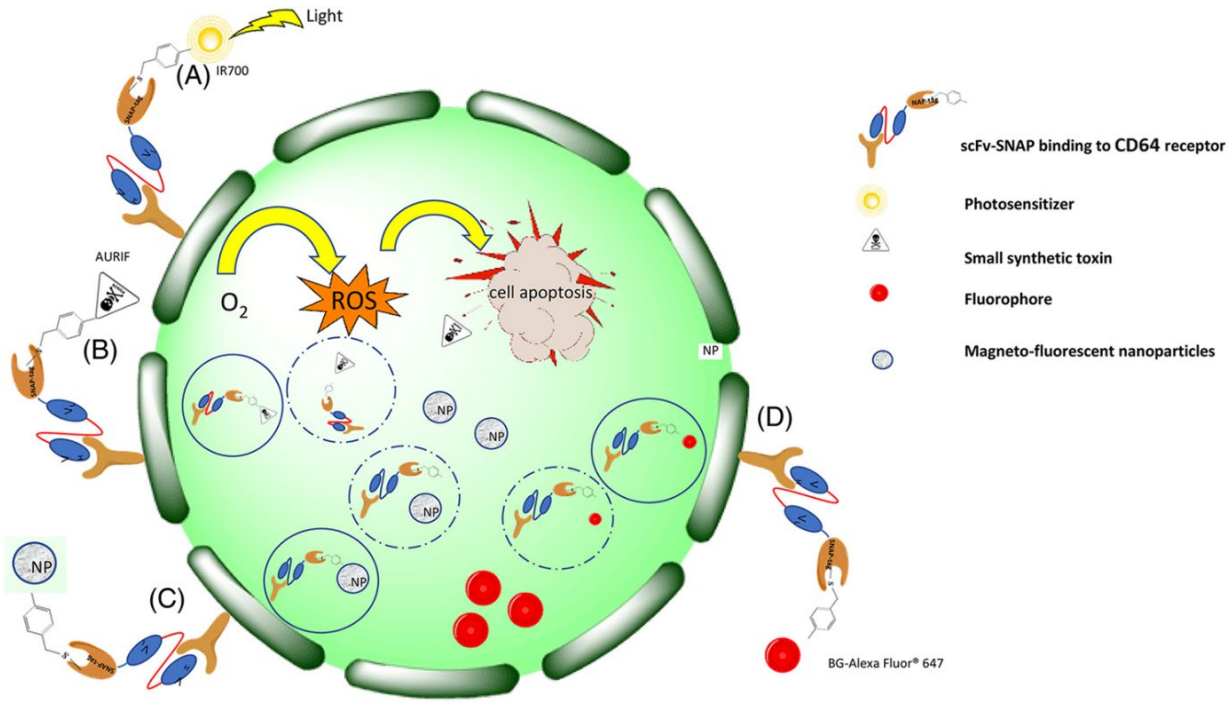

Figure 1.11. Mechanism of action of SNAP-tag Immunoconjugates: A cell-specific scFv-SNAP-tag FP conjugates with BG-modified substrates and exerts cell killing mechanisms via: (A-B) IR700-SNAP-tag conjugate (PIC), and Auristatin F-SNAP-tag conjugate (ADC) gets internalized and released into the cytosol where it induces apoptosis via ROS generation and microtubules disruption respectively. (C-D) Magneto-fluorescent nanoparticles and fluorophores enter the cell by receptor-mediated uptake, accumulate within the tumor, and allow for optical detection [123].

1.10.1 SNAP-tag Antibody drug conjugates (ADCs)

ADCs are targeted therapeutics that contain a specific antibody fragment chemically conjugated via a synthetic linker to a biologically active cytotoxic small molecule payload/drug (Figure 1.12) [125-127]. The mechanism of action of ADCs entails the antibody fragment binding specifically to a specific receptor or antigen on the surfaces of diseased cells. Subsequently, via receptor-mediated endocytosis, the toxic payload is internalized into intracellular vesicles like the lysosomes, endoplasmic recticulum and eventually cytosol, where cell death (apoptosis) is induced in the target cell by disrupting microtubule spindle assembly (Figure 1.13) [128, 129]. Several ADCs have been approved by the U.S Food and Drug Administration (FDA) for the treatment of various cancers, including gemtuzumab ozogamicin for the treatment of AML [130], trastuzumab for the treatment of HER2+ metastatic breast cancer [131], and brentuximab vedotin for the treatment of anaplastic lymphomas [132].

Despite the benefits of specificity and reduced off-target toxicities, the clinical applications of ADCs are limited due to (i) The large size of the full-length monoclonal antibody which limits tumor penetration, (ii) unspecific conjugation chemistry (coupling) between the antibody and toxic payload which results in heterogeneous conjugation products [82, 133]. However, these limitations are resolved with next-generation SNAP-tag antibody-drug conjugates. To increase tumor penetration, SNAP-tag ADCs are prepared using single-chain variable fragments (scFv) antibody fragments of molecular weight (~ 25 – 30 kDa) compared to full-length antibodies of considerable molecular weight (~ 150 kDa). Also, SNAP-tag protein covalently reacts in a 1:1 stoichiometry with its BG-modified substrates; this specific conjugation chemistry has resulted in the generation of homogeneous products and prevents the off-target release of unconjugated cytotoxic drugs [122, 133].

Monomethyl auristatin E and monomethyl auristatin F (MMAE/MMAF) are anti-mitotic agents (small molecules) derived from dolostatin 10 whose mechanism of action includes blocking tubulin polymerization and altering microtubule dynamics during cell division to induce apoptosis in cells [91, 134]. BG-modified MMAF has the chemical attachment of MMAF for 1:1 stoichiometric conjugation to SNAP-tag-based FP to generate a recombinant ADC [135, 136]. The removal of the monomethyl group from the MMAF ensures the chemical coupling of BG-linker to auristatin F by copper-catalysed azide-alkyne cyclo addition click chemistry [127].

SNAP-tag ADCs have undergone pre-clinical evaluation against human cancers. In a study by Woitok et al, two scFv-SNAP FPs (425(scFv)-SNAP and αHER2(scFv)-SNAP) were conjugated to BG-auristatin F to generate SNAP-tag ADCs targeting breast cancers with overexpressed human epidermal growth factor (HER2/neu) and epidermal growth factor receptor (EGFR) respectively. The results show compromised cell viability and apoptotic induction on EGFR+ cell lines with EC_{50} values ranging from 0.6 to 2.0 nM [137]. In another study, Woitok and colleagues compared the therapeutic efficacy of murine-derived SNAP-FP (425(scFv)-SNAP) and human-derived SNAP-FP (1171(scFv)-SNAP derived from FDA-approved panitumumab) conjugated to BG-auristatin F, targeting overexpressed EGFR in embryonal Rhabdomyosarcoma and TNBCs. The results in both ADCs show comparable pro-apoptotic and cytotoxic activity with EC_{50} values ranging from 4 to 12 nM [138]. Also, no unspecific conjugation or off-target cytotoxic effects were observed on cell lines, which confirms the specificity and clinical efficacy of SNAP-tag therapeutics for human application.

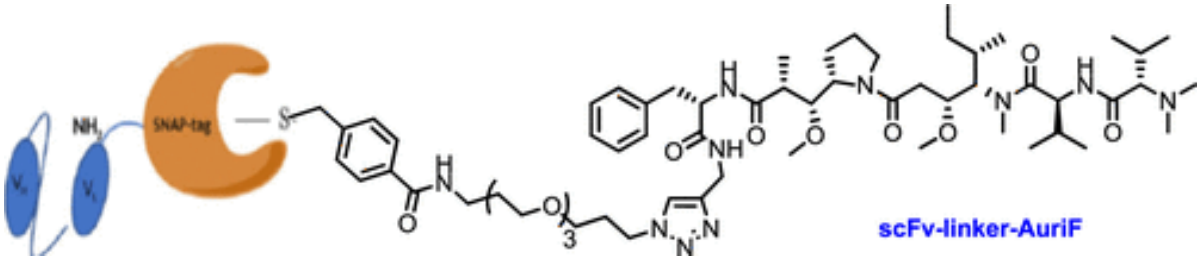

Figure1.12 Structure of novel ADC , scFv−linker−Auristatin F (AuriF)

The structure of the recombinant ADC target containing a scFv bonded to a relatively short linker containing a triazole generated from the click chemistry followed by AuriF as an amide at its C-end with a dimethyl amino N-terminus. Image accessed from [127].

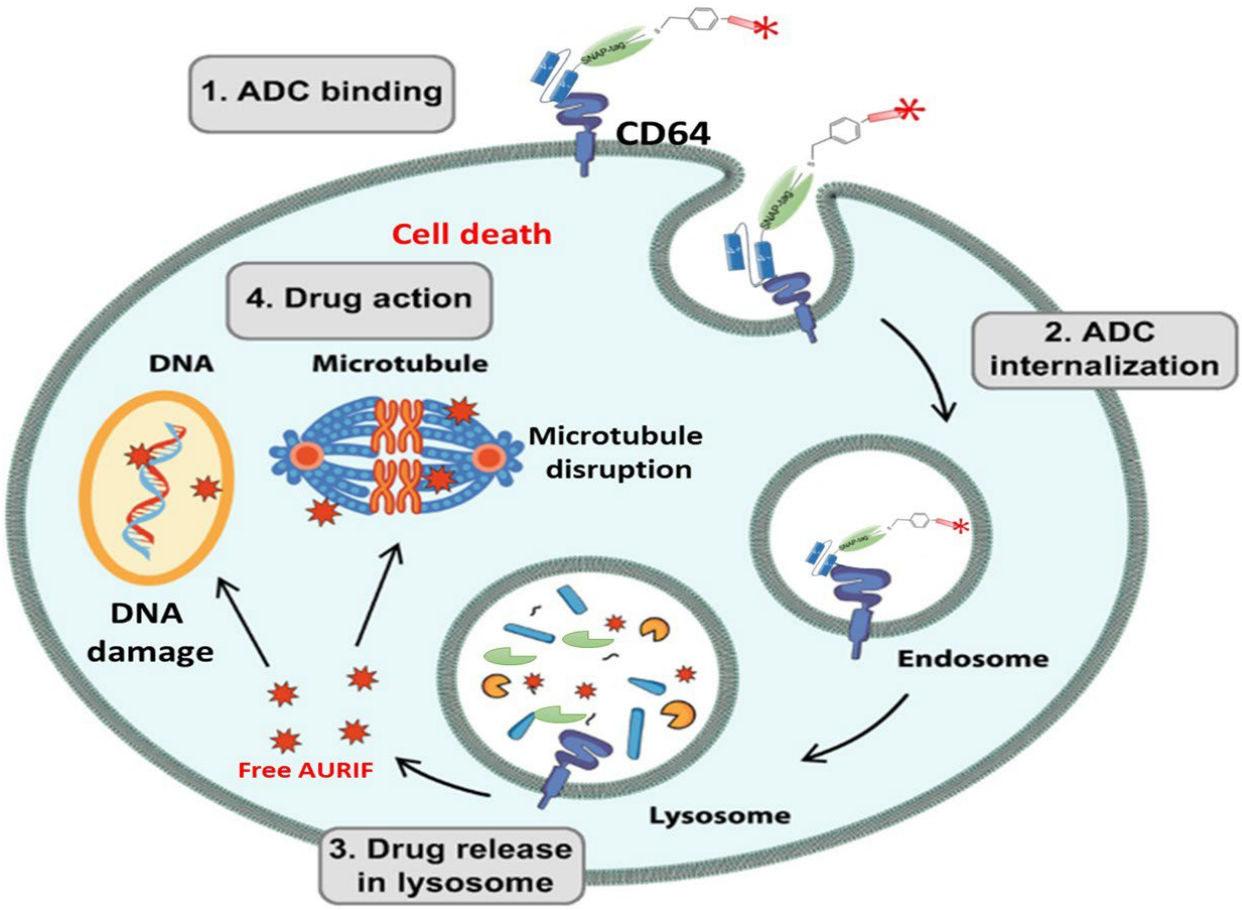

Figure 1.13. Schematic diagram of the specific mechanism of action of SNAP-tag based (novel) ADC (AURIF/MMAF): Upon receptor-mediated internalization and lysosomal processing of novel SNAP-tag ADC , Free circulating Auristatin F (AURIF/MMAF) is released into the cytosol where it induces cell death by disrupting microtubule assembly or cause DNA damage. Imaged modified and adapted from [129].

1.10.2 SNAP-tag recombinant photo immunoconjugate (PIC)

A recombiant PIC contains an antigen-specific antibody fragment conjugated to a photosensitizing agent, which can be used for targeted treatment of diseased cells via photoimmunotherapy (PIT) [139]. A photosensitizer (PS) is a non-toxic light sensitive dye which can be activated by visible light when bioaccumulated in cells. The activation of PS produces reactive oxygen species (ROS) generation leading to DNA damage, cell disruption and necrotic cell death. Furthermore, ROS-induced necrosis activates the immune system towards immunogenic cell deaths mechanisms like autophagy and apoptosis (Fig.1.14) [139-142]. Examples of common photosensitizers used in PIT include Photofrin, Chlorins, Foscan, and IR700. Chlorins and IR700 are photosensitizers in the near-infrared (NIR) region, and due to their non-invasive penetrative potentials, they are explored in the photoimmunotherapy of cancers [141, 143]. Specifically, IR700 is a unique NIR fluorescent dye with more beneficial qualities than conventional photosensitizers, especially its low light absorbance and scattering, with increased tissue penetration depth. It absorbs light at wavelengths 658 nm – 758 nm, with a peak absorbance of 689 nm [143]. IR700 is currently used in photoimmunotherapy as a theranostic agent – a single molecule with both diagnostic (imaging) and therapeutic (cytotoxic) properties [142, 144], applied to solid tumors [145].

In a clinical study involving the treatment of patients with recurrent head and neck squamous cell carcinoma, a PIC (RM-1929) consisting of an anti-EGFR monoclonal antibody, cetuximab, was conjugated to IR700. The results show a decrease in tumor density after a single cycle treatment in 85% of patients sampled, which iterates the clinical efficacy of IR700 PICs [146]. As well, another study involving the treatment of HER2+ overexpressing breast cancer with TMPC (a PIC consisting of an anti-HER2 antibody, trastuzumab conjugated to a NIR, chlorin e6) shows selective tumor destruction both *in vitro* and *in vivo* [147, 148].

Although the clinical efficacy of conventional PICs in photoimmunotherapy has been documented, its significant drawbacks lie in random conjugation and suboptimal stoichiometry ratio of the antibody to photosensitizer. Fortunately, the SNAP-tag technology offers a solution to this limitation by leveraging on the covalent binding between the SNAP-tag FPs and BG-modified photosensitizer (e.g., BG-IR700) in a 1:1 stoichiometry, which provides a simple, homogeneous conjugation system [149]. On binding to overexpressed antigens and internalization into tumor cells, an introduced light source induces excitation of the photosensitizer within the tumor, thereby limiting the risk of off-target accumulation and toxicities. In a study conducted by von Felbert and colleagues, an anti-EGFR single chain variable fragment (scFv-425) was genetically fused to the SNAP-tag protein and conjugated to BG-IR700 to generate a SNAP-tag

PIC, scFv-425-SNAP-IR700. The PIC was evaluated and found to selectively compromise the cell viability of EGFR+ skin cancer cell lines [150].

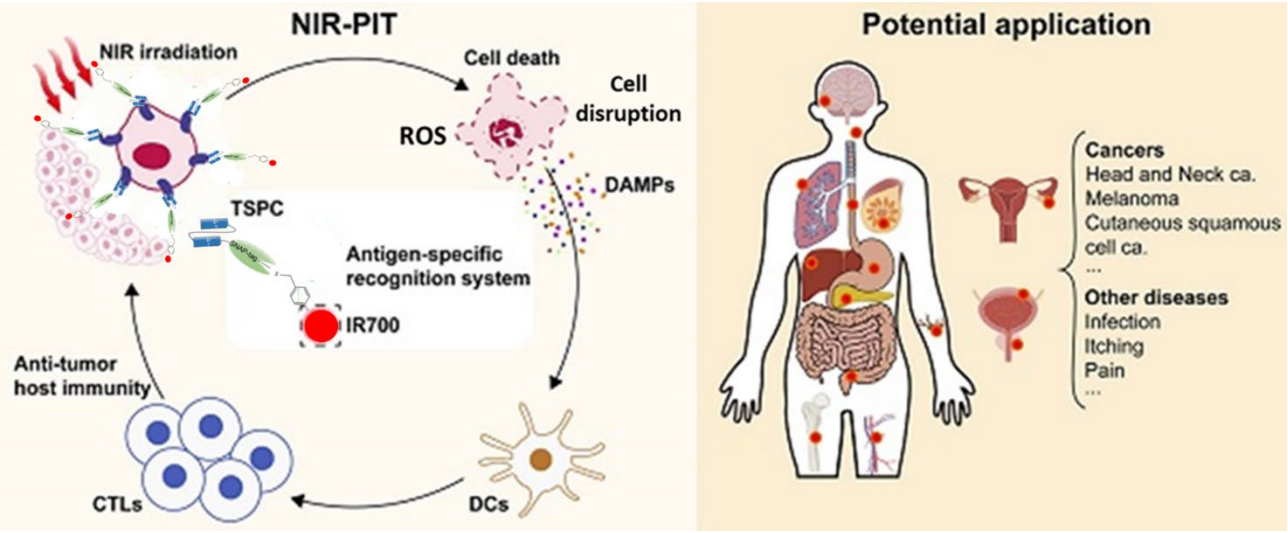

Figure 1.14. Targeted delivery of a SNAP-tag based PIC and mechanism of action in host cells: A cell-speciifc scFv-SNAP-tag photoimmunoconjugate (TSPC) upon receptor-mediated endocytosis and internalization can be locally irradiated with NIR light to induce physical stress induced cell membrane damage via ROS generation and subquently necrotic cell death. Disrupted cells releases damage-associated molecular patterns (DAMPs) which can activate the immune system – dendritic cells and cytototoxic T lymphocytes to induce immunogenic death on residual disease cells. Tumors. The application of NIR-PIT includes chronic inflammatory diseases, and solid cancers. Image modified and adapted from [142, 145].

1.11 Research aims and objectives

1.11.1 Research aims

CD64 receptor is a pivotal therapeutic target for recombinant immunotherapeutics towards elimination of dysfunctional macrophages/monocytes. Hence in this study, different CD64-targeting immunotherapeutics are generated and evaluated for their therapeutic potential.

The specific aims are:

- To demonstrate the therapeutic potential of deimmunized version of the anti-CD64 rIT , H22(scFv)-dETA`(RG7787-MT2) versus the wild-type variant, H22(scFv)-ETA`.
- To evaluate and compare the therapeutic potential of SNAP-tag ADC, H22(scFv)-SNAP-AURIF on IFN-γ stimulated/unstimulated U937, HL60 cells, and PIC, H22(scFv)-SNAP-IR700 on *ex vivo* differentiated human macrophages.

.[37].

The positive outcome of this study would allow further validation of these recombinant CD64-targeting immunotherapeutics in preclinical studies (3D cultures, animal models) to provide further proof of concept for treatment of monocytic/macrophage-mediated chronic diseases like chronic skin inflammation, skin cancers, myeloid-derived leukemia and solid tumors (lungs, breast etc).

1.11.2 Research objectives

The specific aims of the research will be achieved by investigating these research objectives:

- Insilico and Molecular cloning of recombinant plasmid DNA encoding CD64-recombinant proteins into bacteria (pMT) or mammalian (pCB) expression vectors by DNA recombineering techniques
- Bacteria expression of H22(scFv)-ETA` and H22(scFv)-dETA`(RG7787-MT2) in the periplasmic space of *Escherichia coli (E. coli)* BL21(DE3) using the compatible solute-supported stress expression protocol [151]
- Transient expression of H22(scFv)-SNAP in Human Embryonic Kidney (HEK 293T) cells
- Recombinant protein extraction and purification using affinity chromatography: immobilized metal-ion chromatography (IMAC) and size exclusion chromatoraphy (SEC).
- Protein analysis and validation of full-length recombinant proteins using Sodium dodecyl sulfate-polyacrylamide gel electrophoresis (SDS-PAGE), Western blot (WB) and protein quantification by densitometric analysis.
- Conjugation of BG-modified fluorophores: BG-Alexa488 /BG-Alexa 647 to H22(scFv)-SNAP to validate SNAP-tag domain functionality and generate fluorophore-labeled protein for investigating internalization studies.
- Isolation, *ex vivo* differentiation, and polarization of human monocytes-derived macrophages (differentiated hMDMs).
- Perform functional (binding) assays of anti-CD64 FPs on IFN-γ stimulated and unstimulated U937, HL60 cells and polarized *ex vivo* human macrophages using flow cytometry/analysis.
- Evaluate internalization kinetics of labelled recombinant anti-CD64 FPs on different *ex vivo* human macrophages subtypes by via confocal microscopy imaging.
- Evaluation of biological activities of CD64-targeting immunotherapeutics; (H22(scFv)-ETA`, H22(scFv)-dETA`(RG7787-MT2), H22(scFv)-SNAP-AURIF and H22(scFv)-SNAP-IR700) on IFN-γ stimulated CD64+ monocytic cell lines (U937, HL60) and

polarized *ex vivo* differentiated hMDMs to validate their therapeutic potential by performing cell viability (XTT) assays.

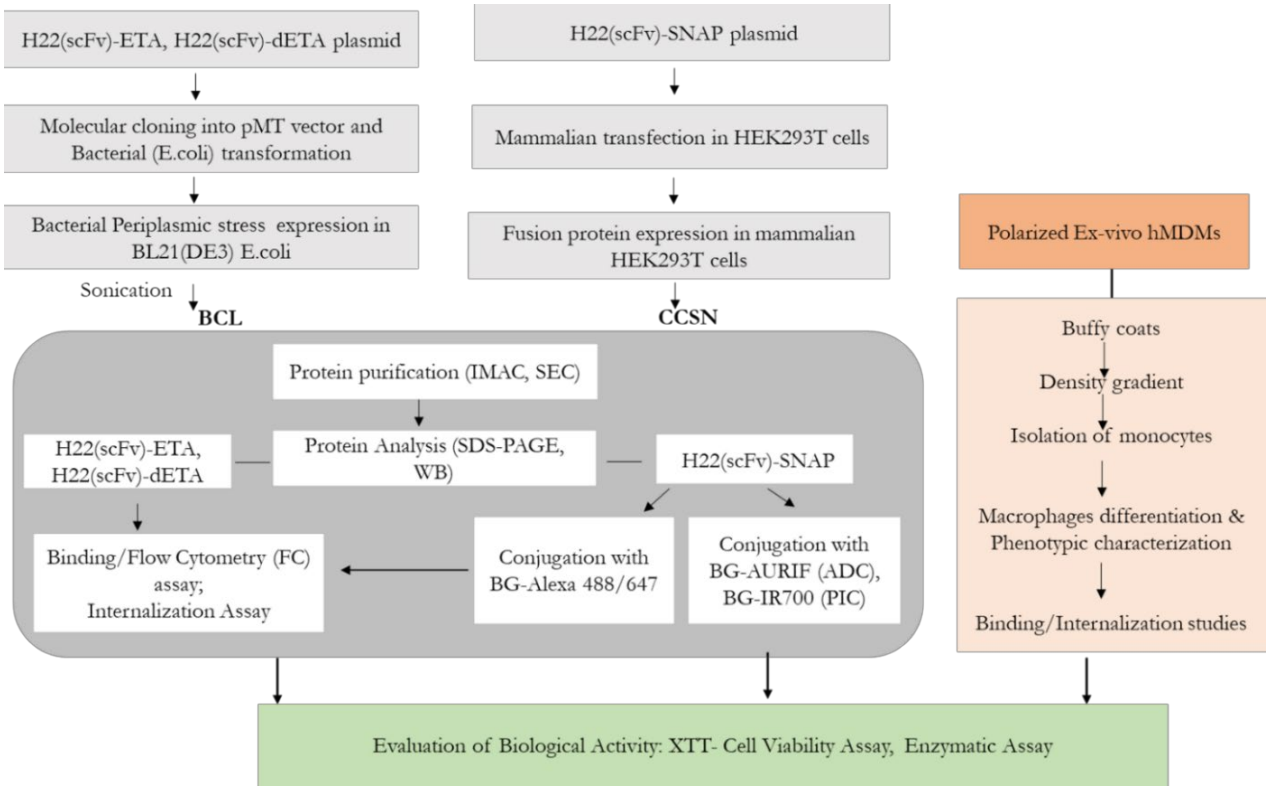

Figure 1.15. Schematic research workflow Abbreviations: BCL: Bacteria cell lysate, CCSN: Cell culture supernatant. differentiated hMDMs: Human monocyte-derived macrophages.

|CHAPTER 2: MATERIALS AND METHODS|

2.1 Materials

2.1.1 Chemicals and consumables

Unless otherwise stated, the following manufacturers supplied the chemicals and consumables used for this research: Peprotech (Hamburg, Germany); Abcam (Massachusetts, USA), Invitrogen (California, USA); Bio Legend (San Diego, USA); New England Bio Labs (NEB) (Massachusetts, USA); Sigma-Aldrich (Missouri, USA); Thermofischer Scientific (Waltham, USA); Roche (Bazel, Switzerland); Qiagen (Hilden, Germany); GE Healthcare (Illinois, USA); Promega (Wisconsin, USA); Merck (New Jersey, USA); Bio-Rad (California, USA); Millipore (Massachusetts, USA); Whatman (Freiburg, Germany); Nalgene (New York, USA); Life Technologies (California, USA); Bio Smart Technologies (South Africa), Lasec (South Africa).

2.1.2 Buffers and media solutions

Buffers and stock solutions were prepared according to standard procedures using distilled or ultrapure water (d/dH_2O). The pH of buffers was adjusted with concentrated HCL and NaOH solution as required. Where necessary, the sterilization of media and solution was done using a sterile microfilter (0.20 µm or 0.45 µm) or autoclaving at 121°C for 20-30 minutes. IMAC his-tagged protein purification Buffers were filtered and degassed using 0.45 µm Polyvinylidene difluoride (PVDF) membrane. RPMI-1640 culture medium was purchased from Invitrogen and supplemented with 10% foetal bovine serum and 1% Penicillin and Streptomycin. Zeocin® (Invitrogen) was added to the medium of transfected cells at a final concentration of up to 100 µg/mL. Stock solutions of ampicillin or kanamycin (Sigma-Aldrich) was prepared, filter-sterilized (0.2 µm) and added to Luria broth media after cooling below 50°C at a final concentration of 1 mg/l. The composition of all standard buffers and solutions (Table 2.1) and media (Table 2.2) used during my research is documented below:

Table 2.1 Buffers and solutions

Buffers	Composition	Concentration	Application
10x Tris-acetate-EDTA (TAE) buffer	Tris base Glacial acetic acid EDTA	400 mM 200 mM 10 mM	Agarose gel electrophoresis, DNA analysis
10x Phosphate-buffered saline	NaCl Na_2HPO_4	1.4 M 88 mM	Protein analysis

(PBS)	KCl KH_2PO_4	27 mM 17.5 mM	
10x Tris-buffered saline (TBS) pH 7.6	Tris base NaCl	200 mM 1.5 M	Protein analysis, WB
1x TBS-Tween	10x TBS dH_2O Tween 20	10 % (v/v) 90 % (v/v) 0.1 % (v/v)	
10x Transfer buffer	Tris Glycine	250 mM 2 M	
1x Transfer buffer	10x Transfer Buffer Methanol dH_2O	10 % (v/v) 20 % (v/v) 70 % (v/v)	
4x Incubation buffer pH 8.0	NaH_2PO_4 NaCl Imidazole	200 mM 1.2 M 40 mM	IMAC, Protein purification
Equilibration buffer pH 8.0	NaH_2PO_4 NaCl	50 mM 300 mM	
Elution buffer pH 8.0	NaH_2PO_4 NaCl Imidazole	50 mM 300 mM 250 mM	
Lysis solution 1	Tris-HCl pH 8.0 Glucose EDTA	50 mM 50 mM 10 mM	DNA isolation and purification
Lysis solution 2	NaOH, SDS	0.2 M 1 % (w/v)	
Lysis solution 3	Potassium acetate pH 6	3 M	
Tris-Glycine SDS (pH 8.3)	Tris-HCl (pH 8.3) Glycine SDS	25 mM 192 mM 0.1% (w/v)	

Stacking Gel	Acrylamide/Bisacrylamide (30/1) Tris-HCl (pH 6.8) SDS TEMED APS	12% (w/v) 375 mM 0.1% (w/v) 0.1% (w/v) 0.1% (w/v)	SDS-PAGE, Protein analysis
Separating/Resolving Gel	Acrylamide/Bisacrylamide (30/1) Tris-HCl (pH 8.8) SDS (10 %, w/v) TEMED APS	5 % (w/v) 150 mM 0.1% (w/v) 0.1% (w/v) 0.1 % (w/v)	
Lysis buffer	Tris-HCl pH 8.0 NaCl DTT Protease inhibitor cocktail Glycerol (Sigma-Aldrich)	75 mM 300 mM 5.0 mM 1 tab./50 mL 10 % (v/v)	Sonication and Protein preparation
Fluorescent Activated Cell Sorting (FACS) buffer	PBS pH7.4 FCS EDTA	1X 3% (v/v) 2mM	Flow cytometry, Protein binding affinity

Table 2.2 Medias and transfection/transformation reagents

Medium	Composition	Concentration	Source, Application
RPMI 1640	GlutaMAX™ Sodium pyruvate Phenol red Fetal bovine serum Penicillin Streptomycin	2 mM 3.7 g/L 15.0 mg/L 10 % v/v 100 I.U/ml 100 µg/ml	Gibco 618, Tissue culturing (CD64+/Macrophage cell lines, Suspension cells, Adherent cells)
DMEM	GlutaMAX™ Sodium bicarbonate Phenol red	2 mM 3.7 g/L 15.0 mg/L	Gibco 18,

	Fetal bovine serum Penicillin Streptomycin	10 % v/v 100 I.U/ml 100 µg/ml	Tissue culturing (CD64-, Cancer cell lines, Adherent cells)
Luria-Bertani (LB) Media	Tryptone Yeast Extract Sodium Chloride (NaCl) Agar (Agar plates)	1.0% (w/v) 0.5% (w/v) 0.5% (w/v) 1.5% (w/v)	Solid/Liquid bacterial (*E. coli*) culturing,
Terrific Broth with compatible solutes	Glucose Sorbitol NaCl $ZnCl_2$ Glycine-betaine	3.5% (w/v) 5.0 M 4% (w/v) 0.5 mM 40 mM	Periplasmic expression in *E. coli* BL21(DE3)
SOC outgrowth media	Peptone Yeast extract NaCl KCl $MgCl_2$ $MgSO_4$ Glucose	2.0% (w/v) 0.5% (w/v) 10 mM 25 mM 10 mM 10 mM 20 mM	*E. coli* BL21(DE3) or DH5α plasmid transformation
Xtremegene Transfection reagent	Proprietary blend of lipids and other components supplied in 80% ethanol		Thermofischer Scientific, Mammalian transfection of recombinant plasmids
Zeocin™ Selection reagent	Zeocin was supplied in sterile water in one 1.25ml eppendorf tube.	100 mg/ml	Thermofischer Scientific, Mammalian expression/ transfection of recombinant plasmids

2.1.3 Antibodies

These specific binding antibodies were used during the research for the following purposes: (i) immunodetection of recombinant proteins on western blots (WB), (ii) analysing of surface receptors on mammalian cells by flow cytometry (FC): These antibodies are summarized (Table 2.3)

Table 2.3: Specific antibodies and their applications

Names	Supplier	Applications
Mouse-anti-Penta-His*	Sigma Aldrich/ Bio-Rad	WB, Primary Antibody
Goat-anti-rabbit-IgG Horseradish peroxidase	Sigma Aldrich	WB, Secondary antibody for protein detection
Mouse-anti-Human CD14*	Biolegend	FC
Mouse-anti-Human CD206*	Biolegend	FC
Anti-His Tag-PE antibody	RnD systems	FC, Protein detection via 6X, 10X His-tag
Goat anti-mouse IgG-Alexa 647	Abcam	Surface receptor, FC
Mouse anti-human CD64 Alexa fluour ® 647 antibody	Biorad	CD64 surface receptor, FC

2.1.4 Chromatography resins and membranes

Chromatographic resins and membranes were used during chromatographic techniques. Immobilized metal-ion affinity chromatography (IMAC) was performed with an XK16-20 column filled with Ni-Sepharose 6 Fast Flow resin (GE Healthcare) for the enrichment of Histidine (His)-tagged proteins. Preparative size exclusion chomatography (SEC) was carried out using an XK16-70 column packed with Superdex^{TM} 75 / 200 resin. Amicon ultrafiltration filter 10 kDa (Millipore) was used to concentrate the purified proteins for proper detection of His-tag recombinant proteins; Polyvinylidene fluoride or polyvinylidene difluoride (PVDF) is used as a transfer membrane during WB.

2.1.5 Cloning reagents and kits

Molecular cloning reagents include Restriction enzymes (*SfiI, NotI, BlpI, MauBI),* CutSmart® buffer, T4 DNA ligase and T4 ligase buffer supplied by New England Biolabs (USA) and Zymo Research (USA). The reagents were used according to the stipulated manufacturer's guidelines. Also, cloning kits, including DNA purification kits, ligation, etc., are summarized in the table below (Table 2.4):

Table 2.4 Cloning kits and their applications

Kit	**Source**	**Application**
Nucleobond PC 100 Miniprep, Midi prep kit	Machery-Nagel, Germany	Plasmid isolation & and purification
Zyppy ™ Plasmid Miniprep Kit	Zymo Research, USA	Plasmid extraction and purification
QIAquick Gel Extraction Kit	Qiagen, Germany	Plasmid extraction
Quick Ligation (T4 Ligase) Kit	NEB	Ligation of plasmids
DNA sample loading dye	New England Biolabs, USA	Plasmid analysis
DNA ladder 1kb, 100 bp	New England Biolabs, USA	Plasmid analysis
Restriction enzymes (*SfiI*, *NotI*, *BlpI*, *MauBI*)	New England Biolabs, USA	Restriction digest, mapping

2.1.6 Biological materials

2.1.6.1 Bacterial strains

Two bacterial strains (Table 2.5) were used in the cloning and expression of recombinant proteins: *E. coli* DH5α cells was used for all intermediate cloning steps and amplification of plasmid DNA, and *E. coli* BL21(DE3) cells was used for the expression of rITs.

Table 2.5 *E. coli* strains used:

E. coli Strains	Genotype	Reference	Application
DH5α	*fhuA2 (argF-lacZ)U169 phoA glnV44 80 (lacZ)M15 gyrA96 recA1 relA1 endA1 thi-1 hsdR17*	Biolabs	Cloning of recombinant plasmids

BL21(DE3)	*fhuA2 [lon] ompT gal (λ DE3) [dcm] ΔhsdS λ DE3 = λ sBamHIo ΔEcoRI-B int: :(lacI:PlacUV5:T7 gene1) i21Δnin5*	Biolabs	Expression of recombinant proteins

2.1.6.2 Mammalian cell lines

These mammalian cell lines listed below (Table 2.6) were used for recombinant protein production and evaluating the functional activity of recombinant proteins towards CD64 positive/negative cells:

Table 2.6: Mammalian cell lines

Name	Background	Receptor used	Reference
HEK293T	Highly transfectable derivative of human primary embryonal kidney cell line 293	CD64-	ATCC Nr. CRL-11288
U937	Human histiocytic lymphoma cell line	CD64+	ATCC Nr. CRL-1593.2
HL60	Human leukemia cell line	CD64+	ATTC Nr. CCL-240
MDA-MB-468	Human breast cancer cell line	CD64-	ATTC Nr. HTB-132
A2058	Human melanoma cell line	CD64-	ATTC Nr. CRL-11147

2.1.6.3 Human monocyte-derived macrophages (differentiated hMDMs)

The functional activities of CD64-recombinant proteins were evaluated with polarized *ex vivo* differentiated differentiated hMDMs. All experiments on differentiated hMDMs were conducted with the approval of the University of Cape Town Human Research Ethics Committee (HREC) with reference number HREC: 201/2023.

2.1.7 Equipment and software

Table 2.7: Equipment used in this research with their manufacturer/supplier are listed:

Equipment	Manufacturer/supplier
Balances	P5600.R2 (RADWAG)
Centrifuge	Allegra X-30R (Beckman coulter), Prism (Labnet)

Microfuge	Mcf-2360 (LMS Co Ltd)
Cell counter	TC20 (Bio-Rad)
Electrophoresis and Blotting	Mini-Protean (Bio-Rad), Trans-Blot Cell (Bio-Rad)
Transilluminator	DR-89x (Clare chemical research)
Flow cytometer	BD LSR-II (BD Biosciences)
Shaking flask incubator	LM-510RD (Yinder Co Ltd)
Tissue culture incubator	*In vitro* Cell (Nuaire)
Spectrophotometer	Denovix Ds-11 (Denovix Inc)
Microscope	Zoe (Bio-rad), LSM 540 / 880 Airyscan (Zeiss)
Sonicator	Qsonica (Qsonica L.L.C)
Vortex	VTX-3000L (LMS Co Ltd)
Orbital Shaker	Gyrotwister (Labnet)
Chromatography Equipment	Äkta Avant (GE Healthcare, Freiburg)
pH Meter	pH 50+ DHS (XS Instrument)
Heating block	Thermomixer comfort (Eppendorf), Thermostat 5320 (Eppendorf)
iBrightFL1000 imaging system	Thermofischer scientific
SpeedVac	MiVac (Sp scientific)
Serological Pipette	Pipetman (Gilson)
Software	Graph Pad Prism v10.0, Flowjo v10.5, Snapgene v5.0.5, Microsoft office 365.

2.2 Methods

2.2.1 Expression vectors for recombinant protein production

The SnapGene ® software was used to design the open reading frame (ORF) of two plasmid vectors to produce recombinant immunotoxins (rITs) and SNAP-tag FP. The ORF of rITs, H22(scFv)-ETA`, and H22(scFv)dETA` (RG7787-MT2) was cloned into a pMT backbone for protein production in bacteria (Table 2.8). The ORF of SNAP-tag FP, H22(scFv)-SNAP, was cloned into the pCB backbone for protein production in mammalian human embryonic kidney (HEK293T) cells (Table 2.9). In both pMT and pCB backbone, the CD64-targeting antibody; H22(scFv), was flanked by single *SfiI* and *NotI* restriction sites while the toxins, ETA`/dETA` (RG7887-MT2) or SNAP-tag protein was flanked by *NotI* and *BlpI* restriction sites at the 5' – 3' end respectively. Both plasmid vectors have been fully optimized for recombinant protein production at *MB&I* lab, and a summary of the essential features and their functions are documented below:

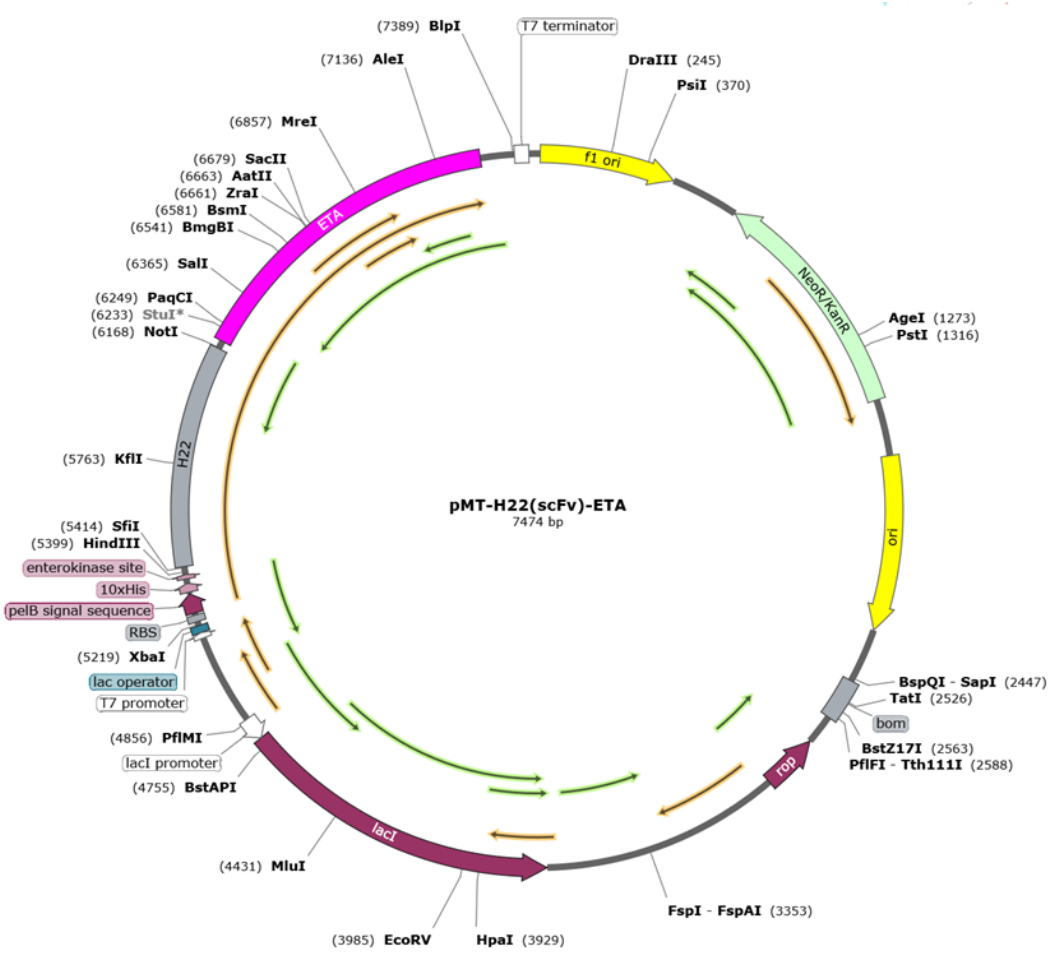

Table 2.8: Features of bacterial (pMT) expression vector and their functions

S/N	Plasmid features	Description/function
i	Lac I	The gene that regulates the Lac operon by producing a lac repressor protein that prevents RNA polymerase from binding to lac operator [152]
ii	LacI promoter	Turns off transcription of the genes required for lactose metabolism [152]
iii	T7 promoter	Regulates gene expression especially transcription and translation of FPs. Also allows induction with IPTG [153]
iv	Lac operator	Regulates the transcription of the lac operon [152]
v	Ribosome binding site (RBS)	Sequence of nucleotide before the start codon of an mRNA transcript that allows ribosomes to bind and initiate translation [153]
vi	PelB signal sequence	A signal peptide that directs the secretion of recombinant proteins into the bacterial periplasm [153]
vii	10xHis-tag	10 repetitive histidine amino acids which allow FP to bind successfully during affinity chromatography and detection of protein using immunoblotting [154]
viii	Enterokinase cleaves site (EKS)	Separate the secretion site (Pel B from single chain variable fragment (scFv) FP [154]
ix	scFv	Gene encoding the cell-specific antibody /target of interest [71]
x	Exotoxin A (ETA`)	A truncated version of external toxin (exotoxin A) derived from bacterial *Pseudomonas aeruginosa,* which inhibit protein synthesis and induce apoptosis [100]
xi	T7 terminator	present in bacteriophages and allows for efficient termination of RNA transcripts [155]
xiii	NeoR/KanR	Neomycin or kanamycin resistant gene that allows for selection of viable plasmid carrying procaryotic cells [156]
xiv	ori	Origin of replication [153]

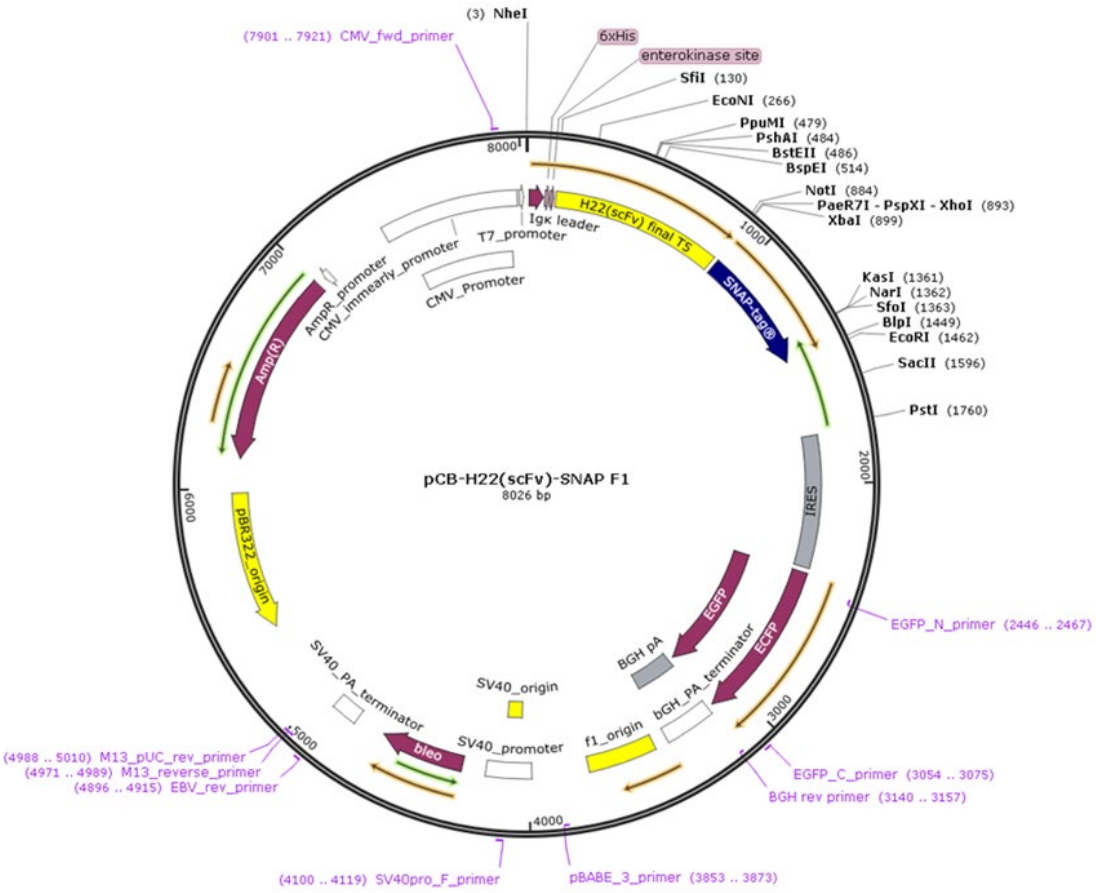

Table 2.9: Features of mammalian (pCB) expression vector and their functions

S/N	Plasmid features	Description/function
i	Bleo^{R}	It allows for antibiotic resistance specifically bleomycin, zeocin in eukaryotic cells, hence selection of viable transfected/cloned cells [156]
ii	SV 40 poly (A) terminator	Termination of mRNA transcript [153]
iii	f1 origin	The origin of replication of bacteriophages[153]
iv	Bovine growth hormone (Bgh) poly adenylation (A) signal	Poly adenylation signal that leads to termination of gene transcription [157]
v	Enhanced green fluorescent protein (eGFP)	A reporter gene that allows for the identification of successfully cloned/ transfected plasmids. Microscopic visualization is monitored based on green fluorescence generated by co-expression of eGFP with FP [156]

.[50].

vi	Enhanced cyan fluorescent protein (eCFP)	eCFP reporter gene for monitoring FP protein expression in mammalian vector. Similar in function to eGFP reporter gene [156]
vii	Internal ribosome entry site (IRES)	Allows co-expression of two genes in a single vector in a regulated manner e.g H22(scFv)-SNAP expressed with eGFP hence green fluorescence involves active protein production [156]
viii	SNAP-tag ®	A self-labelling protein that conjugates antibody to toxin or fluorophores [158]
ix	scFv	Sequence for scFv antibody fragment, allows for the affinity/binding of FPs to cells [71]
x	Enterokinase cleavage site (EKS)	Cleavage site separating leader sequence from recombinant proteins [154]
xi	Poly histidine-tag (6X)	6-repetitive histidine amino acids responsible for binding affinity during purification and detection of his-tag proteins after western blots (WB) [154]
xii	Ig-Kappa leader	A leader sequence peptide of 15-20 amino acids that signals the secretion of FPs into mammalian cell culture supernatant [153]
xiii	T7 promoter	Initiate the transcription of genes using mRNA polymerase [153]
xiv	CMV promoter	Allows expression of genes in the mammalian vector, both the ORF region and non-ORF regions [159]
xv	AMP(R) promoter	Allows transcription of ampicillin resistance gene [160]
xvi	AMP(R)	Ampicillin resistance gene that allows for successful selection of viable transfected clones [160]

2.2.2 Molecular cloning of recombinant plasmid for expression

The methods described below followed standard experimental techniques according to Sambrook and Russell [161], or the instructions provided by the product manufacturer.

2.2.2.1 Bacterial transformation of *E. coli* using the heat-shock method

Bacterial transformation involves the uptake of recombinant plasmid (DNA) by *E. coli* cells, and it is essential procedure for plasmid bulk prep, DNA extraction, and recombinant protein

production. In summary, 50 µL of competent *E. coli* (DH5α/ BL21(DE3)) cells were slowly thawed on ice and mixed gently with 100 ng of the plasmid DNA (encoding recombinant protein of interest). The mixture was then incubated on ice for 30 minutes and heat-shocked at 42°C for 1 minute to allow the plasmid DNA uptake by *E. coli cells*. Thereafter, the transformation mix were cooled on ice for 5 minutes and 950 µl of antibiotics-free super optimal broth with catabolite repression (SOC medium) was added. The mixture was incubated at 37°C for 60 minutes with shaking at 300 rpm to allow the expression of the antibiotic-resistant gene(s) from acquired plasmids. Afterwards, the transformed cells were centrifuged at 3000 x g for 4 minutes and the cell pellet was resuspended in 300 µL SOC medium. Finally, 100 -150 µl of the cell suspension was plated onto warm LB agar plates supplemented with appropriate antibiotics and incubated at 37°C overnight (or approximately 16 hours) for recovery of successful transformants (as single colonies). After recovery, single colonies were selected and inoculated with 50ml of LB medium supplemented with appropriate antibiotics: 50 ng/µl of kanamycin for rIT (pMT)plasmids and 100ng/µl of ampicillin for SNAP-tag fusion (pCB) plasmid. The culture was incubated overnight on a shaking incubator at 37°C with vigorous shaking at 200-200 rpm to induce bacterial growth. The next day, plasmids DNA are retrieved from cell culture and glycerol stocks were prepare for long-term storage plasmids. Glycerol stocks were prepared by mixing 500 µl of overnight culture with 500 µl of 50 % (v/v) sterile glycerol to generate a final volume of 1.0 ml. Each glycerol stock was immediately transferred and stored at -80°C for long-term maintenance.

2.2.2.2 Plasmid (DNA) isolation from bacterial culture

Plasmid isolation involves the retrieval of DNA from bacteria. This is pivotal for bulk preparation, and downstream molecular cloning of plasmids. Following the manufacturer's instructions, all plasmid DαNA was isolated and purified from an overnight bacteria culture (DH5α) using the Zyppy plasmid mini-prep kit (Zymoresearch, USA) or the Nucleobond DNA extraction kit (Macherey-Nagel, Germany). The plasmid preparation could follow a mini-prep, midi-prep or maxi-prep protocol. In summary, *E. coli* (DH5α) cells was pelleted in a Centrifuge (at 4000g for 30 mins), and in a series of alkaline solution lysis of the bacterial cells, the plasmid DNA was released, and bounded to an anion-exchange resin in the Nucleobond ® column, from where it is eluted and precipitated with room temperature 70% Isopropanol. After precipitation, the isolated DNA is dried and solubilized in 30ul of nuclease free water (pre-heated at 50°C for 15mins), and quantified (nanodrop) with Denovix DS-11 spectrophotometer (Thermofischer scientific, USA).

2.2.2.3 DNA quantification: concentration and purity

DNA concentration and purity are important for molecular cloning of recombinant plasmid/DNA. The DNA concentration was determined by measuring absorbance at 260 nm (A260) on the Denovix DS-11 spectrophotometer, and the purity of the nucleic acid was determined by measuring the A260 / A280 ratio which is expected to be 1.8 and above for pure DNA.

2.2.2.4 Restriction digestion

Restriction digestion was used to cleave plasmid constructs into compatible/sticky ends containing the insert fragments and backbone fragments. Briefly, 2 µg of plasmid DNA was incubated with corresponding restriction enzymes and buffer at the recommended temperature for 16hours as suggested by New England Biolabs (Table 2.10). At the end of the restriction digest, the enzymes were deactivated by incubating the reaction mixture at 65°C for 10-15 minutes. The digested DNA fragments were isolated with Agarose Gel Electrophoresis (AGE).

Table 2.10 Restriction digestion reaction set up

Component	**Concentration**	**Incubation temp/time**	**Deactivation temperature**
10X NEB-cut smart buffer	1X		
Plasmid DNA of interest	2 µg		
Restriction enzyme 1 (*NotI*)	2000U/ml	37°C (16hours)	65°C
Restriction enzyme 2 (*BlpI*)	2000U/ml	37°C (16 hours)	65°C
Nuclease free water	Up to 50 µl		

2.2.2.5 Agarose gel electrophoresis (AGE)

To isolate the digested DNA fragments, an analytical agarose gel electrophoresis was performed. Samples containing the digested DNA fragments were gently loaded into a 1.2 % pre-cast agarose gel supplemented with SYBR-safe nucleic acid staining dye (Thermofischer Scientific). A 2-log DNA ladder was used to evaluate the DNA band sizes. DNA fragments of interest were excised from the gel on a UV transilluminator with a sterile blade. The DNA fragments were purified from

the agarose gels using a QIAquick gel extraction kit (Qiagen) according to the manufacturer's instructions and stored at –20°C.

2.2.2.6 T4 ligation of recombinant DNA

Ligation of plasmid DNA is used for inserting different recombinant DNA fragments into a vector backbone. This allows for the generation of several recombinant clones/plasmids or constructs. The ligation of DNA fragments was carried out using the T4 DNA Ligase kit by following the manufacturer's protocol (New England Biolabs). Briefly, reaction components were set up in a final volume of 20 µl and included up to 1 to 5-fold molar excess of vector to insert DNA depending on their relative sizes. The ligation reaction set up (Table 2.11) was thereafter incubated at 16 °C overnight. The next day, the reaction was stopped by heat inactivation at 65 °C for 10-15 mins. Afterwards, the ligated product was transformed into competent *E. coli* (DH5α) cells, and they were cultured overnight on an LB plate at 37°C to retrieve ligated colonies.

Table 2.11 Ligation reaction set-up

Component	**Concentration**		
T4 DNA ligase buffer	1X T4 DNA Ligase		
Vector: Insert DNA	1:1	1.:3	1:5
Vector DNA	50 ng		
T4 DNA Ligase	200 - 400 U		
Nuclease free water	Adjusted to 20 µl		

2.2.2.7 Restriction mapping analysis

Restriction mapping is a molecular cloning protocol for confirmation of successfully cloned plasmids, with the use of restriction endonucleases. The restriction digest protocol above (2.2.2.4) was used for restriction mapping of cloned pMT-H22(scFv)-dETA`(RG7787-MT2), using restriction enzymes *MauBI* and *NotI (*restriction Temp – 37°C) to distinguish it from its parent plasmid, H22(scFv)-ETA`.

2.2.3 Expression of recombinant FPs

2.2.3.1 Periplasmic expression in *E. coli* under osmotic stress conditions

The periplasmic expression protocol for rITs in *E. coli* had been established and documented by Barth et al [151]. Briefly, a freshly transformed *E. coli* BL21(DE3) single colony was used to inoculate 50 ml of terrific broth (TB) media and cultivated overnight (or 16 hours) at 37 °C in shaking incubator at 200 rpm as the starter culture. 15 ml of this starter culture was transferred into a fresh 500 ml of TB medium supplemented with appropriate amount of kanamycin (1:1) until an optimal density, OD 600 of 1.6 was reached (7 hours, 26 °C and 200 rpm). Osmotic stress was induced by the addition of 100 ml of compatible solutes containing 0.5 M Sorbitol, 4 % NaCl, 10 mM Glycin-betaine and 100 ml TB/$ZnCl_2$ media. After incubation for 30 minutes at 26°C, the expression of recombinant protein was induced by the addition of 1 mM Isopropyl ß-D-1-thiogalactopyranoside (IPTG). Induction was continued for 16 hours at 26 °C in a shaking incubator at 200 rpm. Afterwards, the IPTG-induced cells were harvested by ultracentrifugation (4000 × g, 30 mins, 4°C) and the pellets were stored at -80°C. For purification, the frozen pellet was resuspended in ice-cold preparation lysis buffer (pH 8.0) containing; 75 mM Tris/HCl, 300 mM NaCl, 5 mM DTT, 10 mM EDTA, 10% (v/v) glycerol, and complete protease inhibitor (1 tablet / 50 ml, Sigma Aldrich). To release the periplasmic content, the samples were sonicated (60 s at 200 W) and cell debris was removed by ultracentrifugation (30,000 X g, 30 min, 4°C).

2.2.3.2 Mammalian expression of recombinant FPs in human embryonic kidney (HEK293T) cells

Transfection of recombinant plasmid into HEK293T cells was carried out by using the Xtremegene transfection reagent (Merck, USA) according to the instructions provided by the manufacturer. Briefly, a transfection mixture containing 200 µL of plain RPMI, 5 µg of plasmid DNA and 10 µl of X-treme gene transfection reagent was prepared in a sterile tube and incubated for 30 minutes at room temperature to allow complex formation. Afterwards, the transfection mixture was added to the cells without disturbing the cell monolayer. After 48 hours, the transfection medium was replaced with fully supplemented RPMI media. At 72-96 hours post-transfection, the cells were viewed underneath a fluorescent microscope to check for the expression of the eGFP reporter gene as a measure of transfection efficiency. Selection for positively transfected cells was performed by adding 100-200 µg/ml of Zeocin™ (Invitrogen). In a stepwise approach, the HEK293T cells were expanded from T-25 to T-75 to T-175 flasks. Recombinant FPs were recovered by collecting and centrifuging the cell culture media (4500 rpm, 10 minutes, 4°C) and storing the supernatant at 4°C.

2.2.4 Purification of recombinant proteins using immobilized metal-ion affinity chromatography (IMAC)

IMAC is a widely used technique to purify or rapidly enrich poly-histidine-tagged proteins. In order to purify fusion proteins (FPs) expressed in E. coli or HEK293T cells, a purification system called Äkta-Avant (GE Healthcare) was utilized. The Äkta-Avant system was equipped with pre-packed columns for purification: the His-Trap Excel column, which was used for purifying FPs from mammalian cell culture supernatant (CCSN), and the His-trap Chelating column, which was used for purifying FPs from bacterial cell lysate. These columns are specifically designed to exploit the presence of histidine tags on the target proteins, allowing for efficient and effective purification.

2.2.4.1 Purification of recombinant proteins from bacterial (cell) lysate

The bacterial lysate (soluble fraction) from section 2.2.3.1 was clarified by passing it through a 0.45 µm filter (Millipore) before loading it onto a ready-to-use His-Trap Chelating column at a flow rate of 5 ml/minute. Afterwards, the column was washed with a wash buffer containing 30 mM imidazole until the baseline was reached (Table 2.12 - 2.13). Finally, the bound protein was eluted using an elution buffer containing (250 - 500 mM) imidazole at a flow rate of 1 ml/minute. The eluted protein fractions were subsequently screened by SDS-PAGE and WB before concentrating fractions (using the Amicon® ultrafiltration device 10 kDa) with the protein of interest.

Table 2.12: Profile steps for 1st IMAC (rITs)

Procedure	Column volume (CV), Flow rate
Column equilibration (start)	5 CV, 5 ml/min
Sample Application	1 ml/min
Column Wash	10 CV, 3 ml/min
Step Elution (250mM imidazole)	10 CV, 2 ml/min
Equilibration wash (end)	3 CV, 5 ml/min

Table 2.13: Profile steps for 2nd IMAC (rITs)

Procedure	CV, flow rate
Column equilibration (0-10 mM) (start)	5 CV, 5 ml/min

Sample application	1 ml/min
Column wash (30 mM)	5 CV, 3 ml/min
Step elution (225 mM)	1 CV, 2 ml/min
Gradient elution (225 - 250 mM)	4 CV, 2 ml/min
Step elution (250 mM)	5 CV, 2 ml/min
Equilibration wash (end)	3 CV, 5 ml/min

2.2.4.2 Purification of recombinant protein from mammalian cell culture supernatant

Before commencing purification, cell culture supernatants were clarified by filtering through a 0.45 µm filter membrane and adjusted to optimal binding conditions by adding 4x binding buffer (40 mM imidazole pH 8.0). Thereafter, the cell-free culture supernatants were applied to an already equilibrated His-Trap Excel column using these conditions (Table 2.14). Each eluted fraction was analysed by SDS-PAGE and fractions containing the desired protein bands were pooled together.

Table 2.14: Profile steps for IMAC (SNAP-tag FP)

Procedure	**CV, flowrate**
Column Equilibration	5 CV, 5 ml/min
Sample application (start)	3 ml/min
Column wash	15 CV, 5 ml/min
Gradient Elution (0 -150 mM)	20 CV, 5 ml/min
Step Elution (500 mM)	5 CV, 5 ml/min
Equilibration wash (end)	5 CV, 5 ml/min

2.2.4.3 Size Exclusion Chromatography (SEC)

SEC is a protocol used to separate proteins based on differences in their molecular weight. Before samples loading, the Äkta Purifier System (GE Healthcare) with an XK16-70 Superdex^{TM} 75 / 200 packed column (GE Healthcare) was equilibrated with phosphate buffer saline (PBS, pH 7.4) at 1.0 ml/minute for 3 hours. Next, IMAC purified protein samples concentrated in 1 ml using an

Amicon®10 kDa cut-off was loaded to the column and fractions were eluted in 1 ml fractions and analysed by SDS-PAGE for protein size and purity. Selected fractions were pooled, concentrated, filter-sterilized (0.2 μm) and stored at 4°C. Purified proteins were quantified by using the Denovix DS-11 spectrophotometer to measure absorbance at 260 nm.

2.2.5 Protein analysis

The characterization of the structural integrity of expressed recombinant proteins were evaluated using SDS-PAGE and WB techniques. Furthermore, recombinant proteins were quantified using Denovix spectrophotometer to measure total protein concentration, while Densitometry (with BSA standards) was used to specifically quantify the yield of the expressed full-length proteins.

2.2.5.1 SDS-PAGE

To analyse protein samples, a 10 % SDS-PAGE was used to separate proteins based on their specific molecular weight. Briefly, protein samples were denatured by mixing with 4x Laemmli buffer (3:1) and heating for 5 minutes at 95°C. Thereafter, 25 μl of denatured protein samples and 2.5-3 μl of prestained protein molecular weight marker (Thermofischer scientific) were loaded onto a polyacrylamide gel. The proteins were separated by running the gel at 120 volts for 90 minutes in a Mini-PROTEAN II chamber (Bio-Rad) in 1x running buffer. Thereafter, protein bands were visualized and analysed by staining the gel with Aqua-stain for 15- 30 minutes.

2.2.5.2 Western Blotting (WB)

WB (also called protein immunoblot) is a widely used technique that allows the specific detection of poly histidine-tagged proteins separated by SDS gel electrophoresis. Briefly, proteins separated by the SDS-PAGE protocol above were transferred from the polyacrylamide gel onto a PVDF membrane (25V, 1.0A, 30mins) using the Bio-Rad Trans-Blot Turbo system. Afterwards, the membrane was blocked with fat-free milk for 1hr at room temperature on a rocker to prevent unspecific binding of primary antibodies to transferred proteins. Next, the membrane was washed three times with 1x PBST and incubated with 1:1000 anti-His-tag primary antibody at 4 °C overnight (for 16 hours) on a rocker. Thereafter, unbound antibodies were removed by washing the membrane in TBS-Tween thrice and incubating it with horseradish peroxidase-conjugated anti-rabbit-IgG secondary antibody (1:5000; Sigma) for 1 hour at RT. The second set of washes was performed in TBS-Tween three times before staining with the colorimetric TMB blotting solution. To quench the reaction and visualize protein bands, ultrapure (type 1) water was used and the PVDF membrane was captured on Gel Doc.

2.2.6 Labelling of SNAP-tag FP with BG-modified substrates

2.2.6.1 Labelling of SNAP-tag FP with BG-modified fluorophores

To confirm the functionality of the SNAP-tag domain, SNAP-FP were labelled with BG-modified fluorophores: BG-Alexa 488 (SNAP-tag functionality), and BG-Alexa 647 (Binding/Internalization assays). Purified SNAP-tag FPs were labelled with BG-Alexa Flour 488 (NEB) by following the manufacturer's protocol. Briefly, a 30 µl reaction mixture containing 1 mM DTT, 5 µM SNAP-tag purified protein and 15 µM (3-fold excess) BG-Alexa Flour 488/ BG-Alexa 647 in PBS was set up and incubated for 60 minutes at 37 °C in the dark (Table 2.15, Table 2.16). The unreacted SNAP-tag substrate was removed by using a Zeba™ Spin Desalting Column (7 kDa molecular weight cut-off) (Thermofischer Scientific) according to the manufacturer's instructions. Successful conjugation was confirmed by running samples on an SDS-PAGE gel and the detection of fluorescence signals on a transilluminator.

Table 2.15: Reaction mix for BG-Alexa 488 conjugation

Component	Final
DTT	1 mM
BG-Alexa 488	15 µM
SNAP-tag FP	5 µM
1xPBS	Adjusted to 30 µl

Table 2.16: Reaction mix for BG-Alexa 647 conjugation (binding/internalization)

Component	Final
DTT	1 mM
BG-Alexa 647	15 µM
SNAP-tag FP	5 µM
1xPBS	Adjusted to 30 µl
Volume of fluorescent protein prepared	1000 µl

2.2.6.2 Labelling of SNAP-tag FP with BG-modified Auristatin F

For the generation of an ADC, SNAP-tag FP was conjugated to a BG-modified Auristatin F (From Prof. Roger Hunter Group at University of Cape Town, South Africa). Briefly, a three-fold

molar excess of BG-modified Auristatin F was incubated with purified SNAP-tag FPs for 3 hours at 37°C. Afterwards, the complete saturation /labelling for ADC development was confirmed with a secondary label, BG-Alexa 488 conjugation (Table 2.17). After this, buffer-exchange was done to remove residual unbound fluorophores and the final construct was named, H22 (scFv)-SNAP-AURIF.

Table 2.17: Reaction mix for generation of ADC

Component	Final
DTT	1 mM
BG-AURIF	15 µM
BG-Alexa 488	5 µM
SNAP-tag FP	5 µM
1xPBS	adjusted to 30 µl
Volume of ADC prepared	1000 µl

2.2.6.3 Labelling of SNAP-tag FP with BG-modified IR700

For the generation of a PIC, SNAP-tag FP was conjugated to a photosensitiser (PS), BG-modified IR700 (from Prof. Matthias Peipp at the University of Kiel, Germany). Lyophilized BG-IR700 was solubilised in 50% DMSO, and purified H22 (scFv)-SNAP was incubated with a three-fold molar excess of BG-IR700 at room temperature in the dark for 2 hours. After labelling, the labelled protein was conjugated to BG-Alexa 488 to confirm complete saturation/labelling of PIC (Table 2.18), and afterwards buffer exchange was used to remove unbound IR700. The final construct was called H22 (scFv)-SNAP-IR700.

Table 2.18: Reaction mix for generation of PIC

Component	**Final**
DTT	1 mM
BG-IR700	15 µM
BG-Alexa 488	5 µM
SNAP-tag FP	5 µM
1xPBS	Adjusted to 30 µl
Volume of PIC prepared	1000 µl

2.2.7 Mammalian cells culturing

All cell lines (CD64+/CD64-) used in this study (Table 2.6) were cultured in a complete medium (RPMI 1640 or DMEM) supplemented with 10% (v/v) fetal bovine serum (FBS) (Gibco), 1% penicillin and streptomycin (Invitrogen). Cell cultures were placed in an Incubator and maintained under standard conditions (37°C, 100% humidity and 5% CO_2). Cell passaging was carried out twice a week for both adherent and suspension cells. Adherent cells were detached from the culture flask using 0.25% Trypsin-EDTA or Accutase solution before reaching confluency and suspension cells were maintained at a density below 1 x 10^6 cells/ml. The cell number was monitored using a T20 cell counter (Bio-Rad). Unless indicated otherwise, before any functional assay, both CD64 positive cell lines, HL60 and U937 cells were stimulated with 300 units (U)/ml and 500 U/ml of hIFN-γ for 24 hours respectively.

2.2.8 Preparation of polarized *ex vivo* differentiated hMDMs

Before the commencement of this study, the protocol was approved by the Human Research Ethics Committee (HREC/201/2023) of the University of Cape Town, South Africa. differentiated hMDMs are derived from peripheral blood mononuclear cells (PBMCs) isolated from blood buffy coats obtained from the Western Province Blood Transfusion Service (WPBTS), Cape Town, South Africa. Briefly, two blood buffy coats collected within 24 hours of donation from healthy male donors were transported on ice in a closed container under sterile conditions. The content of the buffy coat (approximately 50 ml each) was diluted equi-volumetrically with sterile PBS (without $MgCl_2$ and $CaCl_2$), and 25 ml of the resulting dilution was carefully layered on 15 ml of lymph prep density gradient (d = 1.077 g/ml, Axis-Shield). Following several slow-speed centrifugations (400 x g, 20 minutes, 26°C) and wash steps (200 x g, 8 minutes, 26°C), human peripheral blood mononuclear cells were isolated and cultured in plain RPMI 1640 for 3 – 4 h to select for monocytes by adherence. Non-adherent cells (e.g., B-and T-cells) were removed by four washing steps and the adherent cells were harvested by gentle scraping in a pre-warmed standard medium to allow seeding of appropriate cell numbers in 96- or 24-well assay plates. Afterwards, monocytes were cultured in an end-assay plate in fully supplemented RPMI media for 8 days to differentiate them into mature macrophages. At the end of day 8, macrophages were polarised into M1(IFN-γ/LPS) macrophages by incubation with 20 ng/ml IFN-γ (Peprotech) and 50 ng/ml LPS (Sigma) or M2(IL-4) macrophages using 20 ng/ml IL-4 (Peprotech) for 48 h. non-polarized cells were termed resting macrophages, M(0).

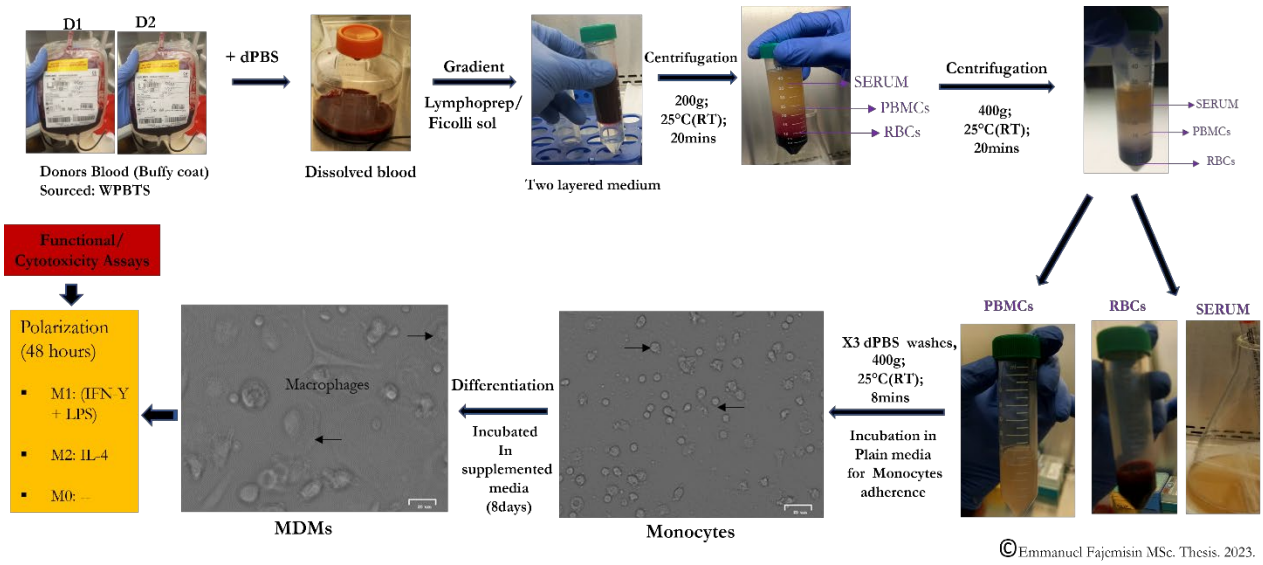

Figure 1.2. Schematic representation of the preparation of differentiated hMDMs. Abbreviation: differentiated hMDMs – Human Monocytes- derived macrophages, dPBS – Dulbecco Phosphate Buffer Saline, PBMCs - Peripheral Blood Mononuclear Cells, IFN-γ – Interferon Gamma, LPS – Lipopolysaccharide, IL-4 – Interleukin 4, RT = Room temperature

2.2.9 Flow cytometric analysis

2.2.9.1 Binding assay of anti-CD64 recombinant proteins

Flow cytometry was used to confirm the functional (binding) activities of anti-CD64 recombinant proteins to IFN-γ CD64+ monocytic cells and polarized differentiated hMDMs. Briefly, about 5 x 10^5 cells were suspended and incubated with 30 µg of each recombinant protein (SNAP-tag FP and rITs) for 1hour. The labelled cells were incubated in FACS buffer (PBS pH 7.4, 2 mM EDTA, 0.5% (w/v) BSA (Sigma)). Afterwards, a secondary antibody, anti-His PE or anti-His-Alexa647 was incubated with the cells for another 1 hour. Thereafter, double-stained cells were washed twice with PBS (pH 7.4), suspended in FACS buffer, and the binding acquired on a BD LSR-II flow cytometer (BD Biosciences). After acquisition, the results are analysed using the flow analysis (FlowJo) software.

2.2.9.2 Profiling of polarized *ex vivo* differentiated hMDMs

Flow cytometry (FC) analysis of cell surface receptors among the differentially polarized macrophage sub-types followed standard protocol. Briefly, 5 x 10^5 differentiated hMDMs were gently harvested from culture plates and washed twice in dPBS (pH 7.4) before incubation with markers (anti-human CD14, and anti-human CD206) for profiling pro- and anti-inflammatory macrophages. After 40 minutes, cells were washed twice and incubated with a secondary antibody, Goat anti-mouse IgG-Alexa 647 on ice for 1 hour. Before data acquisition by flow cytometric, the

cells were washed twice in ice-cold PBS and kept on ice in FACS tubes. The fluorescence was then acquired immediately using the BD LSR-II flow cytometer (BD Biosciences) and analysed using the flow analysis (FlowJo) software.

2.2.10 Confocal microscopy analysis of polarized *ex vivo* differentiated hMDMs

2.2.10.1 Cytoskeletal actin staining of polarized *ex vivo* differentiated hMDMs

Differentiated hMDMs were cultured and polarized to different macrophage sub-types on glass coverslips in a 96-well tissue culture plate. The differentiated hMDMs were fixed in 4% Paraformaldehyde (PFA) for 15 minutes and afterwards permeabilised with 0.1% Triton X-100 for 15 mins. Afterwards, the cells were washed twice with PBS and cytoskeletal actin stained with FITC-phalloidin (1:500 in PBS for 30 minutes). Afterwards, the cell nuclei were counterstained with DAPI (1:5000 in PBS for 15 minutes). A drop of mowiol (plus antifade) was added to the middle of each coverslip before mounting it on a microscopic slide.

2.2.10.2 Internalization studies of SNAP-FP on polarized *ex vivo* macrophages

Confocal microscopy was used to analyse the internalization of labelled SNAP-tag FP, H22(scFv)-SNAP-Alexa647 on polarized *ex vivo* macrophages. Briefly, each polarized macrophage, M(0)(resting), M1(IFN-γ + LPS) and M2(IL-4) were washed twice with dPBS (without $MgCl_2$ and $CaCl_2$) and fixed with 2% PFA on ice for 15 minutes. Next, 0.5% Trixton X was incubated with macrophages for 20 minutes to permeabilize cells. Afterwards, 1 μM of H22(scFv)-SNAP-Alexa 647, was incubated with macrophages for 60 minutes under cold conditions and washed off with dPBS. Finally, the cells are labelled with phalloidin actin (1:500 in PBS for 30 minutes) and DAPI/Hoest (1:5000 in PBS for 15 minutes), including the single stain controls (unstained, phalloidin actin and alexa647 alone) at RT, and resuspended in dPBS before visualization on the Zeiss LSM 880 confocal microscope (Zeiss).

2.2.11 ADP-ribosylation (enzymatic) assay of rITs

rITs induce cell death by mediating ADP-ribosylation of EF2 which subsequently stops protein synthesis. To compare the enzymatic activity of rITs, H22(scFv)-ETA` and its deimmunized variant, H22(scFv)-dETA`(RG7787-MT2); the ADP-ribosylation assay was used as previously described [162, 163]. Briefly, 100 nM of each rIT (H22(scFv)-ETA` and H22(scFv)-dETA`(RG7787-MT2)) was incubated with wheat germ extract (Promega) and 50 nM biotinylated NAD+ (R&D systems, USA) in 20 mM Tris-HCl buffer (pH 7.4) containing 1 mM EDTA and 1 mM DTT at 37 °C for 1 hour. Afterwards, the reaction was quenched by SDS-PAGE sample

.[63].

buffer. The biotinylated EF2 was detected by WB (section 2.2.5.2) using a streptavidin HRP conjugate (Thermofischer Scientific) as the detection probe, and the bands extrapolated with ImageJ software.

2.2.12 Cytotoxicity studies

2.2.12.1 Cell viability (XTT) studies

The XTT cell viability assay is a colorimetric cell assay that quantifies metabolic /cellular viability by the reduction of the XTT reagent to an orange water-soluble formazan dye that absorbs light at 450 nm. The cell viability assay is used to access the cytotoxic killing of anti-CD64 rITs and ADC towards CD64+ monocytic cells and *ex vivo* macrophages. For rITs, H22(scFv)-ETA`, and H22(scFv)-dETA`(RG7787-MT2), 100 nM of protein was used as starting cytotoxic concentration. Before treatment, CD64 + cells (U937 and HL60) are seeded into 96 well plates, with 5 x 10^3 cells per well and stimulated with IFN-γ. In a like manner, the same seeding set up was implemented with evaluation of ADC. 500 nM of H22(scFv)-SNAP-AURIF was used as a starting concentration towards IFN-γ stimulated and unstimulated CD64+ monocytic cells. A2058 was used as a negative control. The 50% Inhibitory concentration on cells (IC_{50}) was calculated by normalizing data to untreated control (0%) and zeocin control (100%) using the GraphPad Prism v10.0 software.

2.2.12.2 Photoimmunotoxicity studies of H22(scFv)-SNAP-IR700

To evaluate the toxicity profile of H22(scFv)-SNAP-IR700 mediated near-infrared photoimmunotherapy (NIR-PIT) on polarized *ex vivo* differentiated hMDMs, cell viability assay was used (2.2.12.1). Briefly, polarized differentiated hMDMs: M1(IFN-γ +LPS), M2(IL-4) and M(0) (resting) macrophages were treated with three different doses (– 500 nM, 100 nM and 20 nM) of H22(scFv)-SNAP-IR700, and incubated for 3 hours at 37°C, 5% CO_2 Incubator. After incubation, cells are washed with sterile dPBS (without $MgCl_2$ and $CaCl_2$) and irradiated for 15 minutes. After irradiation, cells are washed with sterile dPBS and replaced with sterile RPMI media for 48 hours after which XTT reagents are added to evaluate dose-dependent killing.

2.2.13 Statistical analysis

GraphPad Prism v10.0 software was used for statistical analysis in this thesis. Data were expressed as mean ± standard error of mean (SEM) unless otherwise indicated. The cytotoxicity, IC_{50} values evaluated was specified within [90-95 %] Confidence Intervals (CIs). Also, graphical analysis for phototoxicity was evaluated with one-way analysis of variance (ANOVA) to test significant

differences in means of PIC doses (>2), and student parametric (t-test) to compare significance difference in mean between the lowest doses vs untreated samples.

|CHAPTER 3: RESULTS|

CD64 (FcγRI) exhibits overexpression on activated monocytes and dysfunctional macrophages, which play a key role in the pathogenesis of chronic skin inflammatory diseases such as atopic dermatitis (AD) and haematological cancers like monocyte-derived leukemia (e.g., AML). Consequently, the development of immunotherapeutics targeting CD64 offer potential for effective therapy against these chronic diseases compared to conventional non-targeted treatments. In this thesis, four CD64-targeting immunotherapeutics were evaluated for their therapeutic potentials. They include: (1) Recombinant immunotoxin (rIT), H22(scFv)-ETA`; (2) Deimmunized recombinant immunotoxin (d-rIT), H22(scFv)-dETA`(RG7887 (R456T)-R490A/ (RG7787-MT2) (3) SNAP-tag antibody drug conjugate (ADC), H22(scFv)-SNAP-AURIF and (4) SNAP-tag Photoimmunoconjugate (PIC), H22(scFv)-SNAP-IR700.

3.1 In silico cloning of expression vectors for anti-CD64 recombinant proteins

The insilico cloning (and optimization) of expression vectors was done using snapgene ® software. The expression construct H22(scFv)-ETA` was a pMT-plasmid vector which allows for recombinant protein expression in bacteria host, *E. coli* while SNAP-tag FP, H22(scFv)-SNAP was a pCB- plasmid vector which allows for recombinant protein expression in mammalian cells, HEK293T cells (2.2.1). The pMT-H22(scFv)- ETA` contains 7474 bp of nucleotides while the pCB-H22(scFv)-SNAP contains 8026 bp of nucleotides. To prevent premature termination of protein expression, the absence of stop codon (TGA, TAA) within the ORFs was confirmed .The plasmid maps of both pMT-H22(scFv)-ETA` and pCB-H22(scFv)-SNAP with essential ORF features and restriction enzymes sites (*SfiI, NotI and BlpI*) flanking the genes endocing the fusion proteins are summarized below (Figure 3.1 A and B).

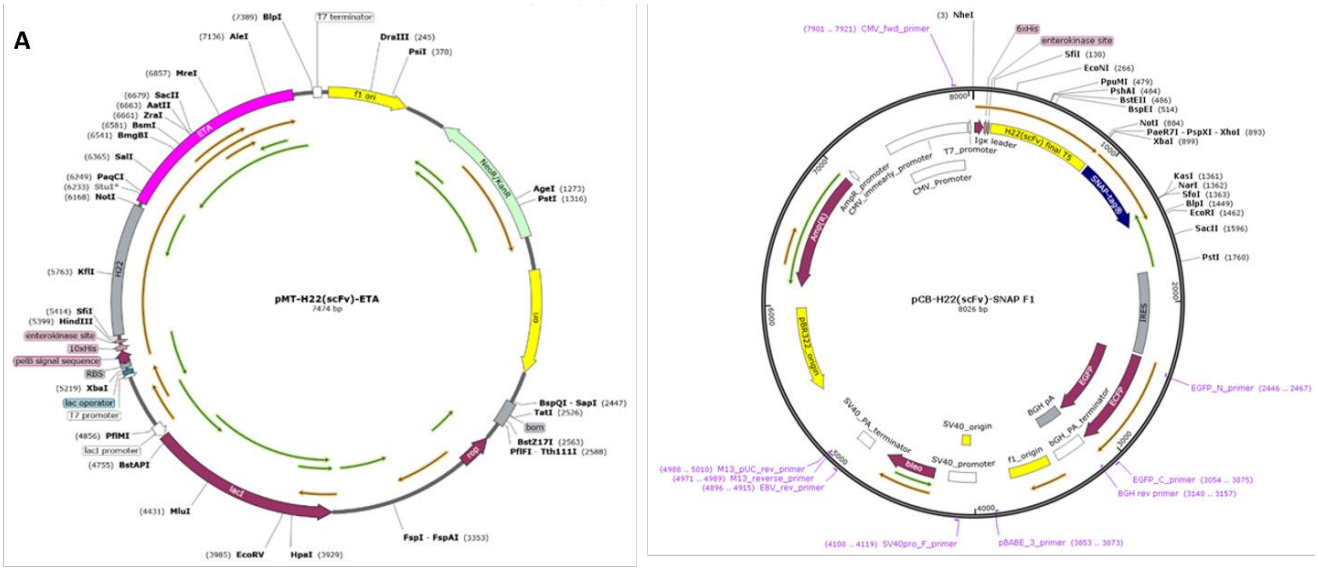

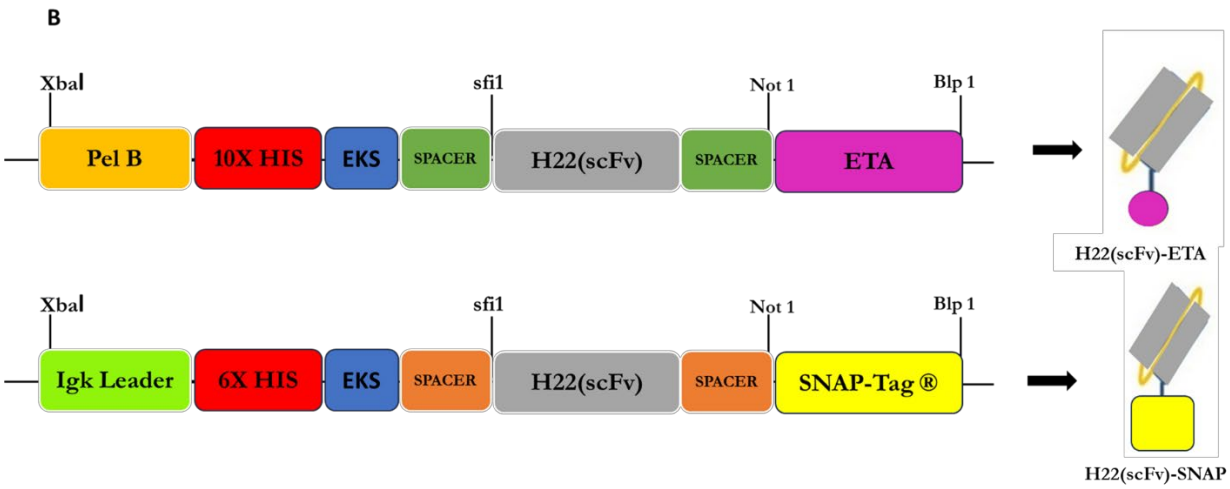

**Figure 3.1. *Insilico* design of expression vectors for production of recombinant immunotoxin (rIT), H22(scFv)-ETA` and SNAP-tag FP, H22(scFv)-SNAP.** (A) Plasmid map representation of pMT-H22(scFv)-ETA` (7474bp) for bacterial expression of rIT and pCB-H22(scFv)-SNAP (8026 bp) for mammalian expression of SNAP-tag FP. The maps are exported from snapgene ® software (B) Open reading frame (ORF) of pMT-H22(scFv)-ETA` with 10xhis-tag and PelB signal peptide to initiate rIT production, and pCB-H22(scFv)-SNAP with 6xhis-tag and IgK leader sequence to initiate SNAP-FP production. The H22(scFv) is flanked by *SfiI* and *NotI* restriction sites, and the ETA` and SNAP fragment is flanked by *NotI* and *BlpI* restriction sites.

3.2 Molecular cloning of anti-CD64 plasmid constructs

3.2.1 Plasmid isolation and quantification of pMT-H22(scFv)-ETA`

The glycerol stocks of pMT-H22(scFv)-ETA` in *E. coli* DH5α cells (- 1 ml) was thawed into 50 ml of LB medium and grown overnight (for 16 hours) in a shaking incubator at (200 rpm, 37°C) (2.2.2.1). Afterwards, the bacterial culture was pelleted, and DNA was isolated and purified with Nucleobond ® extraction (2.2.2.2). A high concentration and purified plasmid DNA were obtained (Table 3.1) for downstream molecular cloning.

Table 3.1. Quantification of purified pMT-H22(scFv)-ETA`

pMT-H22(scFv)-ETA`	Conc (ng/ul)	A260/A280	A230/A260
A	15422.653	2.05	2.62

3.2.2 Restriction digest of pMT-H22(scFv)-ETA` and pUC57-dETA`(RG7787-MT2)

Restriction digest was conducted to replace the ETA` the pMT-H22(scFv)- ETA` vector with its deimmunized varaint, dETA`(RG7787-MT2) to generate an expression vector encoding the drimmunized recombinant immuntoxin, pMT-H22(scFv)-dETA` (RG7787-MT2). A double restriction digest was performed on the plasmids DNA of pMT-H22(scFv)-ETA` and pUC57-dETA` construct (RG7787(R456T)-490A) using *NotI* and *BlpI* restriction endonucleases (2.2.2.4) to generate recombinant deimmunized immunotoxin plasmid, pMT-H22(scFv)-dETA`(RG7787-MT2) (Figure 3.2). is showing the cloning process. After restriction digest, a 1.2% agarose gel electrophoresis was prepared to separate out the restriction digest products. The gel image (Figure 3.3) showed successful cleavage of plasmid DNA of the insert, dETA`(RG7787-MT2) at 1221bp and vector backbone, pMT-H22(scFv) at 6253 bp using the DNA ladder (NEB) as reference. Next, each fragment was excised from the gel, and purified for ligation.

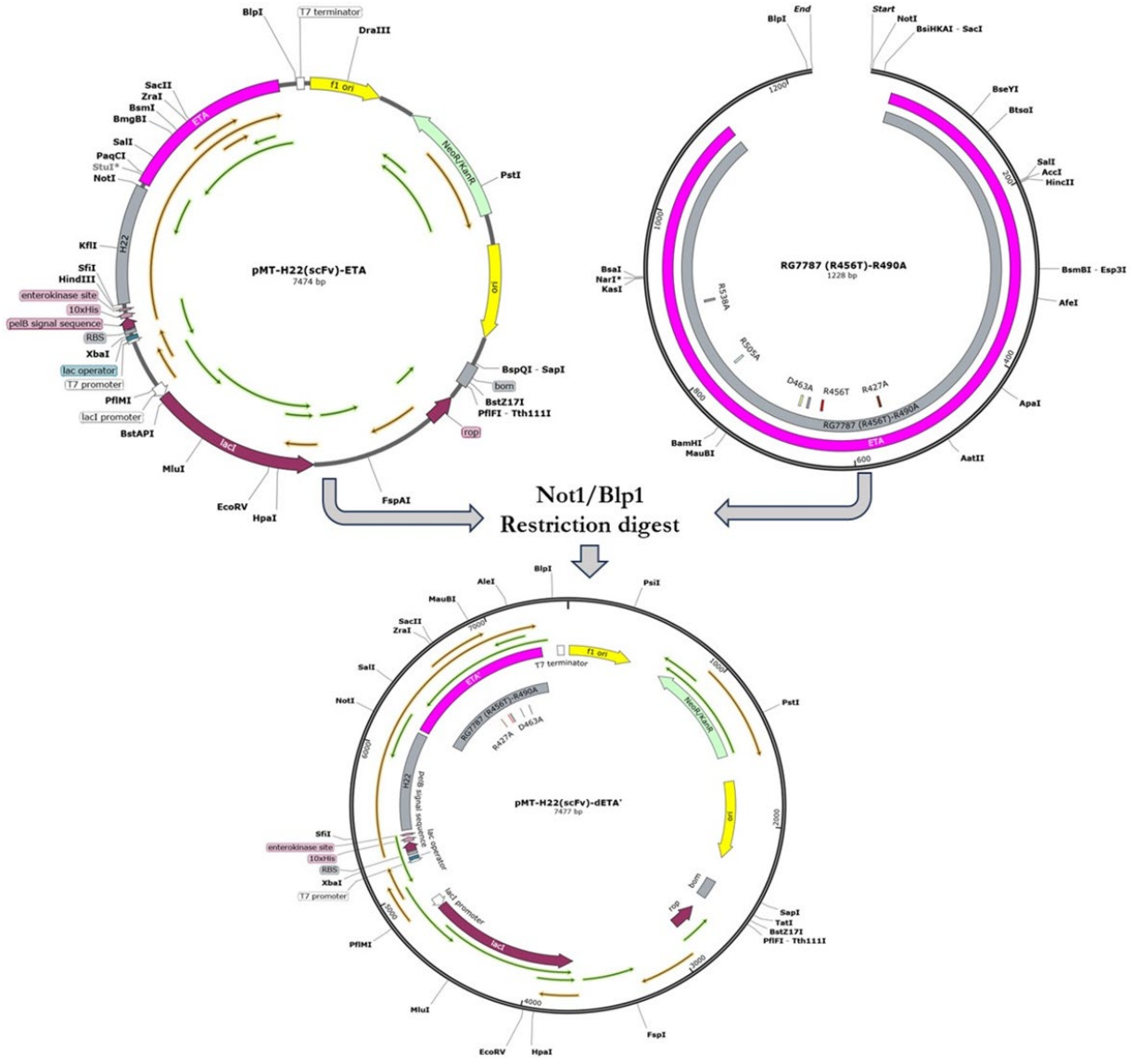

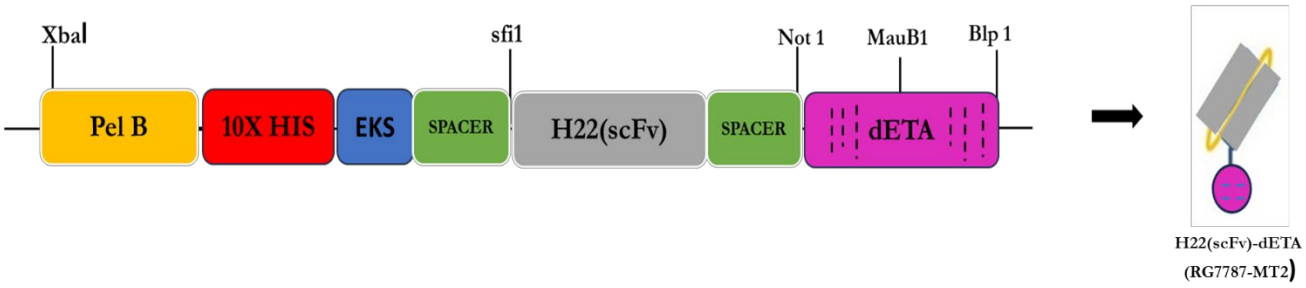

Figure 3.2. Plasmid map showing the molecular cloning of pMT-H22(scFv)-ETA` and pUC57-dETA`(RG7787-MT2). The dETA`(RG7787-MT2) fragment was inserted into the pMT-H22(scFv) backbone successfully using restriction endonucleases *NotI* and *BlpI* to generate pMT-H22(scFv)-dETA`(RG7787-MT2).

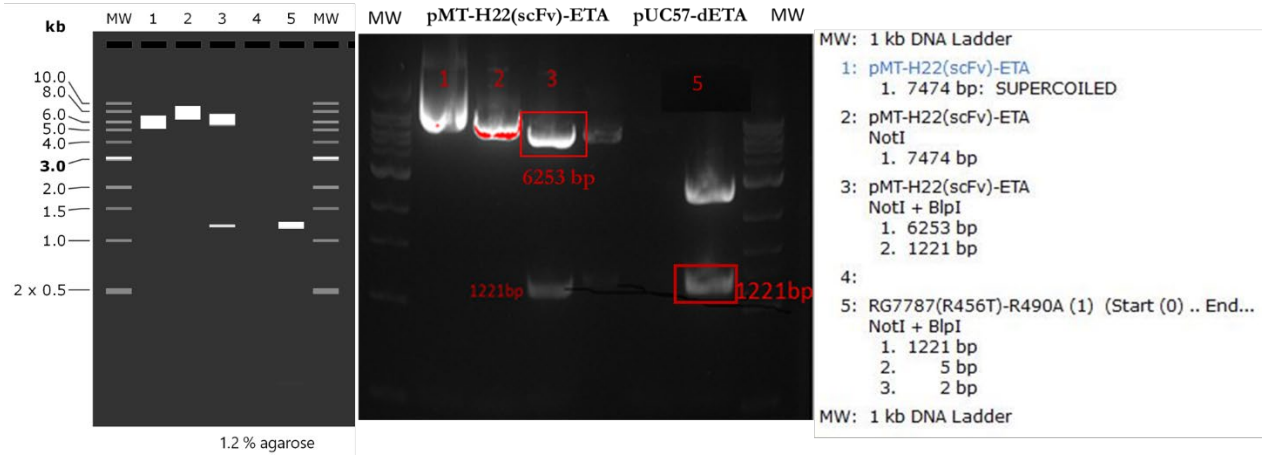

Figure 3.3. Agarose gel of restriction digest product of pMT-H22(scFv)-ETA` and pUC57-dETA` (RG7787-MT2). 1=undigested control pMT-H22(scFv)-ETA`, 2 = single digest (*NotI*) of pMT-H22(scFv)-ETA`, 3 = double digest (*NotI* + *BlpI*) of pMT-H22(scFv)-ETA`, 5 = double digest (*Not I*+ *BlpI*) of pUC57-dETA` (RG7787-MT2).

3.2.3 T4 Ligation of pMT-H22(scFv) backbone and dETA`(RG7787-MT2) fragments

The pMT-H22(scFv) backbone (6253bp) and dETA`(RG7787-MT2) (1221 bp) insert fragments from the agarose gel (Figure 3.3) were excised, purified, and ligated using the T4 DNA ligase enzyme. This resulted in the generation of pMT-H22(scFv)-dETA`(RG7787-MT2). Three different backbones to insert ratios (1:1, 1:3, 1:5) was used to increase the chances of successful ligation outcome (2.2.2.6). The ligated product was afterward transformed into chemically competent *E. coli* DH5α cells and cultured on a kanamycin resistant LB agar plate for selective growth of true transformants. The result below (Figure 3.4) shows successful growth of bacterial colonies in the ligation plates and corresponding transfection efficiency as against negligible

control plate. Next, Bacterial colonies were selected from the ligated plates (1:1, 1:3, 1:5), and cultured in LB broth, to extra DNA for downstream processing and restriction mapping.

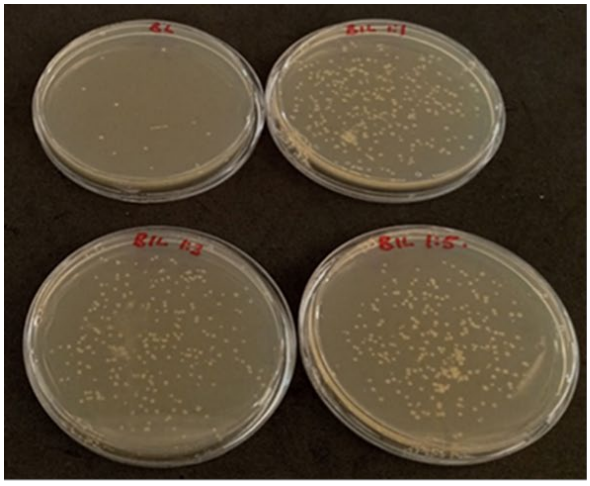

Ligation ratio (Backbone : Insert)	Transformation Efficiency (cfu/ug)
BL (1:0)	--
BIL (1:1)	8.9 X 10^3
BIL (1:3)	1.01 X 10^4
BIL (1:5)	9.1 X 10^3

Figure 3.4. Image of *E. coli* colonies potentially transformed with pMT-H22(scFv)-dETA`(RG7787-MT2) and corresponding transformation efficiency (cfu/ug) after T4 ligation. BL plate: backbone with T4 ligase without insert, BIL plate: backbone with insert and T4 ligase.

3.2.4 Restriction mapping of pMT-H22(scFv)-ETA` and pMT-(H22(scFv)-dETA`(RG7787-MT2)

Single colonies were picked from ligated plates (1:1, 1:3, 1:5) from (Figure 3.4) and cultured in LB broth for 16 hours. Next, plasmids were extracted and purified for restriction mapping. To confirm successful ligation for generation of pMT-H22(scFv)-dETA`(RG7787-MT2), the plasmids extracted in duplicates were compared with pMT-H22(scFv)-ETA` (source plasmid) in a double restriction digest using *MauBI* and *NotI* restriction endonucleases. (2.2.2.7), and the restriction products were resolved on 1.2% Agarose gel. The gel result below (Figure 3.5) shows distinct difference between double digested (*NotI* + *MauBI*) pMT-H22(scFv)-ETA` yielding DNA band size at 642 bp and pMT-H22(scFv)-dETA`(RG7787-MT2) band size at 740 bp. Extracted DNA ligated in the ratio(1:l a; b, 1:3 a; b, 1:5 a; b), which confirms successful ligation and generation of pMT-H22(scFv)-dETA`(RG7787-MT2) as seen in Figure 3.4.

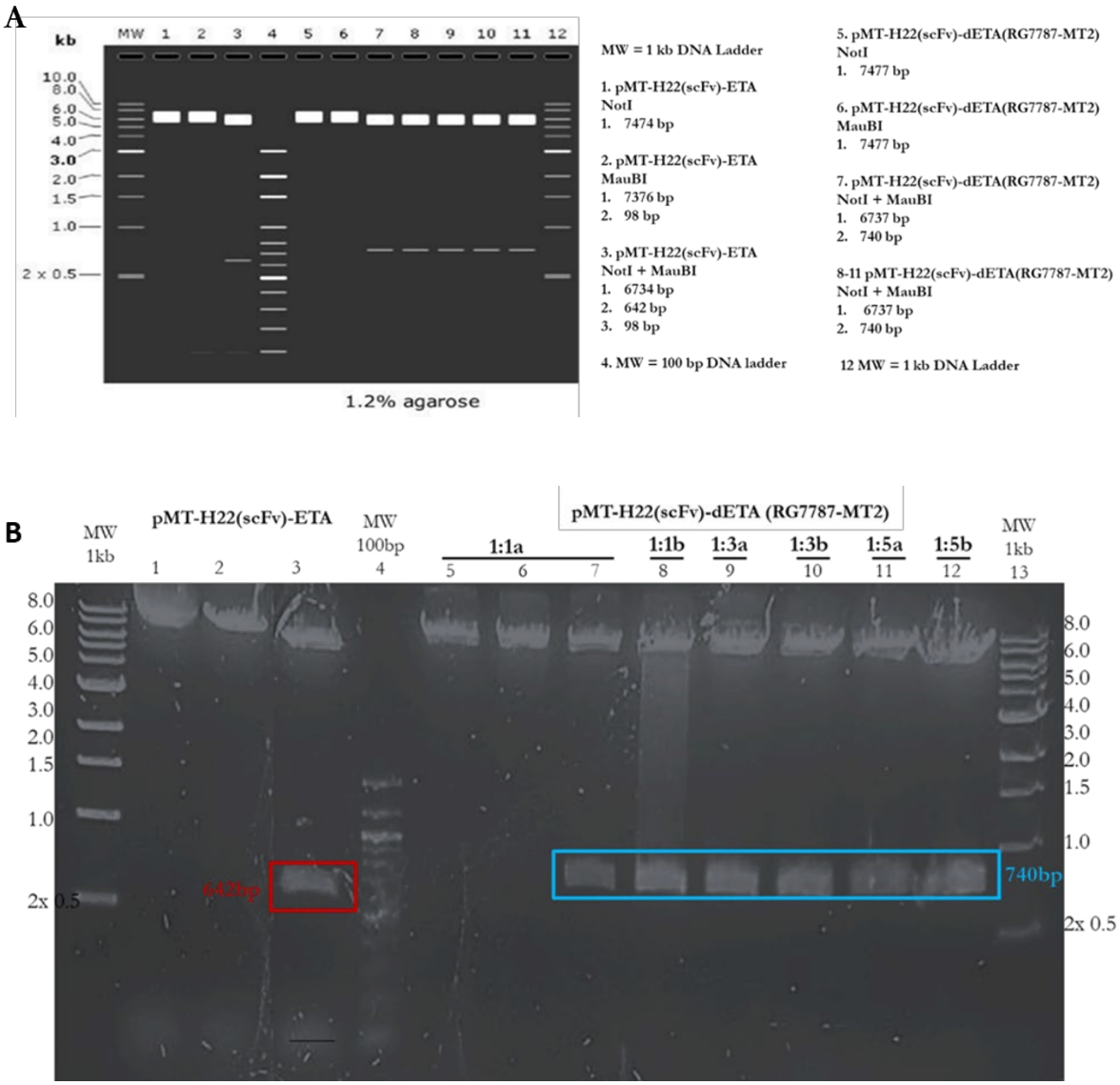

**Figure 3.5 (A-B). Restriction mapping analysis of pMT-H22(scFv)-dETA`(RG7787-MT2).** Recombinant pMT-H22(scFv)-ETA`, and pMT-H22(scFv)-dETA`(RG7787-MT2) clones were restricted with *MauBI*, and *NotI*. The double digested plasmid shows a restriction difference for pMT-H22(scFv)-ETA` (lane 3) (642 bp), compared to pMT-H22(scFv)-dETA`(RG7787-MT2) (lanes 7-12) (740 bp)(3.5B). This difference was also comparable with the insilico simulation of the restriction mapping (3.5A) performed on the snapgene ® software.

3.3 Production of anti-CD64 recombinant proteins

Two host of expression systems were used for production of anti-CD64 recombinant proteins: (i) Bacteria (*E.coli* BL21(DE3)) for production of rITs, and (ii) Mammalian human embryonic kidney (HEK293T) cells for production of SNAP-tag FP.

3.3.1 Expression and characterization of anti-CD64 rITs

The compatible solute stress expression protocol [151] was used for production of anti-CD64 rITs, H22(scFv)-ETA` and H22(scFv)-dETA`(RG7787-MT2) in *E. coli* BL21(DE3) cells. The expressed proteins are transported to the periplasmic space to allow for proper folding and prevention from cytosolic protease degradtion (2.2.2.1). Bacterial pellets of biomass 20 - 25 g were successfully retrieved per liter. Bacteria pellets were thawed in lysis buffer and lysed with a sonicator before clarification by centrifugation. Two IMAC purification were performed according to profile steps (Table 2.13 -Table 2.14) to purify recombiant proteins, forming single protein peaks. As seen in figure 3.6 A (I – II), full-length rITs, H22(scFv)-ETA` and H22(scFv)-dETA`(RG7787-MT2) was present on SDS-PAGE gel run after the two-IMAC purification steps and corresponded to theoretical molecular weights of 72.5 kDa. As observed on gel, , H22(scFv)-ETA` is indicated by (red arrow) with single bands, at 72.5 kDa while H22(scFv)-dETA`(RG7787-MT2) is indicated by (black arrow) with double bands, at 72.5 kDa. Furthermore, to improve protein purity after IMAC, SEC was done (2.2.4.3). The SEC results showed improved protein purity (clear bands) for both rITs compared to IMAC results (Figure 3.6 B and C). Also, The presence of poly histidine-tagged proteins was confirmed in SEC purified proteins by anti-histag antibody-based immunoblotting procedure and the results showed both H22(scFv)-ETA` and H22(scFv)-dETA`(RG7787-MT2) present (at 72.5 kDa) as recombinant proteins observed on the blot membranes (Figure 3.6 B and D). Finally, the recovered yield of H22(scFv)-ETA` was 1.184 mg/L while H22(scFv)-dETA`(RG7787-MT2) yield of 1.05 mg/L from standard lab shaking culture flasks. The recovered purified proteins were stored at 4°C and used for downstream functional studies.

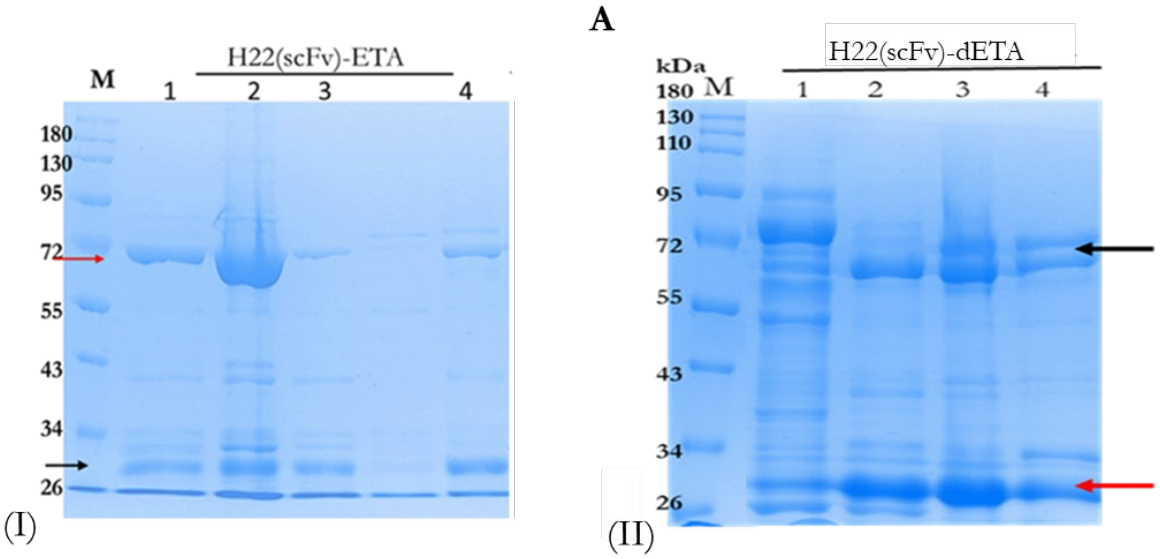

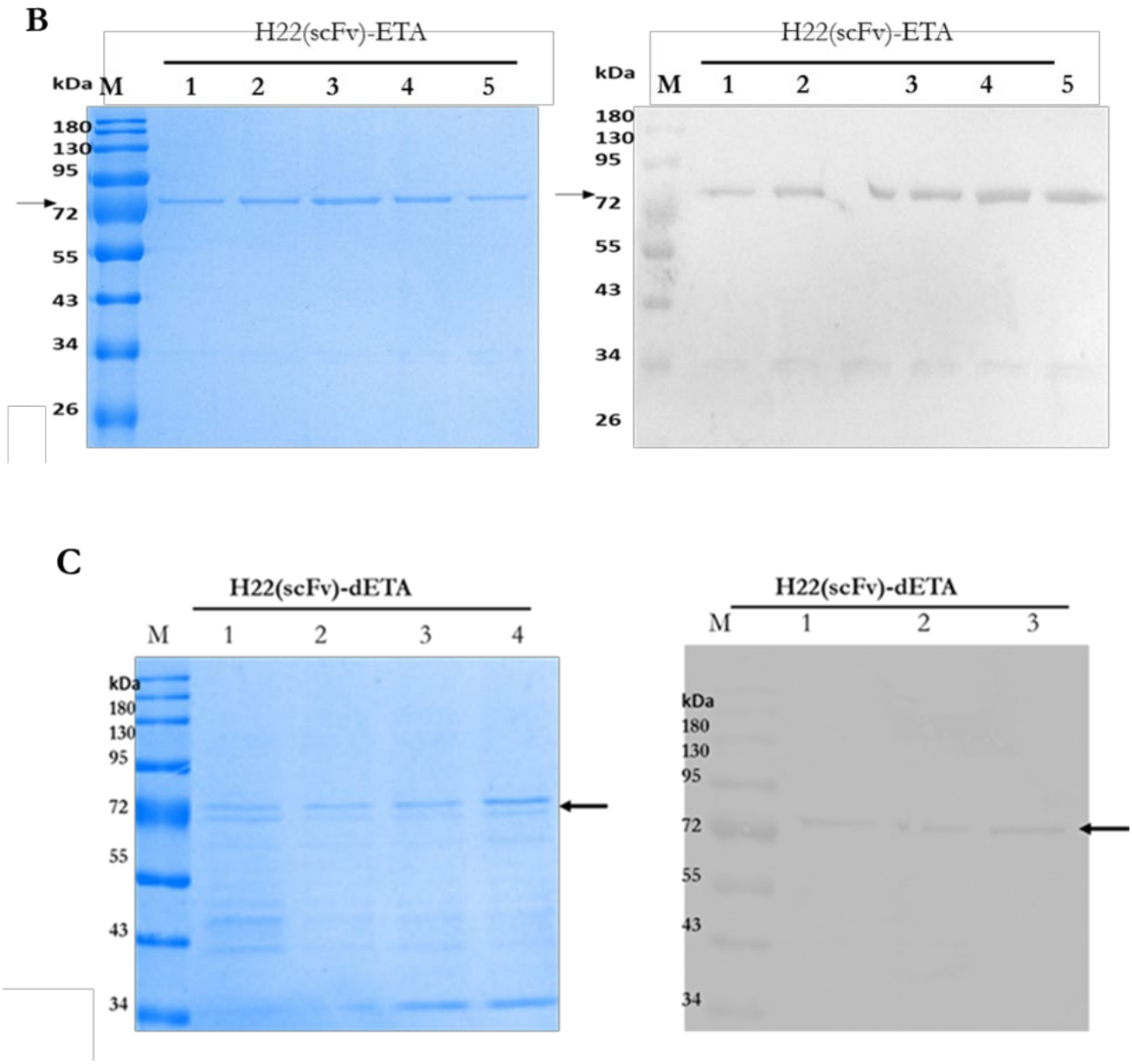

Figure 3.6 Expression and characterization of anti-CD64 rITs.

(A) SDS-PAGE gel analysis of H22(scFv)-ETA` (I) and H22(scFv)-dETA`(RG7787-MT2) (II) after after 2nd IMAC. The full-length protein was present at 72.5 kDa. To improve protein purity of rITs, SEC was used for purification (B and C)) SDS-PAGE and Western blot analysis of H22(scFv)-ETA`and H22(scFv)-dETA`(RG7787-MT2) after SEC. The full-length poly his-tagged protein of anti-CD64 rITs was present at 72.5 kDa on the SDS-PAGE gel and further confirmed with immunoblot (signal: black arrow).

3.3.2.1 Mammalian transfection and expression of H22(scFv)-SNAP

Recombinant SNAP-FP was expressed and produced in HEK 293T cells (2.2.3.2). Transfected cells were selected by Zeocin from untransfected ones. Figure 3.7 showed increasing eGFP fluorescence and gradual expression of H22(scFv)-SNAP plasmid DNA in HEK293T cells over 96 hours. Transfection efficiency via flow cytometric analysis was conducted to quantify successful transfected cells for production of SNAP-tag. According to literature a good chemical transfection efficiencies are to be expected between 60 – 80%, which has been confirmed in my experiments (60%, 75%) (Figure 3.8). Next, Zeocin (1mg/ml) was supplemented to RPMI to deplete non-transfected from successfully transfected cells. Finally, CCSN containing SNAP-tag FP was collected and temporarily stored for purification. Figure 3.9 shows the representative images of each step of CCSN collection. Images were taken 2 months post-transfection. A total of 2.5 liters of CCSN containing H22(scFv)-SNAP was collected over three months period.

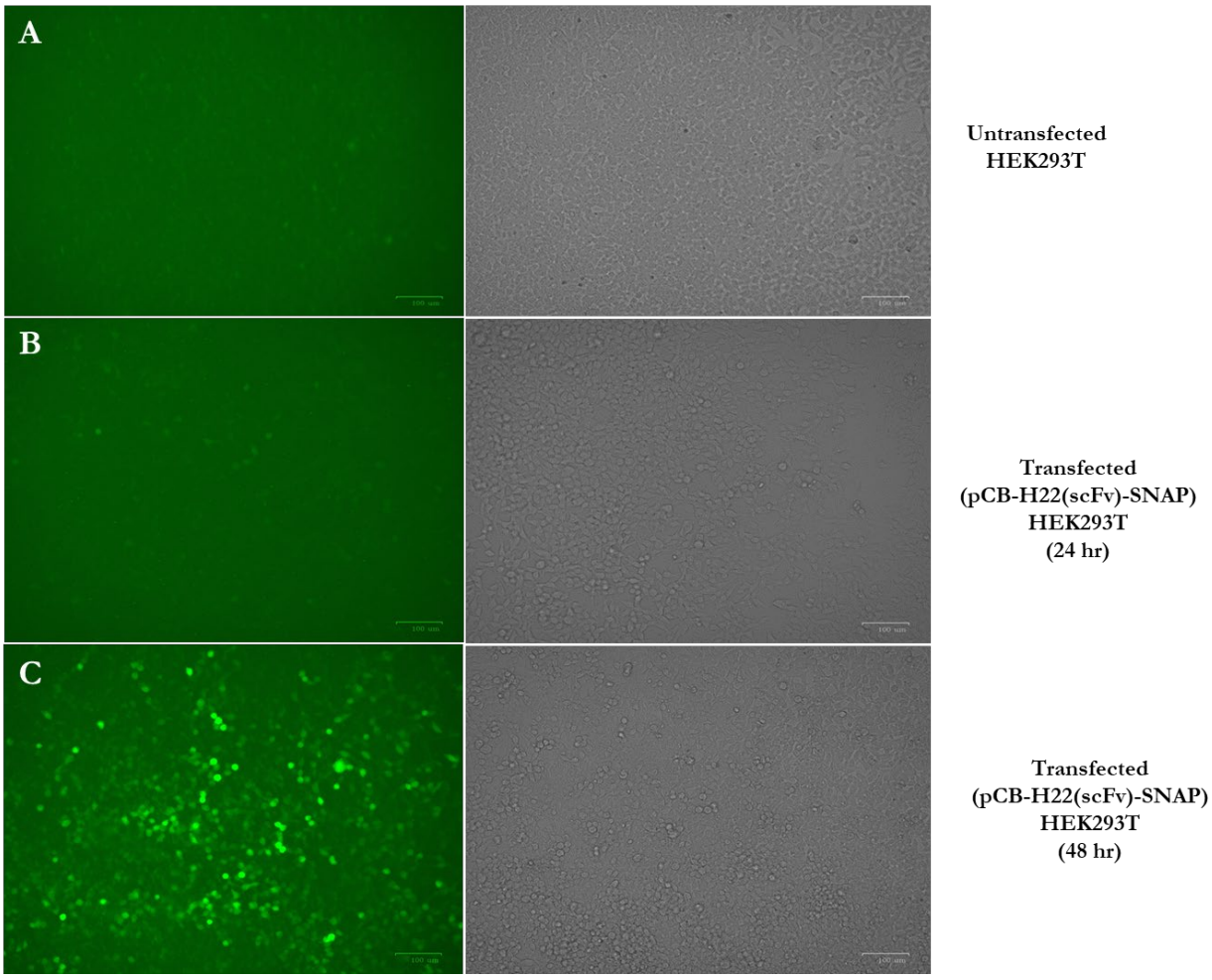

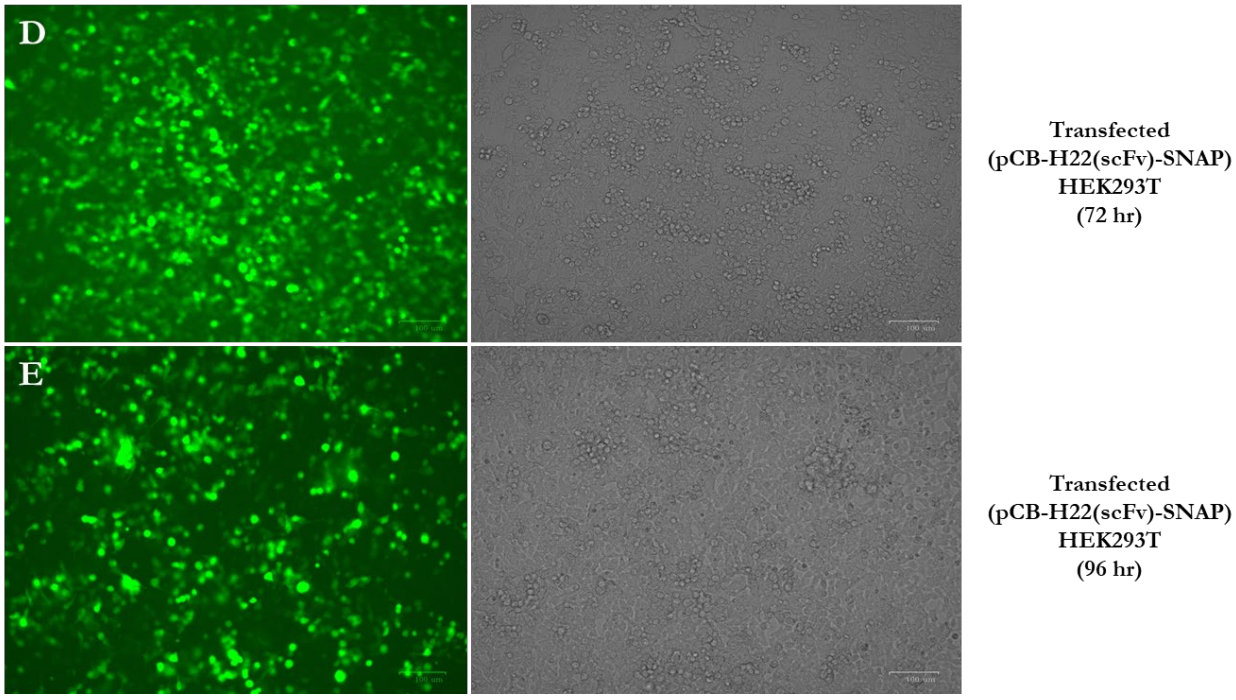

Figure 3.7. Microscopic images (A-E) showing eGFP fluorescence of transfected pCB-H22(scFv)-SNAP in HEK293T cells. A gradual increase in eGFP fluorescence was observed in transfected HEK293T cells over 96 hours evaluation, and the transfection eficiency was confirmed afterwards with flow cytometric analysis.

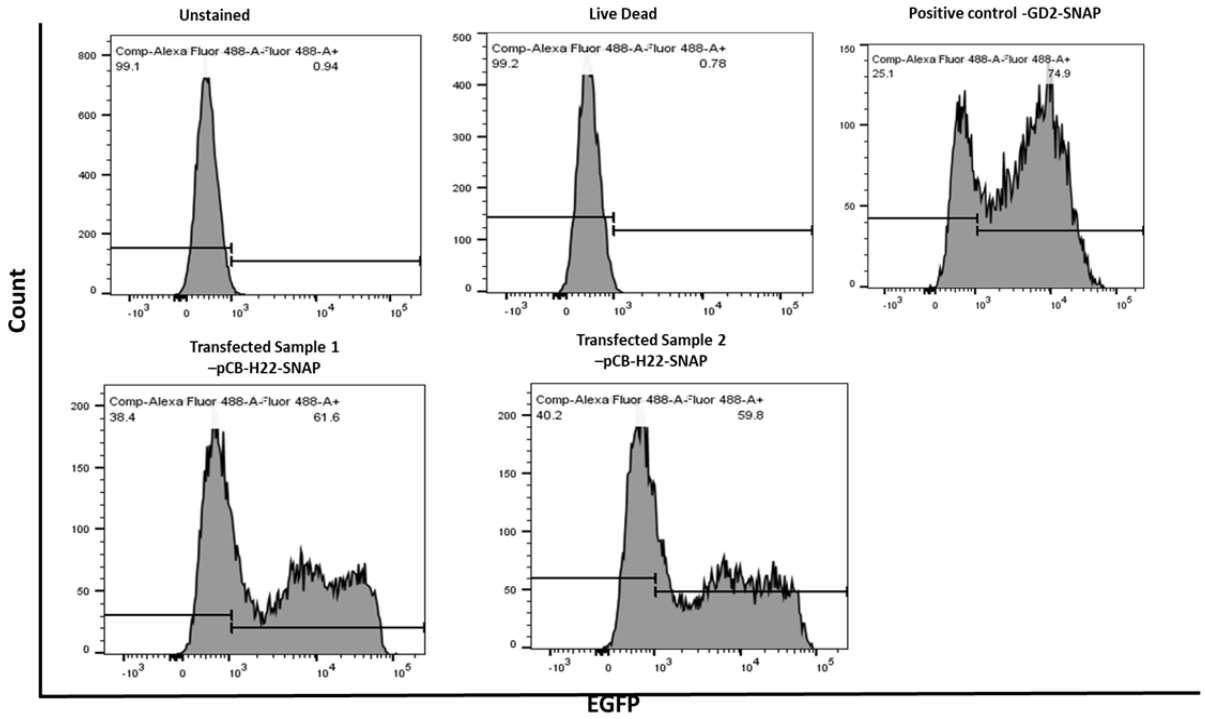

Figure 3.8. Transfection efficiency results of pCB-H22(scFv)-SNAP in mammalian

HEK293T cells by flow cytometric analysis. The results indicate good transfection efficiency of ~ 60%, comparable to good transfection efficency using transfected controls (60-80%).

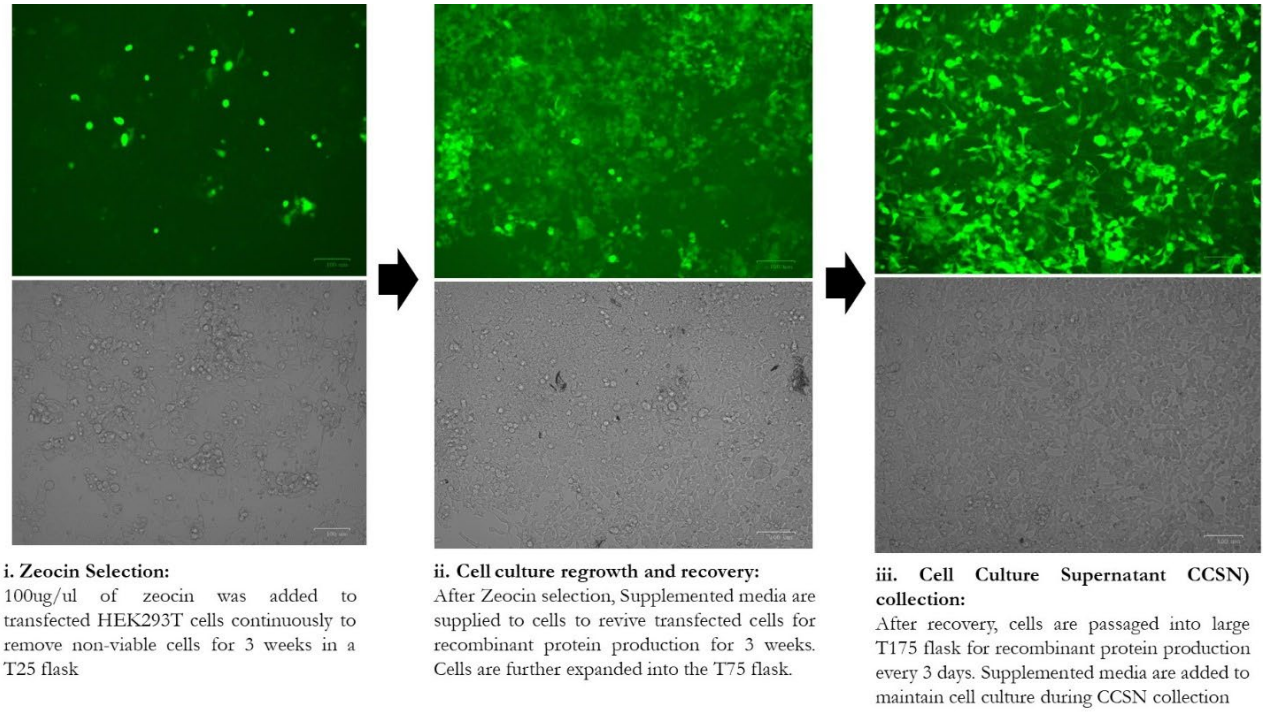

i. Zeocin Selection:
100ug/ul of zeocin was added to transfected HEK293T cells continuously to remove non-viable cells for 3 weeks in a T25 flask

ii. Cell culture regrowth and recovery:
After Zeocin selection, Supplemented media are supplied to cells to revive transfected cells for recombinant protein production for 3 weeks. Cells are further expanded into the T75 flask.

iii. Cell Culture Supernatant CCSN) collection:
After recovery, cells are passaged into large T175 flask for recombinant protein production every 3 days. Supplemented media are added to maintain cell culture during CCSN collection

Figure 3.9. Zeocin selection, culture regrowth and enrichment, and mammalian protein expression of SNAP-tag FP in HEK293T cells. CCSN – Cell culture supernatant containing secreted SNAP-tag FPs are collected and store temporarily for IMAC purification.

3.3.2.2. Purification and characterization of H22(scFv)-SNAP FP

A single purification of mammalian CCSN containing H22 (scFv)-SNAP (2.2.4.2) was done using IMAC based on profile steps in Table 2.14, with ptotein forming double peaks (1,2). After IMAC, protein was characterized using SDS-PAGE (2.2.5.1) and Western Blot (2.2.5.2). As documented below in Figure 3.10A (i and ii), the full-length H22(scFv)-SNAP was present and confirmed in both peaks (1,2) with protein band size at ~ 53 kDa on both the SDS gel and WB. To confirm the functionality of the SNAP-tag domain, a flourescently labelled SNAP-tag substrate (BG-Alexa 488) was conjugated to H22(scFv)-SNAP (Table 2.5) under standard conditions (2.2.6.1). The result (Figure 3.10 B) demonstrate successful conjugation of BG-Alexa 488 to H22(scFv)-SNAP samples (1-6) indicative of the bright green fluorescence at ~53 kDa. Lastly, the total yield of 1.77 mg/L of CCSN containg H22(scFv)-SNAP from culture flasks was retrieved. The recovered proteins are stored at 4°C and used for downstream binding and cytotoxicity assays.

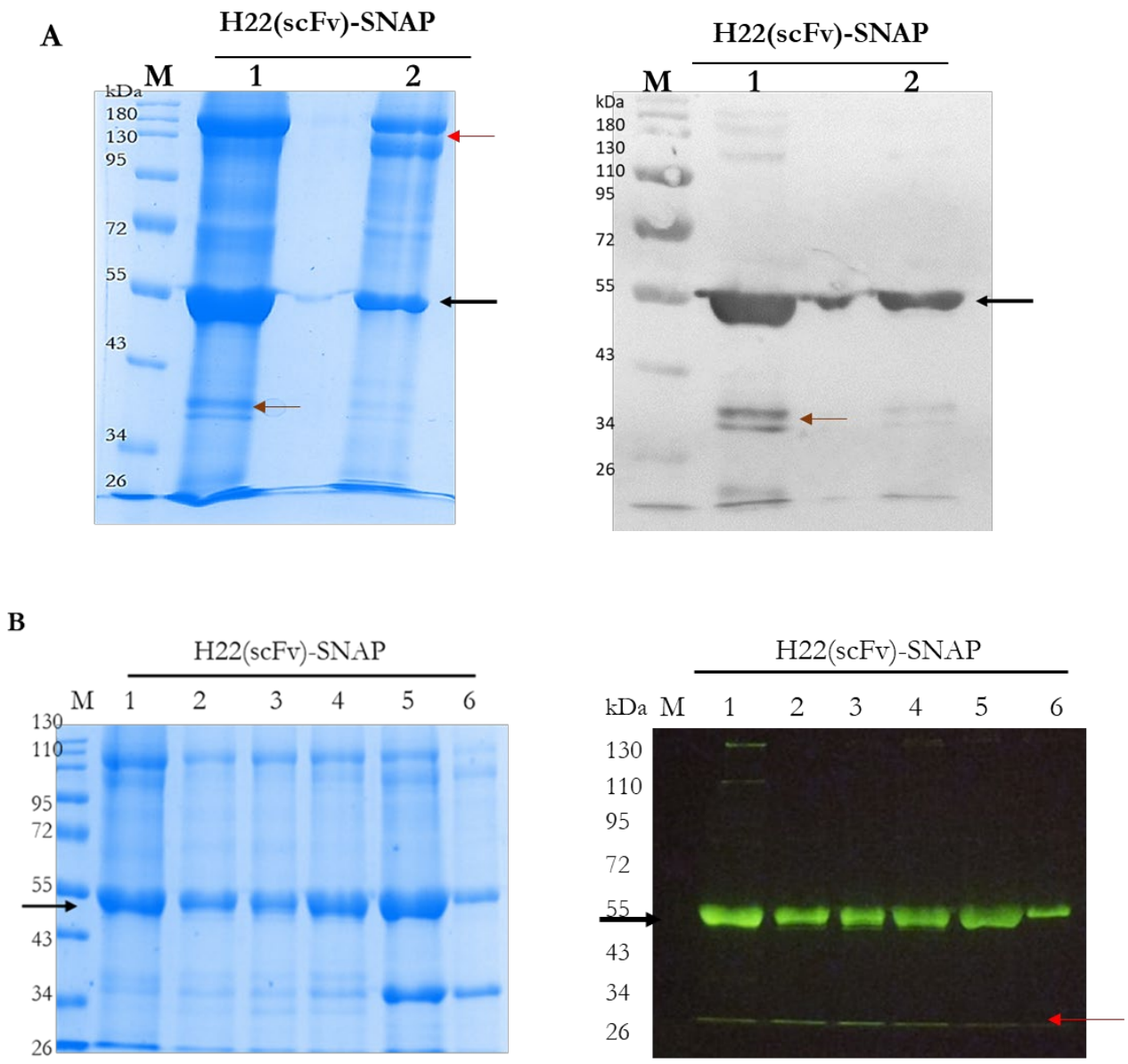

Figure 3.10 Purification and characterization of SNAP-tag FP, H22(scFv)-SNAP.

(A) SDS-PAGE and Western blot analysis of H22(scFv)-SNAP after IMAC. The full-length polyhis-tagged protein H22(scFv)-SNAP was present at ~ 53 kDa on the SDS gel and further confirmed with immunoblot. Other proteins or contaminating bands are indicated by red (~130 kDa) and brown arrows (~34 kDa) (B) Successful BG-Alexa 488 conjugation to H22(scFv)-SNAP fusion proteins samples confirms the functionality of the SNAP-tag domain of the fusion proteins as inidcated by the green fluorescence taken on a DR-89x Transilliminator (Clare chemical research, Germany). The bound protein (by the back arrow) was indicated by the fluorescence at ~ 53 kDa while the unbound residual fluorophore are indicated below by the red arrow. This functionality of SNAP-tag domain is essential for the generation of SNAP-tag ADC and PIC for diagnostics and therapeutic purposes.

3.4 Anti-CD64 FPs demonstrated targeted binding towards antigen-positive cells (IFN- γ U937)

The functional activity of each anti-CD64 FPs was evaluated via flow cytometry to determine selective binding to CD64+ target monocytic cells (U937). Using standard protocols (2.2.9.1), 30 µg of each purified protein (H22(scFv)-ETA`, H22(scFv)-dETA`(RG7787-MT2), and H22(ScFv)-SNAP) was incubated with IFN-γ stimulated U937 cells for 1 hour on ice and afterwards labelled with a detection secondary antibody; anti-Histag-Alexa 647 antibody on ice for 1 hour. As shown in Figure 3.11, all anti-CD64 FPs demonstrated significant binding to U937 cells but not to the CD64 antigen negative cells (MDA-MB 468). Comparably, the bindings results are 87 %, 75.2 % and 85.2 % for H22(scFv)-ETA`, H22(scFv)-dETA`(RG7787-MT2), and H22(scFv)-SNAP respectively. The binding affinity of the H22(scFv) antibody fragment to the overexpressed CD64 antigen is dependent on several factors. Among them, is the overall purity of the recombinant protein and its ability to recognize the targeted antigen, in this case, CD64 [164]. All three proteins show selective binding above 75 % to the CD64 receptor.

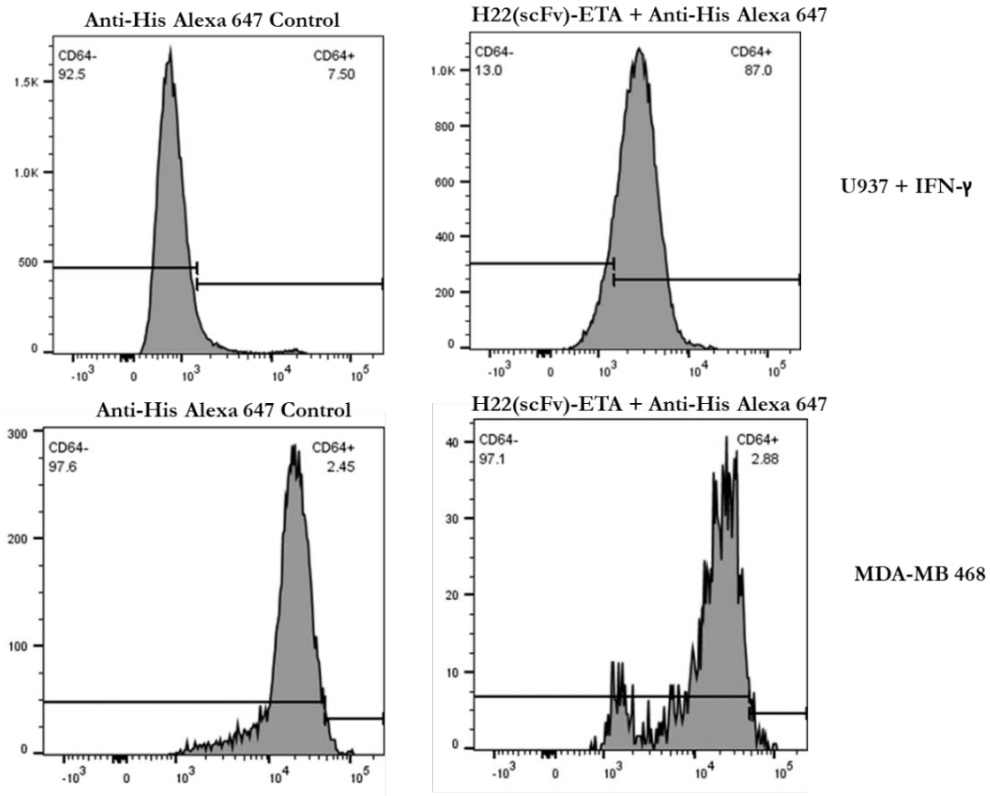

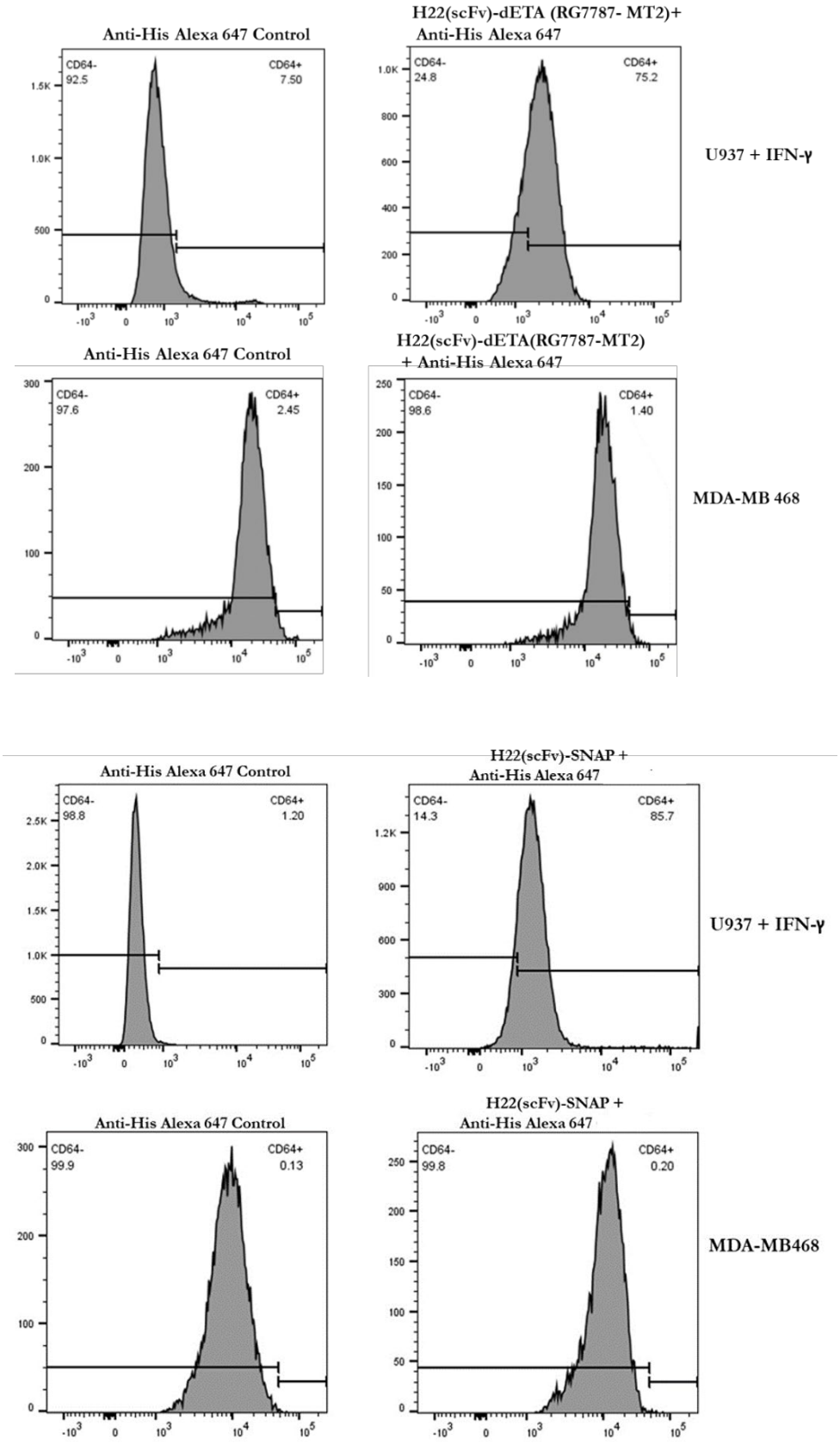

Figure 3.11. Binding analysis of anti-CD64 FPs on IFN- γ stimulated U937 cells.

The functional activities of H22(scFv)-ETA`, H22(scFv)-dETA` (RG7877-MT2), and H22(scFv)-SNAP were investigated by staining IFN-γ stimulated U937 cells with 30 μg of each protein and

.[79].

labelling with anti-Histag-Alexa 647 antibody for detection of bound protein on the surface of the U937 cells (2.2.9.1) Flow cytometric analysis results confirmed significant functional (binding) activities of each anti-CD64 recombinant proteins to IFN-γ stimulated U937.

3.5 Polarization studies of *ex vivo* macrophages

3.5.1.1 Polarized *ex vivo* macrophages show giant multinucleation phenotypic features

Confocal image analysis (2.2.10.1) was performed to evaluate/confirm the phenotypic characteristics of each polarized macrophages. The images captured below (Figure 3.12) show a unique characteristic of macrophages which is their fused/multinucleated nucleus (in blue) [165]. Furthermore, each subtype possesses cytoskeletal actin around their membranes and unique morphology with M1(IFN-γ +LPS) macrophages taking the elongated spindle shape while M2(IL-4) and resting M(0) macrophages have broad/extended shapes [165, 166].

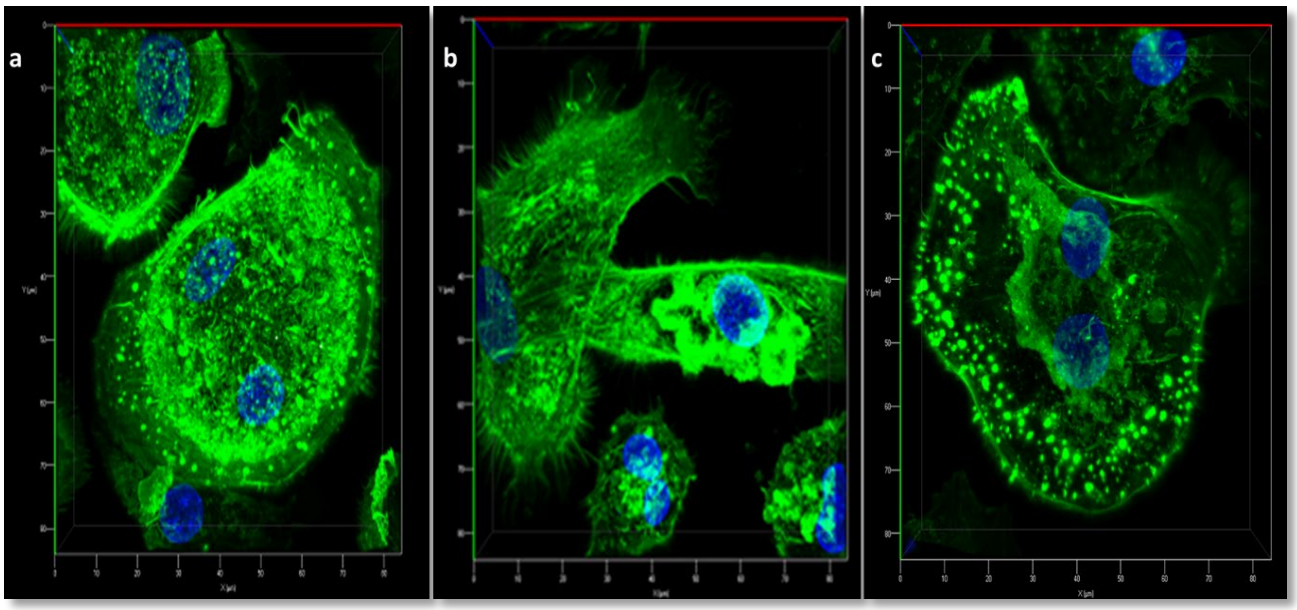

Figure 3.12. Confocal microscopy images of polarized *ex vivo* macrophages.

Green fluorescence highlights cytoskeletal actin (Alexa Fluor™ 488 Phalloidin, green (Invitrogen)) and DAPI nuclear stain (blue) staining of resting macrophages, M(0) (a), M1(IFN-γ & LPS) (b), and M2(IL-4) (c) macrophages. Images were taken with the LSM 880 Airy scan confocal microscope (Zeiss) with resolution of 80 µm (2.2.10.1). As observed for morphology difference, M1(IFN-γ & LPS) macrophages takes more of an elongated shape while M(0) and M2(IL-4) have broad (extensive) shapes.

3.5.1.2 Polarized *ex vivo* differentiated macrophages show different phenotypic surface markers

Flow cytometry analysis (2.2.9.2) was performed to further confirm successful differentiation and polarization of monocytes derived macrophages into the different sub-types. The expression levels of membrane-bound markers (e.g. CD14 and CD206) on macrophages is another approach often used to classify macrophages into different functional sub-types [8]. As shown below, flow cytometric analysis confirmed upregulation of the CD14 receptor (96.1 %) on M1(IFN-γ +LPS) macrophages compared to M(0) (75.3 %) and M2(IL-4) macrophages (53.9 %). In addition, M2(IL-4) macrophages showed upregulation of the CD206 receptor (94.6 %) compared to M(0) (13.9%) and M1(IFN-γ +LPS) macrophages (50.2 %) (Figure 3.13). Both polarization studies (confocal and flow cytometric analysis) confirmed phenotypic differences between polarized *ex vivo* differentiated hMDMs.

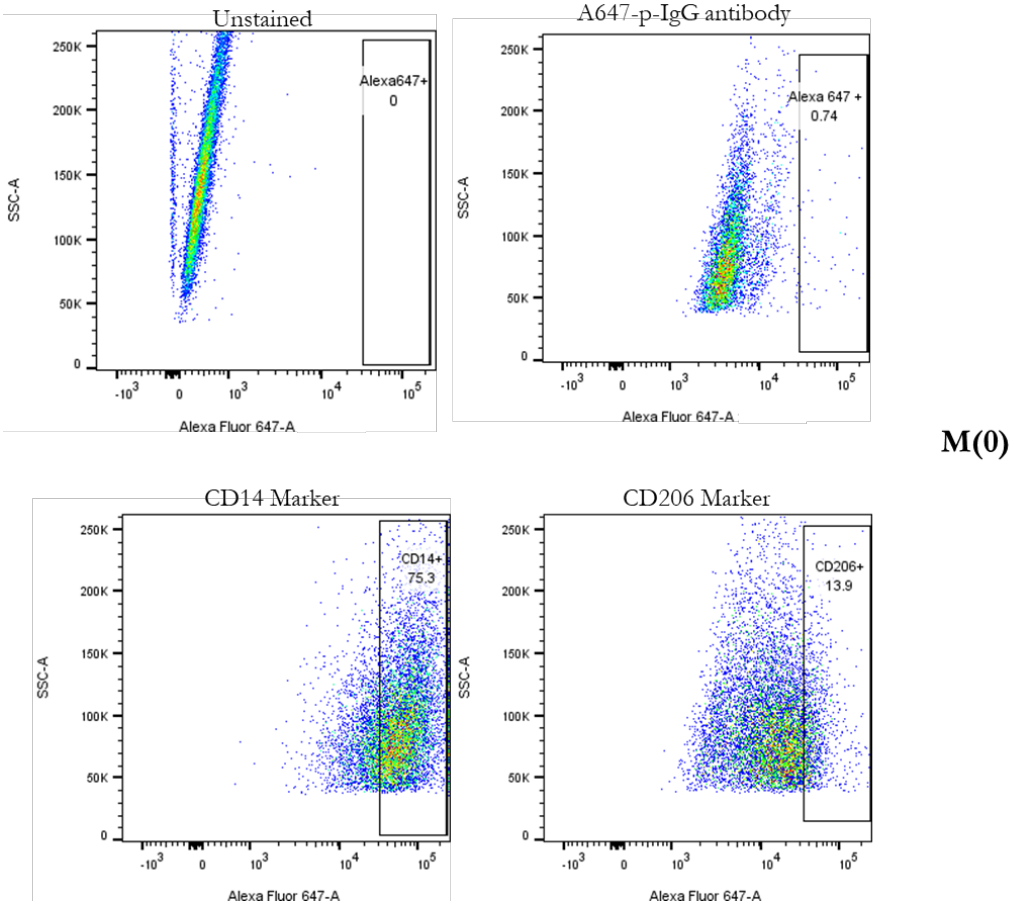

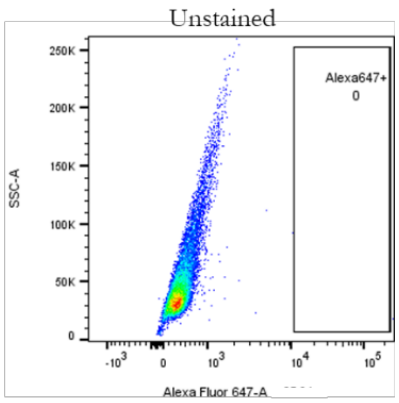

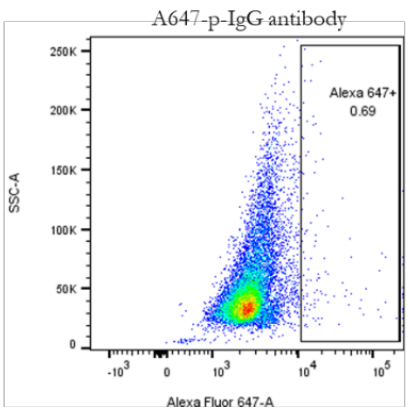

M1
(LPS + IFN-γ)

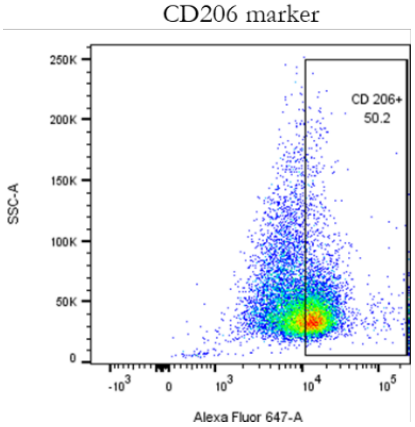

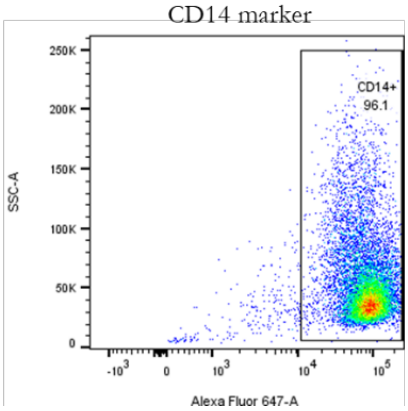

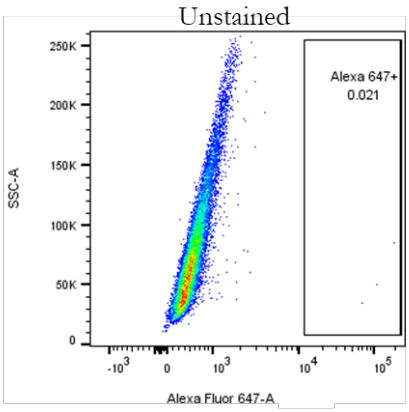

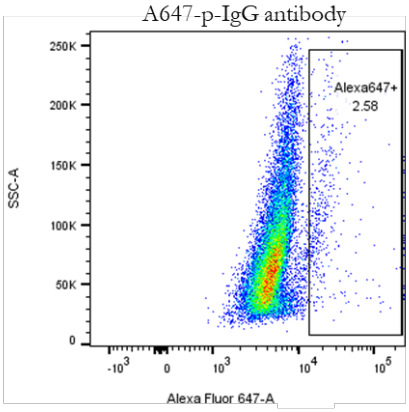

M2 (IL-4)

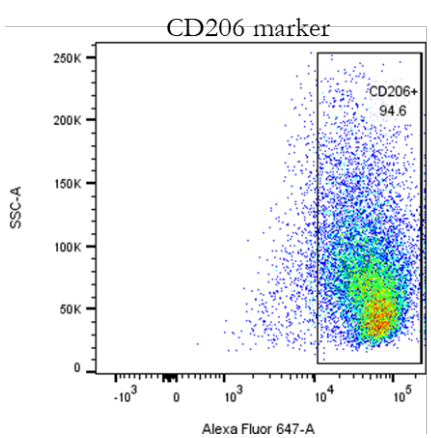

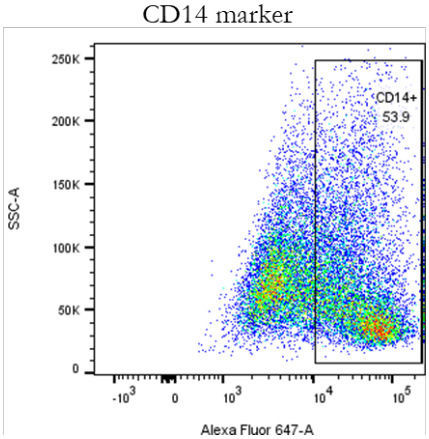

Figure 3.13. Phenotypic surface marker characterization of polarized *ex vivo* differentiated hMDMs.

Surface marker expression on polarized *ex vivo* differentiated hMDMs was investigated by incubation of antibodies against CD206, CD14 with the polarized macrophages for 1 hour on Ice, subsequently labelled with a Goat anti-mouse IgG-Alexa 647 antibody (Sigma Aldrich), before passing the cell through flow cytometer for analysis (2.2.9.2). Comparatively, CD14 is overexpressed on M1(IFN-γ +LPS) macrophages (96.1 %) while CD206 is overexpressed on M2(IL-4) macrophages (94.6 %). These upregulated membrane markers CD14 and CD206 confirm phenotypic differences each polarized differentiated hMDMs. The "A647-p-IgG Antibody" indicated in the plot siagrams = Goat anti-mouse IgG-Alexa 647 antibody. p = polyclonal.

3.5.1.3 Characterization of the CD64 expression on polarized *ex vivo* differentiated hMDMs

Flow cytometry (2.2.9.1) was used to evaluate CD64 receptor expression levels on polarized macrophages. The polarized macrophages were incubated with mouse anti-human CD64 Alexa fluour ® 647 antibody (Biorad, USA) for 1 hour. Thereafter, cells were washed twice with PBS (pH 7.4), suspended in FACS buffer, data captured using the BD LSR-II (BD Biosciences), and analysed on Flow Jo software. The result agrees with literature [167], which showed polarized M1 (LPS + IFN-γ) demonstrated the highest CD64 expression (98.8 %) compared to M2(IL-4) (79.2 %) and M(0) (49.9 %) (Figure 3.14).

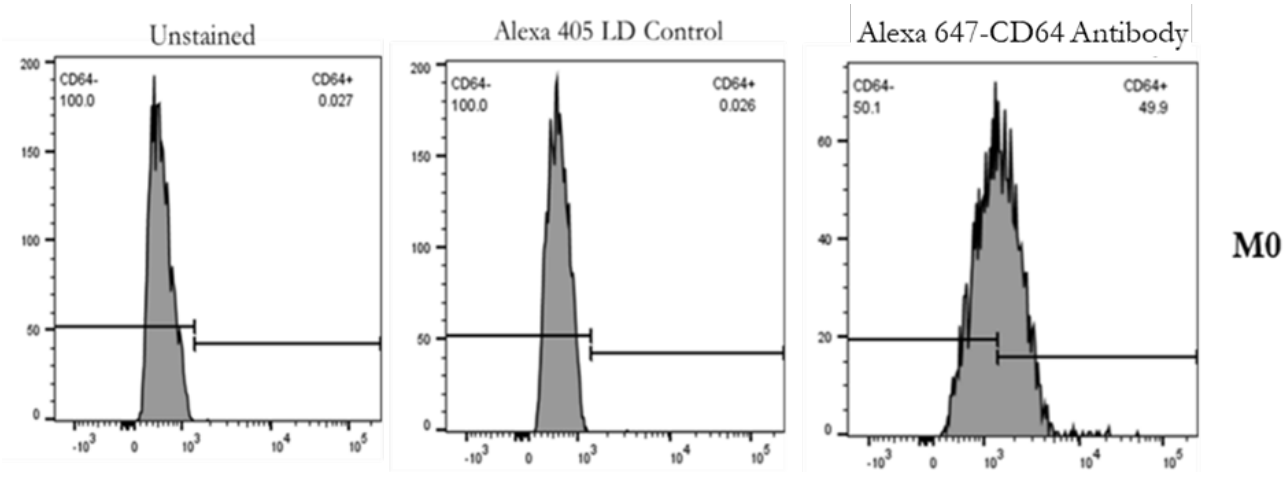

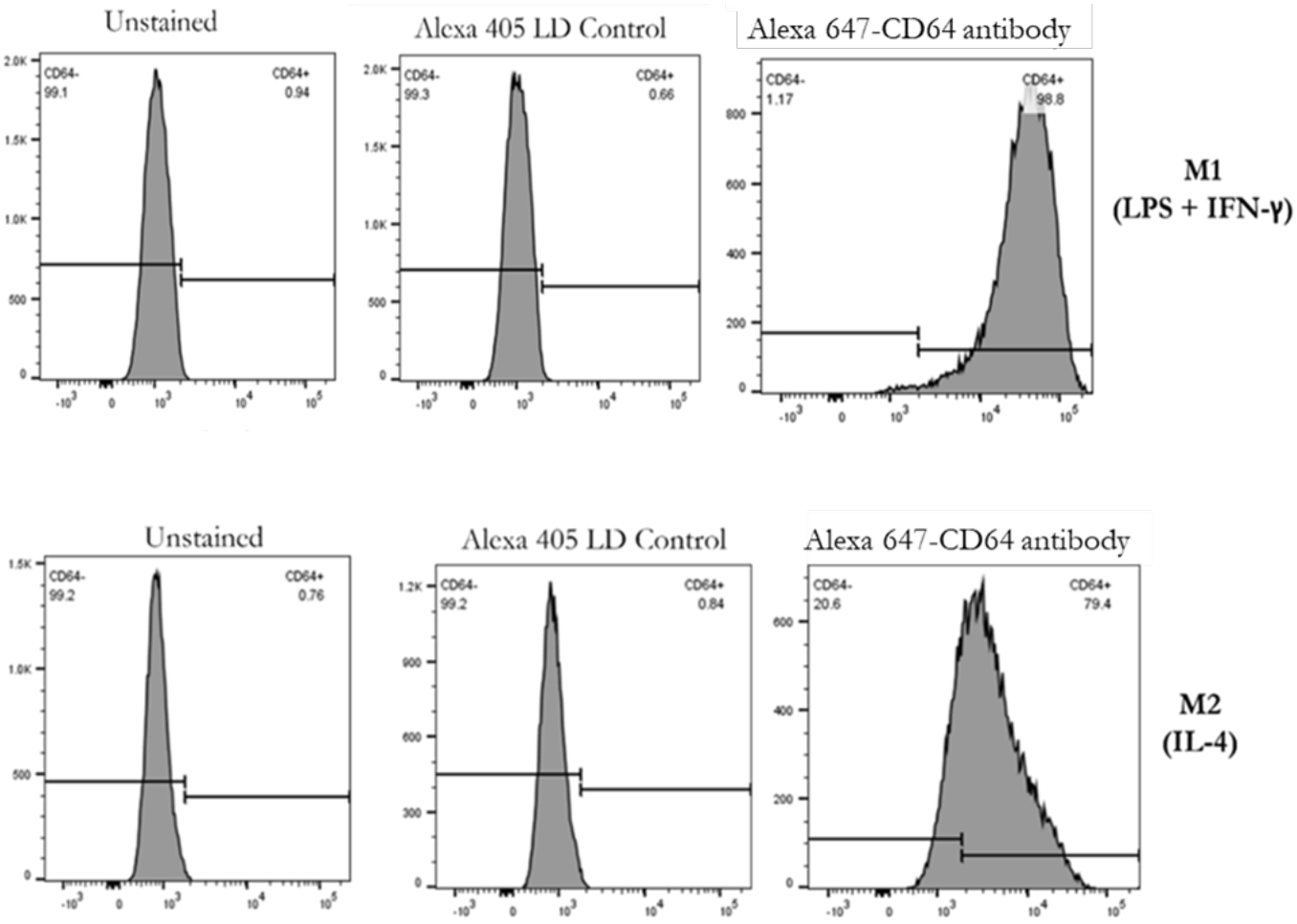

Figure 3.14. Characterization of CD64 expression on polarized *ex vivo* differentiated macrophages.

Alexa 647-CD64 antibody (Biorad, USA) was incubated with each polarized macrophage sub-types on ice for 1 hour. After two washes, the cells were resuspended in the FASC buffer and data was acquired on the BD LSR-II (BD Biosciences) and analysed on Flow Jo software (2.2.9.1). Both M1(LPS + IFN-γ) and M2(IL-4) shows upregulation of CD64 (70-98%) compared to baseline M(0) macrophages (49%). Abbreviations: Alexa 647- CD64 antibody – mouse anti-human CD64 Alexa fluour ® 647 antibody , LD – Live dead marker/control.

3.6 Binding and Internalization Studies of H22(scFv)-SNAP on polarized *ex vivo* differentiated hMDMs

3.6.1 H22(scFv)-SNAP demonstrated selective binding to polarized *ex vivo* differentiated hMDMs

Flow cytometry analysis (2.29.2) was to used to confirm selective binding of CD64-SNAP-tag FP to ex vivo differentiated CD64-positive hMDMs. To run flow cytometry analyses, BG-modified fluorophore (BG-Alexa 647) was conjugated to H22(scFv)-SNAP according to the reaction set-

up (Table 2.16); unlabelled fluorophore was removed by zeba TM spin column. An aliquot of the fluorophore-labelled product generated was run of SDS-PAGE and visualized on iBrightFL1000 imaging system (Thermofischer, USA). The bright red fluorescence indicates the generated labelled product, H22(scFv)-SNAP-Alexa 647 (Figure 3.15A). Afterwards, 30 µg of H22(scFv)-SNAP-Alexa 647 was incubated with the polarized macrophages; M1(IFN-γ + LPS), M2(IL-4) and resting M(0) macrophages for 60 minutes on ice. Afterwards, the cells were washed twice with PBS (pH 7.4), suspended in FACS buffer, and analysed on a BD LSR-II (BD Biosciences). After analysis, results (Figure 3.15B) show that H22(scFv)-SNAP demonstrates binding to all polarized macrophages with resting M(0) macrophages demonstrate binding of 55.6 % while M1(IFN-γ + LPS) and M2(IL-4) polarized macrophages binding are 87.4 % and 73.3 % respectively.

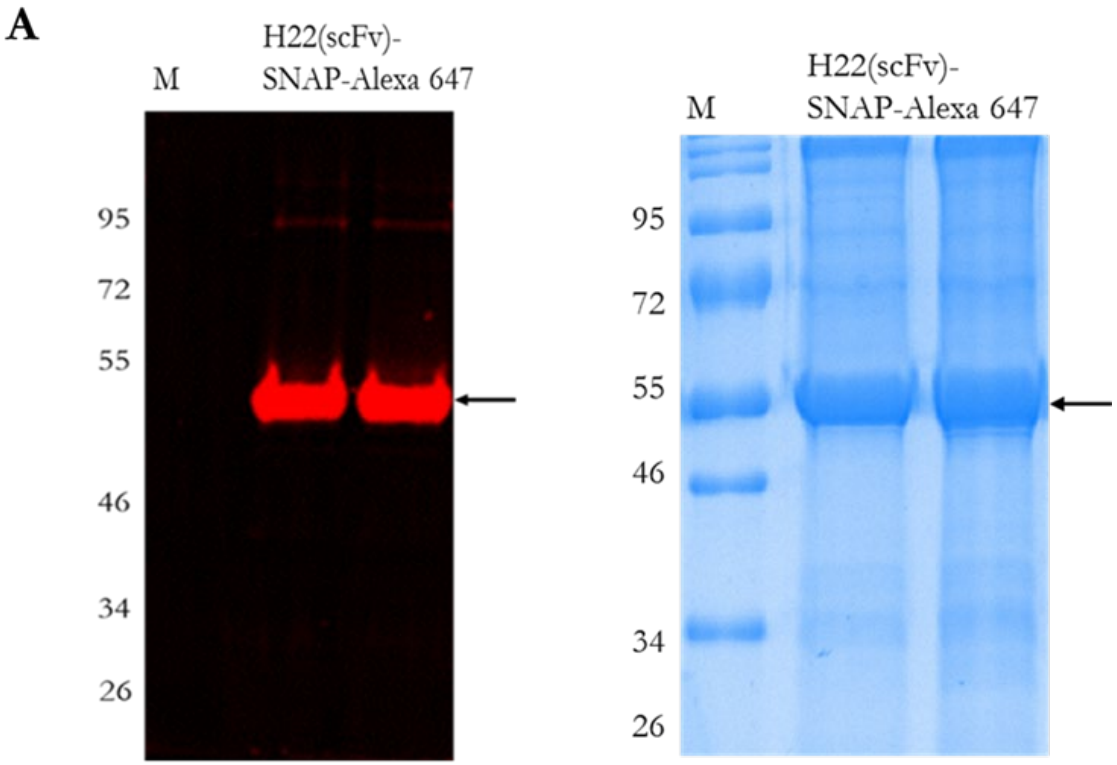

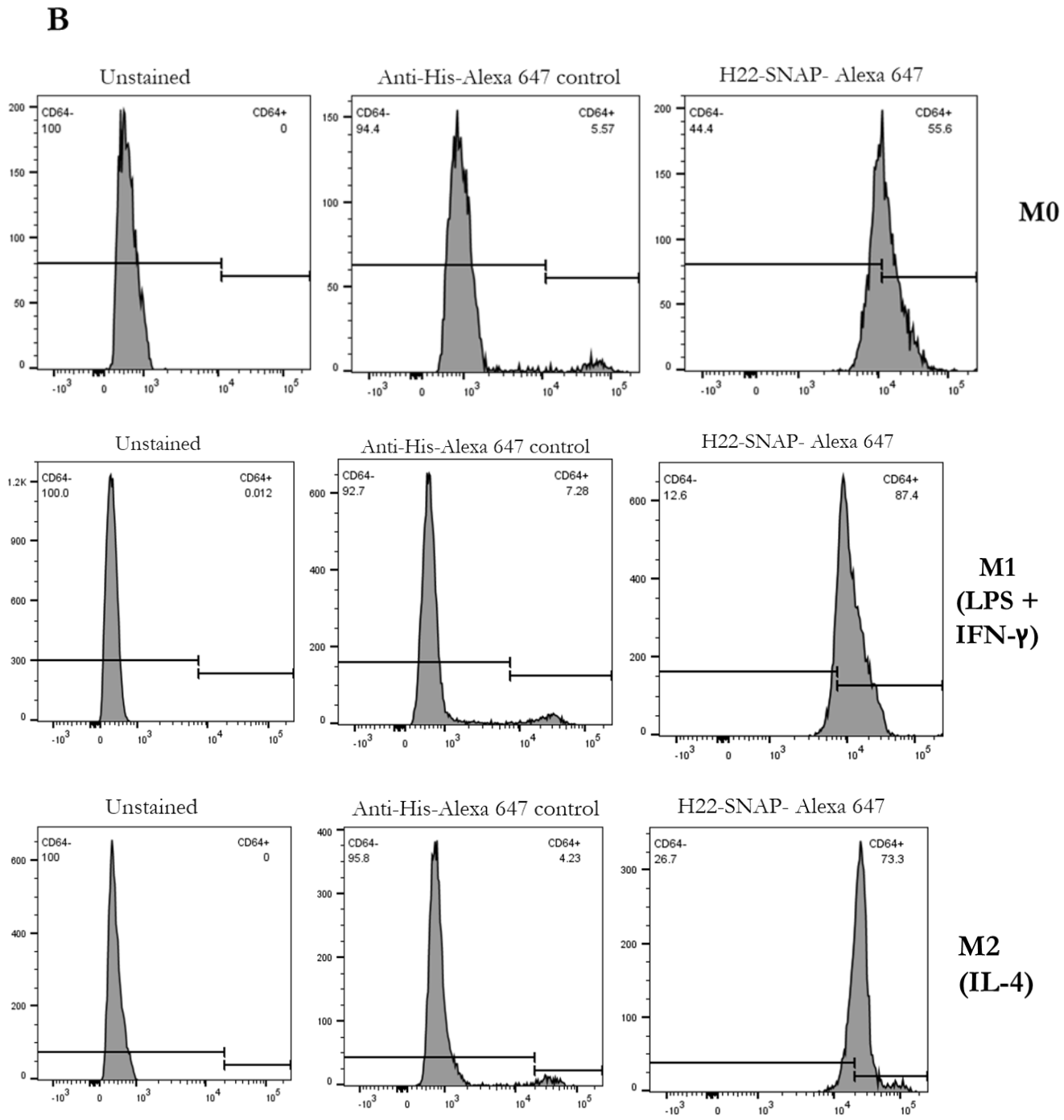

Figure 3.15. Binding of H22(scFv)-SNAP-Alexa 647 to polarized *ex vivo* differentiated differentiated hMDMs.

(A) Gel visualization of labelled H22(scFv)-Alexa 647 used for binding and internalization kinetics. Image taken by iBrightFL1000 imaging system (Thermofischer, USA) and SDS-PAGE gel. Black arrow indicating bound fluophore labelled protein. (B)The binding activity of anti-CD64 FP to *ex vivo* differentiated macrophages was investigated using flow cytometry studies. 30 μg of labelled H22(scFv)-SNAP-Alexa647 was incubated with each macrophage's subtypes for 1 hour on ice. After two washes, the cells were resuspended in the FASC buffer and data was acquired on the

BD LSR-II flow cytometer (BD Biosciences) (2.2.9.1). M1(IFN-γ + LPS) macrophages (87.4%) shows highest selective binding to anti-CD64 FPs compared to M2(IL-4) macrophages (73.3%) and M(0) (55.6%) which corresponds to the CD64 expression levels on each polarized macrophages. Anti-His Alexa 647 antibody was included as a negative control for H22(scFv)-SNAP-647 binding studies to confirm no binding of an irrelevant Alexa 647 labeled antibody in comparison to specific binding to CD64 receptor on hMDMs by H22(scFv). This result was important for the use of this anti-His Alexa 647 as secondary antibody for binding studies with CD64 targeting rITs and hCFPs.

3.6.2 H22(scFv)-SNAP FP demonstrated CD64-dependent internalization in polarized *ex vivo* differentiated hMDMs

Confocal microscopy imaging (2.2.10.2) was used to investigate the internalization kinetics of SNAP-tag FP, H22(scFv)-SNAP on polarized *ex vivo* human macrophages. Briefly, each polarized macrophage sub-types; M(0), M1(IFN-γ + LPS) and M2(IL-4) were washed twice with sterile dPBS and fixed with 2% PFA on ice for 15 minutes. Next, 0.5% Trixton X was incubated with each macrophages for 20 minutes to permeabilize cells. Afterwards, 1 μM of H22(scFv)-SNAP-Alexa 647 (Figure 3.15A) , was incubated with macrophages for 60 minutes under cold conditions and washed off with dPBS. Finally, the cells are labelled with phalloidin actin (1:500 in PBS for 30 minutes) and DAPI/Hoest (1:5000 in PBS for 15 minutes), and images acquired with Airy scan confocal microscope (Zeiss). The result in figure 3.16 showed that all macrophages sub-types internalized the fusion protein, H22(scFv)-SNAP evident by the Alexa 647 signal. Furthermore, as shown in the images in figure 3.16 (B), the M1(LPS + IFN-γ) macrophages presented very bright Alexa 647 signal which can be indicative of a higher FP internalization due to high CD64 expression compared to M(0) and M2(IL-4) macrophages. In Figure 3.16, two channels are included, the red channel (fluorescence) and merged channel. The distinction in the internalization of H22(scFv)-SNAP-Alexa 647 was presented by the intensity of the bright red fluorescence in the red channel. The merged channel shows the generically the cytoskeletal actin for macrophages by phalloidin staining (overview), but when compared.

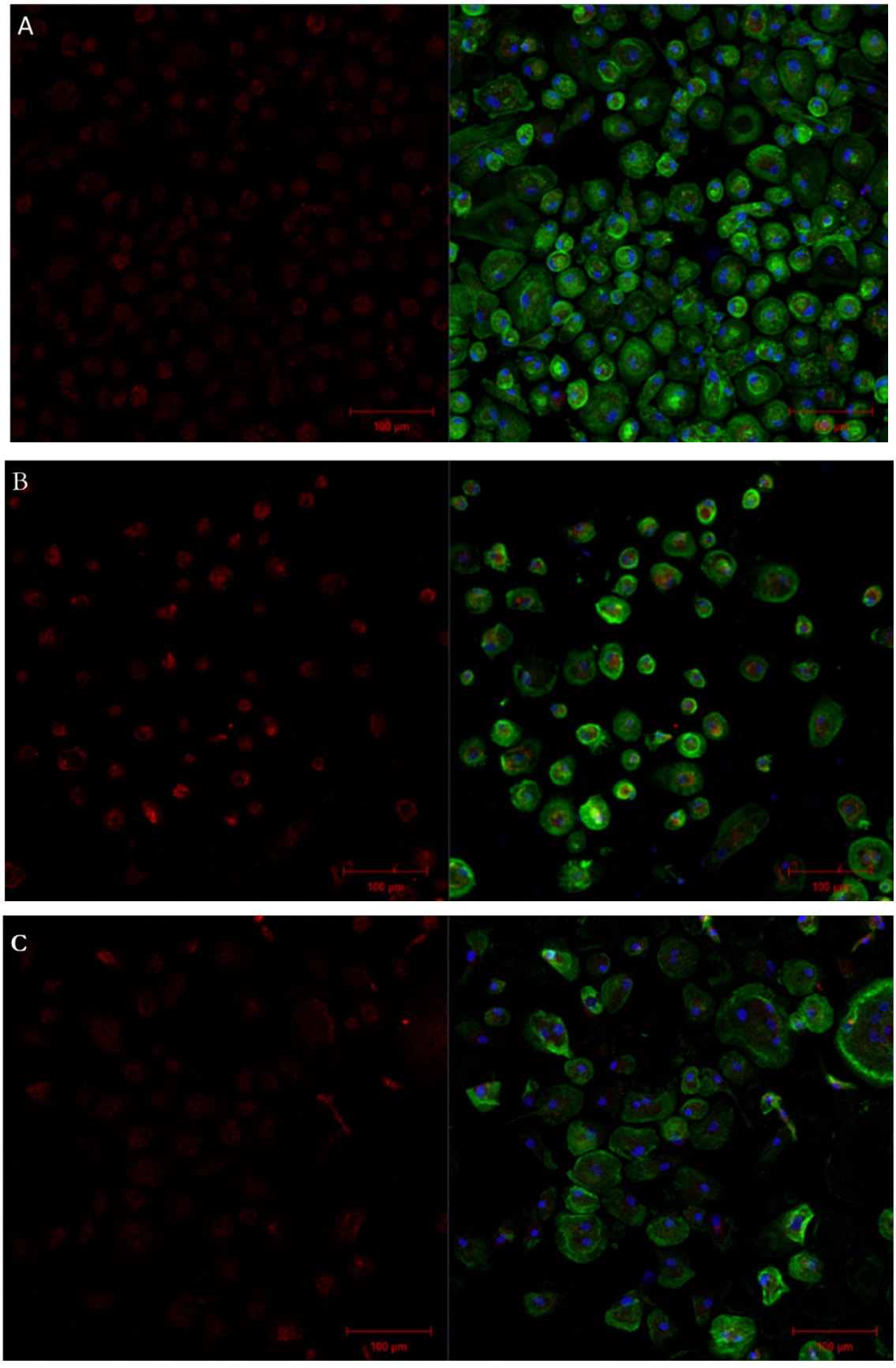

Figure 3.16. Internalization kinetics of H22(scFv)-SNAP-647 FP on polarized *ex vivo* differentiated differentiated hMDMs.

Confocal microscopic imaging was used to evaluate internalization of H22(scFv)-SNAP-647 on each polarized macrophage sub-types: M(0) (A), M1(LPS+IFN-γ) (B), and M2(IL-4) (C). Comparatively, M1(LPS+IFN-γ) (B) macrophages internalize the highest amount of H22(scFv)-SNAP-Alexa647 indicated by the bright fluorescence of BG-Alexa 647which also showed anti-CD64 FPs high selectivity for M1(LPS+IFN-γ) macrophages compared to other macrophage types (M2(IL-4) and M(0)). The images were acquired using the Zeiss LSM 880 Airy scan confocal microscope (2.2.10.2).

3.7 Cytotoxicity studies of CD64-targeting immunotherapeutics on CD64+ monocytic cell lines.

To determine the therapeutic potential of each CD64-targeting immunotherapeutics: H22(scFv)-ETA`, H22(scFv)-dETA`(RG7787-MT2), and H22(scFv)-SNAP-AURIF *in vitro*, the XTT cell viability assay was used to evaluate their ability to selectively induce cell death in target CD64+ monocytic cells compared to CD64- cells in a dose-dependent manner (2.2.12.2). Table 3.5 summarizes the results of the *in vitro* cytotoxicity studies of CD64-targeting rITs and SNAP-tag antibody drug conjugate (ADC) documented in this thesis towards CD64+ monocytic cell lines.

Table 3.2 Summary of *In vitro* cytotoxicity results on CD64+ monocytic cells

Class	CD64-immunotherapeutics	Cell lines	IC_{50} Values
rIT	H22(scFv)-ETA`	U937 +IFN-γ HL 60 + IFN-γ A2058 U937, HL 60	423.3 pM 522.6 pM ---- not available
d-rIT	H22(scFv)-dETA`(RG7787-MT2)	U937 +IFN-γ HL 60 + IFN-γ A2058 U937, HL60	3.846 nM 7.064 nM ----- not available
ADC	H22(scFv)-SNAP-AURIF	U937 +IFN-γ U937 HL 60 + IFN-γ HL60 A2058	14. 58 nM 617.0 nM 135.7 nM 255.2 nM ------
CD	BG-AURIF AURIF	U937 +IFN-γ U937 +IFN-γ	21.57 nM 53.85 nM

--- = no killing/cytotoxic value. Abbreviations: rIT – recombinant immunotoxin, d-rIT – deimmunized immunotoxin, ADC – antibody drug conjugate, CD – cytotoxic drug.

3.7.1. Anti-CD64 rITs selectively induced cell death in CD64-positive antigen cells at nanomolar concentration

Specifically, serial dilutions of rITs (from 100 nM); H22(scFv)-ETA` and H22(scFv)-dETA`(RG7787-MT2) were incubated for 72 hours with IFN-γ stimulated U937 and HL60 monocytic cells. Thereafter, the XTT reagent was added to the cells for four hours after which the plate was read on a Spectrophotometer (2.2.12.2). The results (Figure 3.18) showed that both H22(scFv)-ETA` and H22(scFv)-dETA`(RG7787-MT2) demonstrate selective toxicity towards CD64 positive cells IFN-γ U937 and HL60 but didn't have any effect on CD64 negative cells A2058. Comparably, the IC_{50} (half inhibitory concentration) of H22(scFv)-ETA` demonstrate killing with picomolar concentration (423.3 pM and 522.6 pM) on IFN-γ stimulated U937 and HL60 while H22(scFv)-dETA`(RG7787-MT2) demonstrated killing towards same cells with nanomolar concentration (3.486 nM and 7.064 nM). This suggests that H22(scFv)-ETA` is more cytotoxic compared to its deimmunized version, H22(scFv)-dETA`(RG7787-MT2).

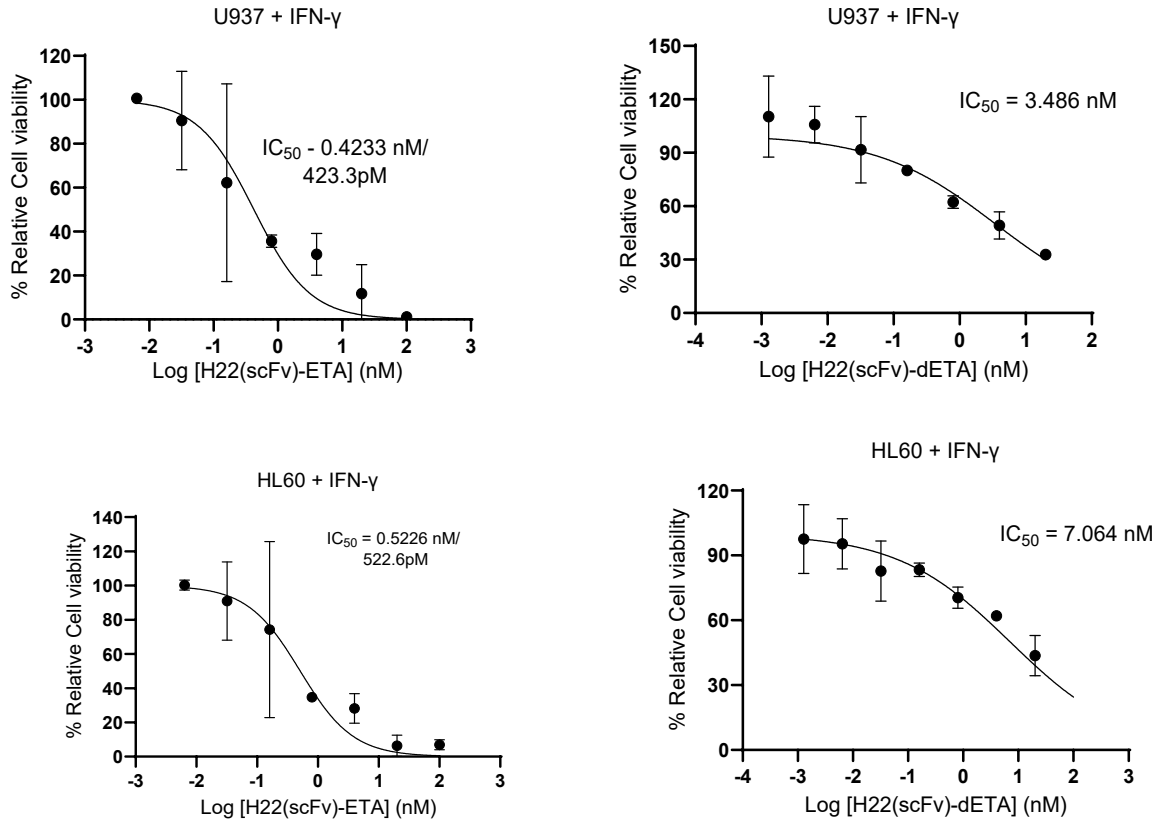

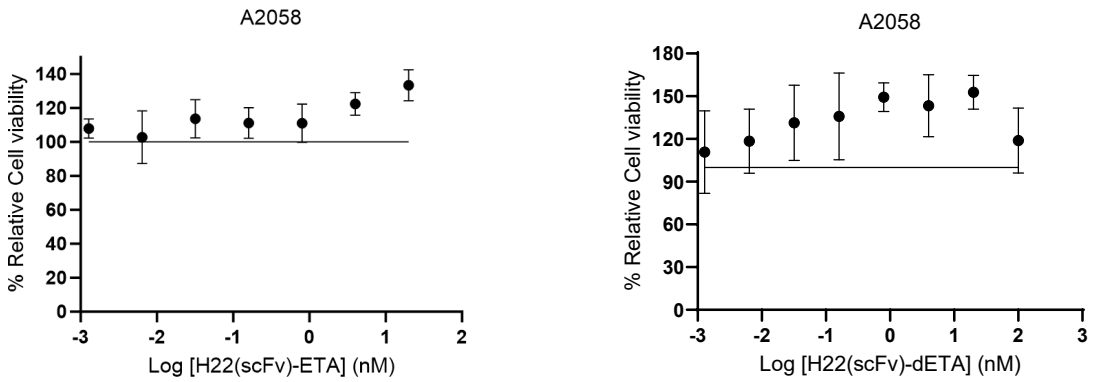

Figure 3.17. Cytotoxicity studies of H22(scFv)-ETA` and H22(scFv)-dETA`(RG7787-MT2) on IFN-γ stimulated U937 and HL60 cells.

Confirmation of cytotoxic activity for the purified H22(scFv)-ETA` immunotoxin was performed as described earlier (2.2.12.1). As shown above, the H22(scFv)-ETA` immunotoxin was selectively toxic in nanomolar concentrations towards IFN-γ stimulated U937 and HL60 cells, but not to the CD64 negative control, A2058 cell. IC_{50} calculations (from non-linear regression) were performed using the GraphPad Prism v10.0 software. pM, picomolar; nM, nanomolar.

3.7.2 Comparative ADP-riosylation assay (enzymatic activity) of anti-CD64 rITs

Anti-CD64 rITs, H22(scFv)-ETA` and its deimmunized variant, H22(scFv)-dETA`(RG7787-MT2) exert cytotoxicity via inhibition of protein biosynthesis. This involves the ADP-ribosylation of elongation factor 2 (EF2) [162, 163]. Hence the ADP-ribosylation assay was used to compare the enzymatic activity of each immunotoxin. Briefly, elongation factor 2 (EF2) extracted from wheat germ was incubated with biotinylated NAD+ in the presence of 100 nM of both H22(scFv)-ETA` and H22(scFv)-dETA`(RG7787-MT2). After incubating for 1 hour at 37°C, the amount of biotinylated-NAD+ incorporated into EF2 was determined by western blot via a streptavidin-horseradish peroxidase (HRP) labelled antibody and extrapolated via Image J analysis. The result documented below (Figure 3.18) shows the comparable difference in band intensities of reduced EF2 by H22(scFv)-ETA` and H22(scFv)-dETA`(RG7787-MT2). Noteworthy is that H22(scFv)-dETA`(RG7787-MT2) retained its enzymatic activity despite the introduced mutational changes to the enzymatic domain of dETA`. However, the enzymatic activities of the deimmunized variant was to some extent reduced when compared to H22(scFv)-ETA`, hence the difference in cytotoxicity above (Figure 3.17).

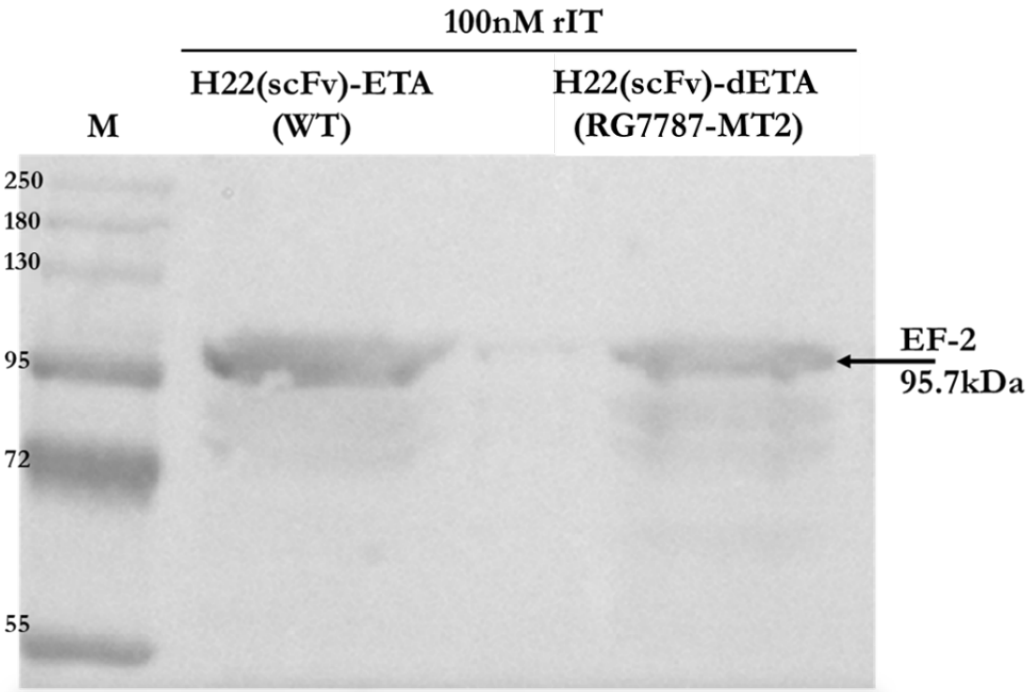

100 nM rIT Variant	Band Intensity (extrapolated from ImageJ)
H22(scFv)-ETA	17470.35
H22(scFv)-dETA (RG7787-MT2)	14612.66

Figure 3.18 Immunoblot showing comparative enzymatic activities of anti-CD64 rITs.

To measure and compare the enzymatic activities of both rITs, an enzymatic assay in which EF2 from wheat germ extract was incubated with biotinylated NAD+ in the presence of 100 nM H22(scFv)-ETA` and H22(scFv)-dETA`(RG7887-MT2) was performed. After incubating the reaction component for 1 hour, the activity of each rIT was determined by western blot using a streptavidin-HRP conjugate and extrapolated with ImageJ (2.2.11). H22)scFv)-ETA` shows higher enzymatic activity compared to H22(scFv)-dETA`(RG7787-MT2).

3.8. Toxicity profile of anti-CD64 antibody drug conjugate (ADC)

3.8.1 Generation and validation of anti-CD64 ADC

ADC contains a cell-specific antibody chemically conjugated to a cytotoxic drug [125]. The SNAP-tag technology [168] was used for the generation of ADC via stoichiometric (1:1) conjugation of H22(scFv)-SNAP to a cytotoxic drug; BG-modified monomethyl auristatin F (MMAF).

Before conjugating BG-modified MMAF (herewith termed BG-AURIF) to H22(scFv)-SNAP, its cytotoxic efficiency was compared to unmodified MMAF (AURIF) via an XTT assay on IFN-γ stimulated U937 cells to confirm retentive cytotoxicity of the BG-modified AURIF. The results showed that BG-AURIF demonstrated retentive cytotoxicity compared to unmodified MMAF (21.57 nM vs 53.85 nM) which makes it a suitable cytotoxic moiety for the generation of SNAP-tag-based ADCs (Figure 3.19).

To prepare the SNAP-tag ADC, H22(scFv)-SNAP was labelled with a three-fold molar concentration BG-AURIF in phosphate buffer at 37°C for 2 hours. The labelled protein was thereafter cleaned up using an Amicon ultracentrifugation filter device (10 kDa MWCO) to remove residual/unbound BG-AURIF. The successful preparation of H22(scFv)-SNAP-AURIF was confirmed by subjecting the H22(scFv)-SNAP-AURIF to a secondary conjugation with BG-Alexa 488 fluorophore (New Englands Biolabs) and analysed on an SDS-PAGE. The failure of Alexa 488 conjugation to H22(scFv)-SNAP-AURIF relative to control, H22(scFv)-SNAP confirmed that prior conjugation of BG-AURIF to H22(scFv)-SNAP was complete and successful (Figure 3.20).

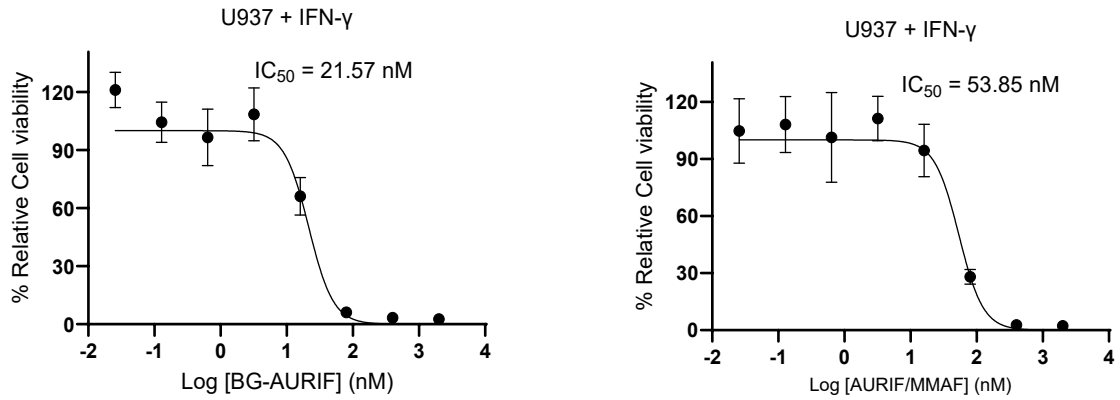

Figure 3.19 BG-modified AURIF demonstrated retentive cytotoxicity compared to unmodified AURIF/MMAF on IFN-γ stimulated U937 cells. The cytotoxic efficiency of BG-modified Auristatin F (BG-AURIF) and unmodified monomethyl auristatin F (AURIF/MMAF) was compared on stimulated U937 cell line using the XTT cell viability assay. The comparative cytotoxicity showed BG-modified AURIF retentive toxic potential hence its good application in the generation of ADC. Nonlinear regression and IC_{50} calculations were performed using GraphPad Prism v10.0 software. nM = nanomolar.

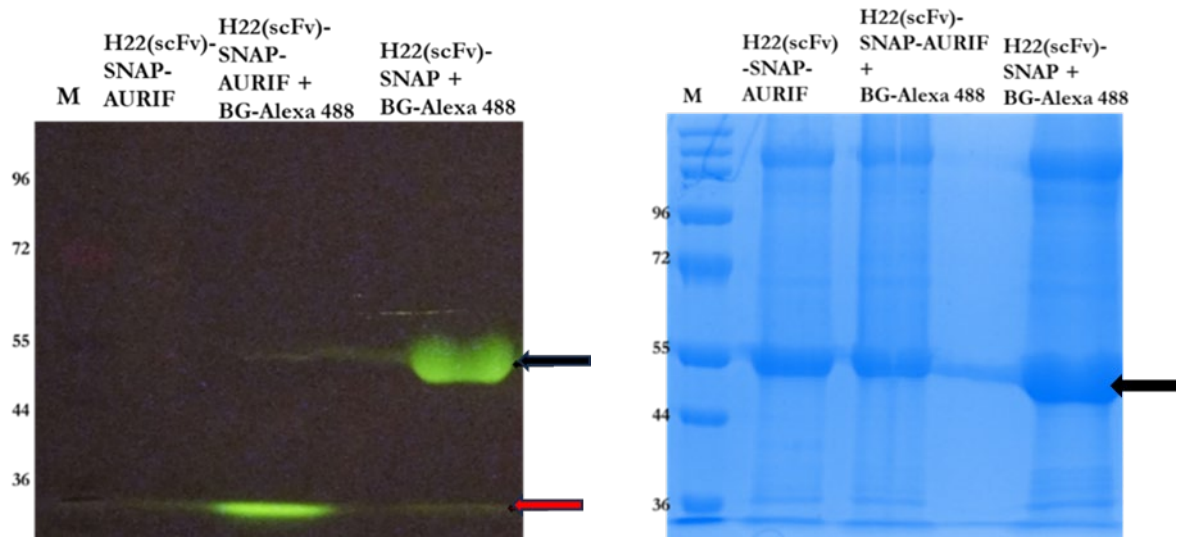

Figure 3.20. Generation of ADC, H22(scFv)-SNAP-AURIF and confirmation of optimal labelling. A one-step site-specific conjugation of CD64-specific antibody, H22(scFv)-SNAP to cytotoxic drug; BG-AURIF was achieved by using the SNAP-tag technology. The corresponding SDS-PAGE gel was used to confirm the conjugation efficiency of BG-AURIF to H22(scFv)-SNAP. The gel showed that prior labelling of H22(scFv)-SNAP with a three-fold molar excess of BG-AURIF was enough to saturate the active site of the SNAP-tag molecule. The black arrow represent labelled/bound H22(scFv)-SNAP while the red arrow represents unbound/residual unconjugated BG-Alexa 488 fluorophore.

3.8.2 H22(scFv)-SNAP-AURIF demonstrated selective toxicity against stimulated and unstimulated CD64+ monocytic cell lines

The XTT cell proliferation assay (2.2.12.1) was used to investigate the cytotoxic activity of H22(scFv)- SNAP-AURIF. For this assay, 5 x 10^3 IFN-γ stimulated U937 and HL 60 cells , and unstimulated U937 and HL 60 cells were seeded in 96 well plates in technical quadruplicates. After 24 hours post-stimulation, the cells were treated with decreasing doses of H22(scFv)-SNAP-AURIF (from 500 nM) for 72 hours after which the XTT reagents was added and viability of the cells was compared with media and zeocin-treated controls. Quantitative analysis of cell viability showed that H22(scFv)-SNAP-AURIF was cytotoxic against both stimulated and unstimulated CD64+ monocytic cells (U937, HL60), but not the CD64- cells A2058 cancer cell line. Also, H22(scFv)-SNAP-AURIF demonstrated improved cytotoxicity in IFN-γ stimulated U937 and HL60 (14.58 nM and 125.0 nM) compared to unstimulated U937 and HL 60 (617.0 nM and 255.2 nM), which further confirms ADC internalization and targeted drug killing is increased with upregulated CD64 receptor on CD64+ target cells (Figure 3.21).

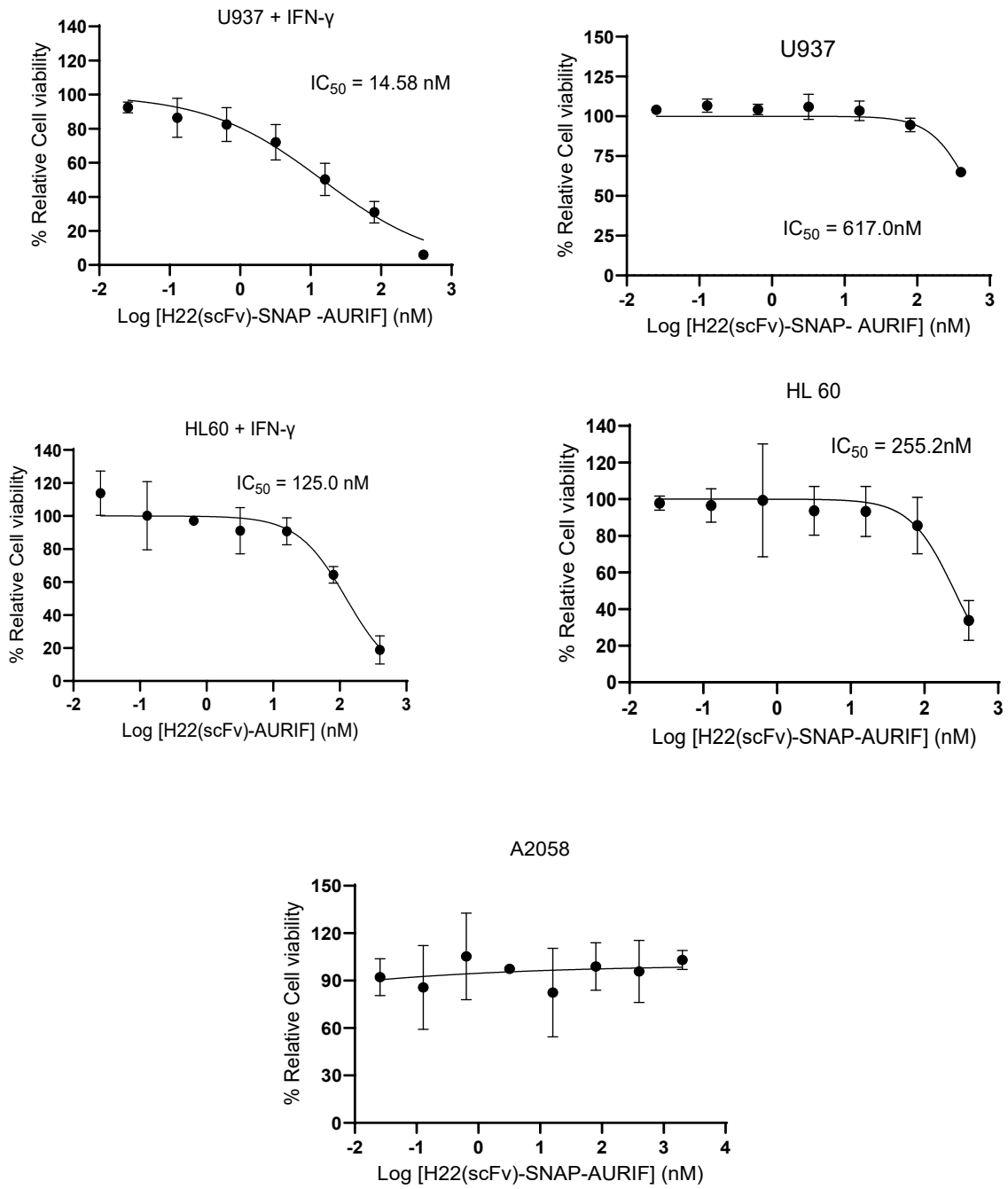

Figure 3.21. Cell viability assays with anti-CD64 SNAP-tag ADC, H22(scFv)-SNAP-AURIF` on IFN-γ stimulated and unstimulated U937 and HL60 cells. Confirmation of cytotoxic activity for the purified H22(scFv)-SNAP-AURIF ADC was performed as described earlier (2.2.6.3). As shown above, the ADC – H22(scFv)-SNAP-AURIF was selectively toxic towards unstimulated and IFN-γ stimulated U937 and HL60 cells (at nanomolar concentartions) and not to the CD64 negative control, A2058 cell. IC_{50} calculations were performed using the GraphPad Prism v10.0 software. pM, picomolar; nM, nanomolar.

3.9 Photoimmunotoxicity studies of anti-CD64 photoimmunoconjugate (PIC) on polarized *ex vivo* differentiated hMDMs

As described above (1.5.2.1.2), a PIC contains a specific cell-binding antibody conjugated to a photosensitizer (PS) for diagnostic or therapeutic applications [139, 169]. Our lab received the PS, BG-PEG_{24}-IR700 from Prof. Matthias Peipp at the University of Kiel, Germany. BG-PEG_{24}-IR700 molecules were conjugated to the H22(scFv)-SNAP at a molar ratio of 3:1 (three-fold) for 2 hours at 37°C. The successful labelling of BG-PEG_{24}- IR700 to H22(scFv)-SNAP was confirmed by visualization of the fluorescence signal on an SDS-PAGE gel (Figure 3.22 a and b) using the iBrightFL1000 imaging system (Thermofischer scientific). To confirm successful labelling and generation of PIC, an aliquot of the labelled H22(scFv)-SNAP-IR700 was labelled with BG-Alexa 488 (New England Biolabs) while using the H22(scFv)-SNAP protein as a control. As shown in figure 3.22 c and d, the failure of the BG-Alexa 488 conjugation to H22(scFv)-SNAP-IR700 confirmed the complete saturation of the SNAP-tag moeity in H22(scFv)-SNAP-IR700 by BG-IR700.

Next, photoimmunotoxicity studies of H22(scFv)-SNAP-IR700 against polarized *ex vivo* differentiated hMDMs was conducted using the XTT cell viability assay (2.2.12.2). Briefly, three different doses of H22(scFv)-SNAP-IR700 (– 500 nM, 100 nM and 20 nM) were each incubated with each polarized differentiated hMDMs sub-types for 3 hours. Afterwards, the cells were washed with sterile dPBS twice and irradiated for 15 mins. After irradiation, cells was washed twice with sterile dPBS and replaced with sterile RPMI media for 48 hours, after which XTT reagents was used to evaluate cell viability. The results in figure 3.23 showed that H22(scFv)-SNAP-IR700 was cytotoxic to all polarized *ex vivo* differentiated hMDMs. However, M1(IFN-γ +LPS) macrophages demonstrated more photokilling at all drug concentrations used in comparison to M2(IL-4) and resting M (0) macrophages, potentially due to the upregulation of CD64 and more bioaccumulation of the photosensitizer (PS).

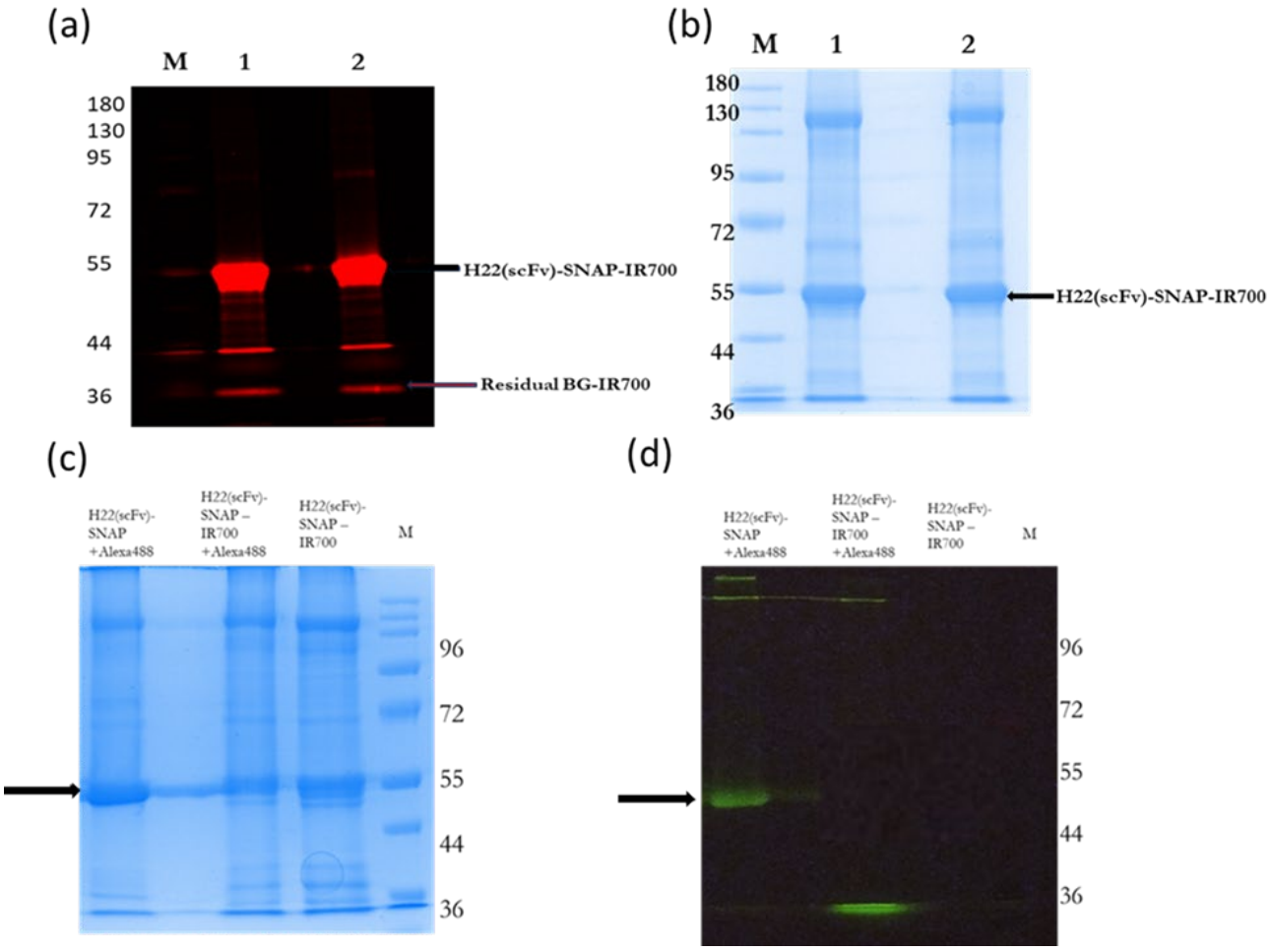

Figure 3.22. Generation of anti-CD64 PIC, H22(scFv)-SNAP-IR700 and confirmation of optimal labelling.

(a-b) SDS-PAGE followed by fluorescence visualization . H22(scFv)-SNAP was incubated with a 3-fold molar excess of BG-PEG$_{24}$-IR700 for 2 hours at 37°C. Images were captured on the iBrightFL1000 imaging system (Thermofischer scientific). BG-PEG$_{24}$-IR700 (red band) was successfully conjugated to H22(scFv)-SNAP (black arrow) with few residual BG-PEG$_{24}$-IR700 (red arrow). (c-d) Generation of PIC, H22(scFv)-SNAP-IR700: Complete saturation of the SNAP-tag FP was confirmed by the failure of BG-Alexa 488 to conjugate to PIC, H22(scFv)-SNAP-IR700, while still conjugating with the control, H22(scFv)-SNAP (indicated by black arrow) at 53 kDa. The generated PIC, H22(scFv)-SNAP-IR700 was used for downstream photoimmunotoxicity studies on differentiated hMDMs.

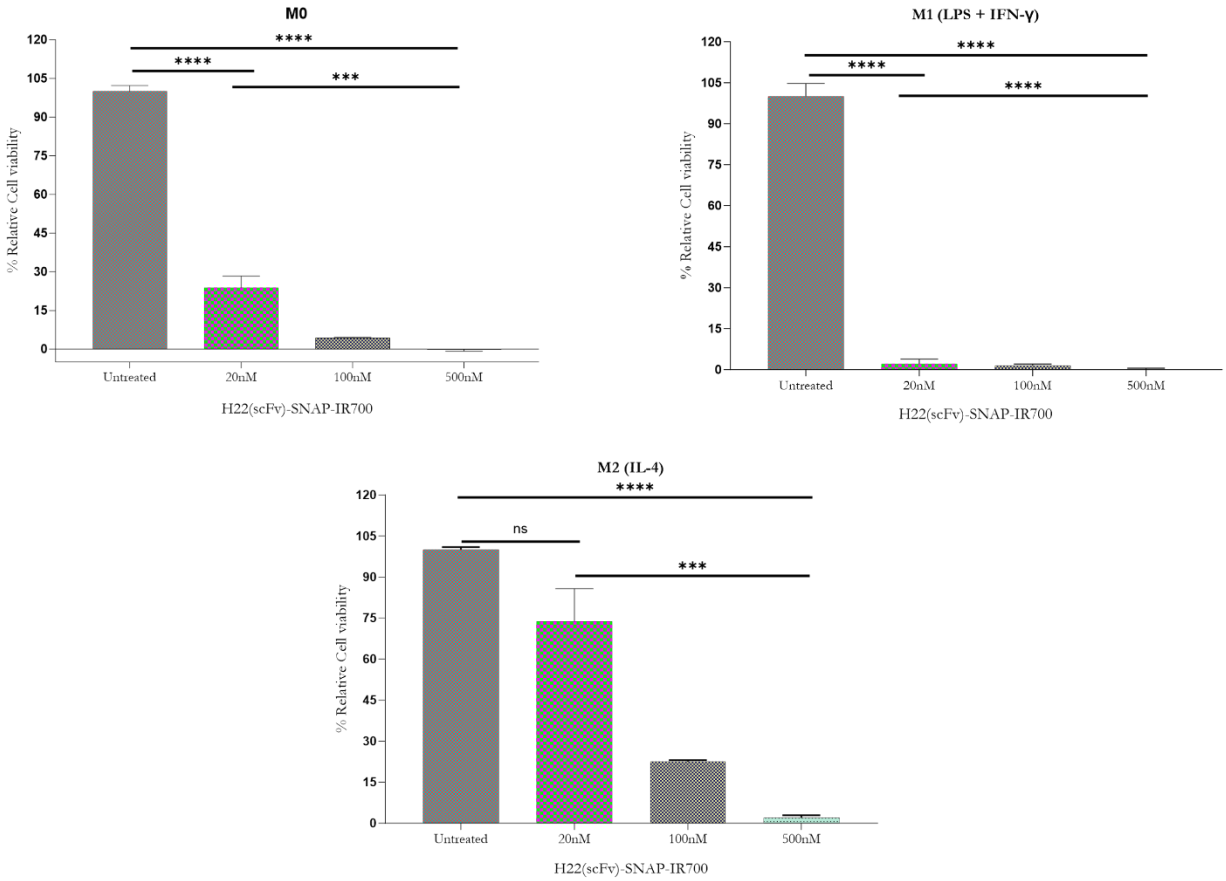

Figure 3.23. Toxicity profile of PIC, H22(scFv)-SNAP IR700 on *ex vivo* differentiated macrophages.

Confirmation of cytotoxic activity for recombinant PIC, H22(scFv)-SNAP-IR700 on polarized *ex vivo* differentiated hMDMs. Photoimmunotoxicity studies were completed with XTT assay (2.2.12.2). The results shows the PIC toxicity towards all polarized differentiated hMDMs . p-values calculated by one-way ANOVA test **** = $p < 0.0001$ across all concentration vs untreated control. p-values comparing killing between concentrations using one-way ANOVA test: M(0), M2(IL-4) ; $p < 0.001$(***), M1(LPS + IFN-γ) ; $p < 0.0001$ (****). Also student parametric t-test to compare lowest dose (20 nM) to untreated shows: M2(IL-4); p =ns, M(0), M1(LPS + IFN-γ); $p < 0.001$ (****). Overall, the photoimmunotoxicity was highest in M1(LPS + IFN-γ) macrophages due to greater amount of bioaccumulation of PS, IR700.

|CHAPTER 4: DISCUSSION|

4.1 Targeted therapy against dysfunctional macrophages

Myeloid-derived cells especially macrophages and monocytes play major physiological roles in the body, especially during homeostasis, immunity, and tissue development. Also, they have been linked to the pathogenesis of a plethora of human diseases, especially those associated with chronic inflammation (and diseases), autoimmunity and cancers [3, 170].

Despite advancements in biomedical research and innovation, there exists an urgent medical need for the development of drugs to effectively treat these ailments in patients. In the past years, nano-based systems have been used for preclinical treatment of macrophage-mediated dysfunctions [171, 172]. Ferumoxytal nanoparticles inhibited tumor growth in breast cancer and liver and lung metastasis (small cell lung cancers) via reprogramming of tumor macrophages to anti-tumor M1(LPS+IFN-γ) macrophages [173], and intraperitoneal injection of novel liposomal clodronate (Clo-Lipo-DOTAP) depletes TAMs involved in tumor angiogenesis and reduces tumor volume in melanoma [172]. Furthermore, Liposomal clodronate has been used to deplete resident tissue dysfunctional macrophages for treatment of obesity complications [174], rheumatoid arthritis [175], and endometriotic lesions [176]. In a study by Ortega and colleagues, mannosylated nanoparticles encapsulating small interfering RNAs (siRNAs) were used to induce cytotoxic and immunostimulatory activity in *ex vivo* macrophages/ TAMs via restoration of NF-ϰB signaling pathways [177]. Unfortunately, due to inability to distinguish normal from aberrant cells, nano-based drugs often result in off-target systemic toxicities despite preclinical efficacy [170].

To overcome this limitation, antibody-based therapy, especially monoclonal antibodies (mAbs) therapies have been developed. Noteworthy is that most hybridoma-derived mAbs are specific gamma immunoglobulins (IgG) with the same specificity and affinity for an overexpressed antigen/protein or receptor on diseased cells. Several monoclonal antibodies have been approved by the Food and Drug Association (FDA) for (pre)clinical applications in cancers and inflammatory diseases [68]. In cancer therapy, Trastuzumab (Herceptin ®) targeting human epidermal growth receptor 2 (HER2) was approved for the treatment of invasive breast cancer [178], Panitumumab (Vectibix ®) targeting Epidermal growth factor receptor (EGFR) was approved for the treatment of colorectal cancer [179], and Gemtuzumab ozogamicin (Mylotarg ®) targeting overexpressed CD33 was approved for the treatment of acute myeloid leukemia (AML) [180]. Also, anti-tumor necrosis factor-alpha (TNF-α) specific drugs, Infliximab (Remicade ®), Certolizumab pegol (Cimzia ®) and Golimumab was approved by the FDA with clinical efficacy and safety in the treatment of rheumatoid arthritis (RA) [181, 182], and anti-amyloid-β mAbs – Aducanumab and Bapineuzumab have been approved for the treatment of Alzheimer's disease

=(AzD) [183], which highlights the use/application of mAbs in treatment of chronic inflammatory diseases [68]. On the other hand while mAbs have demonstrated therapeutic efficacy in the treatment of several cancers either as standalone or combinational therapeutics, their clinical potential is limited by large molecular weight (~150 kDa) which often results in low tumor penetration, difficulty in drug clearance and could possibly lead to drug resistance [69].

To improve treatment outcomes and clinical efficacy, the use of full-length mAbs have now been replaced with antibody fragments such as the small-sized (~25 kDa -30 kDa) single-chain fragment variables (scFv), which are used for the generation of recombinant therapeutics for clinical applications. In this context, the recombinant immunotherapeutics developed in this thesis contains two basic fragments: (1) an H22(scFv) antibody fragment that is cell-specific and binds to the CD64 receptor, (2) a cytotoxic molecule which induces cell death upon internalization in the target cells [184]. Interestingly CD64 (or FcγRI) is primarily expressed on myeloid cells especially macrophages and monocytes, and upon activation, dysregulation, or dysfunction, CD64 is upregulated (or overexpressed). Hence, CD64 was identified as a prime immunotherapeutic receptor/target for the treatment of chronic diseases mediated by dysfunctional macrophages and monocytes [52]. In this thesis, the therapeutic potential of four CD64-targeting therapies was investigated for their ability to selectively eliminate CD64+ monocytic cell lines (mimicking CD64+ monocyte-derived acute myeloid leukemia) and subtypes of CD64+ *ex vivo* differentiated macrophages (implicated in the etiology of most chronic inflammatory diseases and cancers).

4.2 Production and evaluation of anti-CD64 recombinant proteins for their immunodiagnostic potential

While targeted therapy and the use of recombinant antibody-based therapy has shown some success in the clinics [69], the production of recombinant antibody fusion proteins remain challenging for several reasons. Such challenges include the selection of a suitable host of expression (bacteria, yeast, or mammalian cells) for the fusion protein to maximize yield, achieving correct protein folding and post-translational modification to obtain consistent quality and activity, problems with protein purification and stability etc. In this thesis, the successful expression of anti-CD64 fusion proteins was dependent on three factors: (i) identifying a suitable host of expression, (ii) high-quality plasmids DNA, and (iii) optimized expression conditions [185]. Interestingly, genetic engineering and biotechnology have allowed the production of recombinant proteins with desired functional properties from diverse expression systems. These recombinant proteins are currently applied in (pre)clinical use as novel biopharmaceuticals [185, 186]. In this study, two

major hosts of expression were used to produce anti-CD64 recombinant proteins: the bacterial *E coli* BL21(DE3) [187], and mammalian HEK293T cells [186].

H22(scFv) ETA` and H22(scFv)-dETA`(RG7787-MT2) were expressed in E. coli BL21(DE3) using the compatible solute-supported periplasmic stress expression protocol established by Barth et al. [151]. Aside from the benefits of fast growth kinetics, high cell culture density, readily available rich culture medium and fast exogenous DNA transformation in *E. coli,* BL21(DE3) strain has the advantage of deficient genes expressing proteases which can destroy recombinant proteins [188, 189]. Furthermore, it is well suited for compatible solute stress induction as proteins can easily be directed into the periplasmic space to avoid proteolytic degradation [151, 190]. Before expression, pMT-H22(scFv)-ETA` plasmid DNA was retrieved from glycerol stocks in the MB&I lab storage and purified (Table 3.1). The high-quality plasmid was used as a template via molecular cloning for the generation of a deimmunized variant, pMT-H22(scFv)-dETA`(RG7787-MT2) (Figure 3.3-3.5) to be transformed for recombinant protein production in *E. coli.* In this study, successful expression of difficult to expres rITs, H22(scFv)-ETA` and H22(scFv)-dETA`(RG7787-MT2) was possible with the compatible solutes – supported stress expression protocol [151]. This expression medium allows for the production of structutal and functional proteins in *E. coli* BL21(DE3). First the osmotic stress expression protocols prevents protein misfolding and accumulation of fusion proteins into inclusion bodies. Fusion proteins shunt into inclusion bodies are difficult to recover, and requires demanding denaturing and renaturing procedure which produces low yield proteins functional proteins [151, 191]. Second, the protocol used direct proteins into intracellular environment and oxidative milieu in the periplasmic space which is necessary for proper protein folding, disulfide bond formation and protein stability [187]. Lastly, in this study, an optimized IPTG concentration of (1mM) to induce protein expression for 16 hours contributed to good recovery and production of full-length proteins in the periplasmic space of *E. coli* [151, 192]

After protein expression, the fusion proteins were successfully purified using a two-step IMAC purification protocol (at physiological pH 8.0). After purification, the SDS-PAGE gel after 2nd IMAC showed full-length proteins at 72.5 kDa for both H22(scFv)-ETA` and H22(scFv)-dETA`(RG7787-MT2) but also observed is the presence of contaminating protein bands (Figure 3.6 A). To improve the purity of the IMAC-purified proteins and remove the containminants, SEC was used through exchanging the elution buffer into PBS (pH 7.4) [193]. The SEC-purified proteins - H22(scFv)-ETA` and its deimmunized version, H22(scFv)-dETA`(RG7787-MT2) were structurally validated with SDS-PAGE and and western blot analysis. Like IMAC, both full-length proteins were present at 72.5 kDa with cleaner protein bands (purity) on the SDS gel and presence

.[101].

of poly-histidine ptoteins on the western blot (Fig 3.6 B and C). After structural validation of full-length purified rITs, the yield recovered from lab shaking culture flasks was 1.185 mg/L of H22(scFv) ETA` and 1.05 mg/L H22(scFv)-dETA`(RG7787-MT2) which was preferably good yield and used succesfully for downstream functional assays.

H22(scFv)-SNAP was produced via transient expression in mammalian HEK293T cellsIn this study, transfection of HEK293T cells with pCB-H22(scFv)-SNAP using X-tremeGENE transfection reagent (Merck, USA) yielded a transfection efficiency of 60% (Figures 3.7-3.8) which is comparable to previous studies [194]. Subsequently, zeocin (selection) treatment improved the enrichment of viable eGFP-expressing cells and H22(scFv)-SNAP production in the CCSN of HEK293 T cultures (Figure 3.9). After IMAC purification of CCSN containing H22(scFv)-SNAP, the full-length protein was successfully confirmed with SDS-PAGE and western blot analysis present at ~ 53 kDa(Figure 3.10A). Furthermore, H22(scFv)-SNAP showed considerable conjugation to BG-Alexa 488 , confirming functionality of the SNAP-tag domain of the full-length proteins to react with BG-modified substrates which is essenttial in the production of SNAP-tag antibody conjugates especially recombinant ADC and PIC evaluated in this study (Figure 3.10B). Also observed on gel samples (Figure 3.10A and B) are negligible protein protein bands at ~130 kDa and 34 kDa respectively. These bands could be removed by further purification such as SEC [193], and protein proteolysis could be prevented by the addition of protease inhibitors into CCSN before IMAC purification to improve protein stability [195]. As well, the recovered yield of H22(scFv)-SNAP was 1.77mg/L of CCSN which was a good yield from standard lab flask-based systems and was sufficient for successful downstream functional assays. However, therapeutic proteins yield in HEK29T could be further improved with high density fermentation in small -scale bioreactors under standard lab cultivation conditions [196].

Following structural validation of each anti-CD64 fusion proteins using a mix of SDS-PAGE and western immunoblotting, functional antigen-dependent binding was confirmed using flow cytometric analysis on IFN- γ stimulated U937 cells, with each recombinant protein, H22(scFv)-ETA`, H22(scFv)-dETA`(RG7787-MT2), and H22(scFv)-SNAP demonstrating significant binding of 87%, 75.2%, and 85.7% respectively (Figure 3.11). Interestingly, this functional binding by anti-CD64 recombinant proteins also confirms its potential towards stimulated CD64+ monocytic cells, and not CD64- cells (MDA MB 468) (Figure 3.11), hence indicative that the scFv antibody of each recombinant protein are well folded and maintains sufficient functional antigen-binding properties.

4.3 Phenotypic characterization and biological activity of H22(scFv)-SNAP on polarized *ex vivo* differentiated hMDMs

Naïve macrophages are myeloid-derived cells usually produced from the differentiation of circulating monocytes [197]. They are highly plastic cells which can be polarized into distinct phenotypic features based on stimulus within the microenvironment milieu [11]. *Ex vivo* differentiated hMDMs (Figure 2.1) are polarized to M1(LPS+IFN-γ) macrophages upon stimulation with LPS and IFN-γ, M2(IL-4) macrophages are stimulated by IL-4, while unstimulated cells are referred to resting M(0) macrophages [9]. In this study, macrophage subtypes (M1(LPS+IFN-γ), M2(IL-4) and M(0)) were profiled/investigated for distinguishing phenotypic features [10].

Confocal imaging analysis showed the morphology of all macrophage subtypes including their multinucleated fused nuclei [165]. However, the morphology of each macrophages subtypes was unique. Most M1(LPS+IFN-γ) macrophages have elongated shapes/appearance compared to M(0) and M2(IL-4) macrophages which have a more flattened or broad (extended) appearance (Figure 3.12) [198]. Furthermore, surface receptor validation was used to characterize successful polarization of the macrophages sub-types using flow cytometry analysis. The result (Figure 3.13) showed upregulation of CD14 present on M1(LPS+IFN-γ) macrophages compared to M2(IL-4) and M(0). This aligned with lieterature as CD14 is essential for phagocytosis and activation of immune cells towards inflammatory response against bacterial infections [199]. In contrast, CD206 (otherwise referred to as mannose receptor) is upregulated on M2(IL-4) macrophages compared to M1(LPS+IFN-γ) and M(0) macrophages (Figure 3.13). CD206 influences anti-inflammatory responses in M2(IL-4) macrophages and potentially plays a role in innate and adaptive immunity against infectious diseases [200]. Once the *ex vivo* differentiated macrophages were confirmed to be successfully polarized to different sub-types, they were then used for downstream assays.

Based on the background that CD64 is upregulated on polarized macrophages and activated monocytic cells, a flow cytometric analysis using a labelled CD64 antibody was used to validate its upregulation. The results indicate baseline expression in M(0) (49 %), while M1(LPS+IFN-γ) and M2(IL-4) demonstrate upregulated CD64 receptor of 98.8 % and 79.4 % respectively (Figure 3.14), which preferably highlights M1(LPS+IFN-γ) macrophages as a prime target for anti-CD64 immunotherapeutics, although M2(IL-4) and M(0) macrophages could be targeted as well due to their CD64 expression [167]. Subsequently, the immunodiagnostic potential of H22(scFv)-SNAP-Alexa 647 conjugate on stimulated macrophages was validated both with flow cytometry and confocal analysis. The labelling of SNAP fusion protein, H22(scFv)-SNAP with a BG-modified flurophore, BG-Alexa 647 to generate a targeted diagnostic probe, H22(scFv)-SNAP-Alexa 647

.[103].

(Figure 3.15A) which upon internalization by localized macrophages subpopulations can be useful as a visualization tool to determine the target sites for the anti-CD64 immunotherapeutics. The result from the flow cytometry (binding) analysis of H22(scFv)-SNAP-647 demonstrated binding to all macrophages sub-types. However, the highest binding was observed in M1(LPS+IFN-γ) macrophages (87.4 %) compared to M2(IL-4) macrophages (73.3 %) and M(0) (55.6 %) which corresponds to the CD64 expression levels on the surface of the polarized macrophages (Figure 3.15B). Furthermore, confocal microscopic imaging allows to validate the proportionate internalization of labelled SNAP-FP, H22(scFv)-SNAP-Alexa647 in different macrophage subtypes – M(0), M1(LPS+IFN-γ) and M2(IL-4) (Figure 3.16) based on their CD64 expression levels. This result confirms that all macrophage subtypes are able to internalize CD64-targeting immunotherapeutics, and can serve as a precise theraoy for macrophages-mediated diseases depending on the dominat subpopulation in the disease model. For example, a specific CD64-based therapeutic agent can be used for targeted elimination of M2-protumor macrophages in cancers (i.e solid tumors, hematological cancers e.g AML), treatment or M2-type parasite-hosted macrophages in cutaneous leishmaniasis, dysregulated M1-proinflammatory macrophages in treatment of chronic inflammatory diseases (e.g rheumatoid arthritis, chronic skin inflammation etc), and infected M(0) macrophages unactivated in host cells. Overall, these phenotypic and functional evaluations validate CD64 as an attractive immunodiagnostic/immunotherapeutic target in different macrophages subtypes [167, 168].

4.4 Immunotherapeutic potential of CD64-targeting recombinant immunotoxin (rITs)

As described in section 1.7, rITs are fusion proteins containing a cell-binding domain (e.g. scFv) genetically fused to plant or bacterial toxins and induce apoptosis in target diseased cells via inhibition of protein biosynthesis [201]. Most rITs are produced with bacterial *pseudomonas* exotoxin A (called PE) and diphtheria toxin instead of plant toxin , ricin A due to high production yield and potency, and relatively low non-specific toxicities [100, 201].

Over the last three decades of rIT development, they have been preclinically evaluated for treatment of several human pathologies like autoimmune diseases [202] and cancers [102] either hematological [203, 204] or solid tumors [205]. In addition, previous studies from our lab have demonstrated successful preclinical outcomes with the use of rITs against inflammatory diseases [92, 104] and cancers [85, 93]. In this study, H22(scFv)-ETA` was evaluated for its selective cytotoxic potential towards IFN-γ stimulated U937 and HL-60 cells, which both express CD64 at high levels. The result showed that H22(scFv)-ETA` demonstrate cytotoxicity at picomolar concentrations with IC_{50} of 423.3 pM and 522.6 pM on IFN-γ stimulated U937 and HL-60 cells

.[104].

respectively but do not affect A2058 (CD64-) cells (Figure 3.17). This further strengthens the pool of scientific evidence demonstrating the cytotoxicity of H22(scFv)-ETA` against activated CD64+ monocytic cells which has been applied in the treatment of acute myeloid-derived leukemia [93] and chronic cutaneous inflammation or skin lesions [94, 103].

As mentioned earlier in section 1.9, immunogenecity remains a limiting factor in the use of rITs in patients, oweing to the generation of neutraliizng antibodies against the toxin domain of the rIT. Against this background, we developed the H22(scFv)-dETA`(RG7787-MT2) as a next generation deimmunized immunotoxin (Figure 3.3 – 3.5) . After employing some site-directed alanine mutagenesis on ETA`(RG7787 (R456T)- R490A) otherwise refereed (RG7787-MT2), the ADP ribosylation assay was used to investigate if the dETA` toxin moeity retains its enzymatic potential. This assays involves the evaluation of the activity of immunotoxins (ETA`/dETA`) by their ability to reduce elongation factor 2 (EF2)(sourced from wheat germ) in cells. This also represents the immunotoxin's mechanism of apoptotic induction by the termination of the protein translation process [163]. As documented in the immunoblot visualization and ImageJ extrapolation, H22(scFv)-dETA`(RG7787-MT2) demonstrate retentive enzymatic activity with distinct bands which corresponds to ribosylated/reduced EF2 (95.7 kDa). However, when compared with wild-type H22(scFv)-ETA`, the enzymatic activity was lower (Figure 3.18).

On a final note, the biological activity of H2(scFv)-dETA`(RG7787-MT2) was evaluated towards IFN-γ stimulated U937 and HL60 cells. The result showed that H22(scFv)-dETA`(RG7787-MT2) demonstrated cytotoxic killing at nanomolar concentrations with IC_{50} values of 3.486 nM and 7.064 nM on IFN-γ stimulated U937 and HL60 cells respectively but does not affect A2058 (CD64-) cells (Figure 3.17). Although both immunotoxins are enzymatically active and exerts selective cytotoxicity towards IFN-γ stimulated CD64+ monocytic cells , H22(scFv)-ETA` exert better enzymatic activity and cytotoxicity compared to its deimmunized variant, H22(scFv)-dETA`(RG7787-MT2) *in vitro*. Conclusively, the results generated from the enzymatic and biological activities of both anti-CD64 immunotoxins variants highlight the immunotherapeutic potency of rITs against CD64+ monocytic cells/ mediated diseases especially those characterized by activated cell types with elevated CD64 levels.

4.5 CD64-targeting SNAP ADC as novel immunotherapeutic agent

Antibody-drug conjugates (ADCs) represent a special class of highly potent biopharmaceuticals designed as targeted therapy for cancer treatments. They contain a cell-specific antibody chemically linked to drug molecules that induce cell death in tumors [125]. As of November 2022, 12 ADCs has been approved by the United States Food and Drugs Administration (US FDA) including

.[105].

Blenrep ® (relapsed/refractory multiple myeloma), Mylotarg ® (acute myelogenous leukemia), Kadcyla ® (metastatic breast cancer), Baspona ® (acute lymphoblastic leukemia), etc. [206, 207]. Currently, over 100 different ADCs are been investigated in several clinical trials towards the treatment of cancers and chronic diseases [208].

One of the challenges associated with conventional ADCs has been variable drug-to-antibody ratios (DAR) due to non-specific chemical conjugation strategies between the drug moiety and antibody [125]. This often results in heterologous ADC formation, reduced clinical efficacy and off-target systemic effects of dissociated payload [209]. The advent of SNAP-tag technology has provided an efficient strategy to overcome the challenge of variable DARs and the development of novel ADC formats by allowing site-specific conjugation of the antibody to the drug in a stochiometric 1:1 ratio [168, 210]. In this study, CD64-targeting SNAP FP, H22(scFv)-SNAP undergoes chemo-enzymatic site-selective conjugation with benzyl guanine (BG) modified monomethyl auristatin F (referred to as BG-MMAF or BG-AURIF) to generate novel ADC format, H22(scFv)-SNAP-AURIF. Monomethyl Auristatin F (referred to as MMAF or AURIF) is a natural chemotherapeutic and anti-mitotic agent derived from dolostatin-10 that disrupts tubulin assembly in target cells, hence inducing apoptosis [134, 135].

Furthermore, the H22(scFv)-SNAP-AURIF ADC possesses a polyethene glycol (PEG) linker sequence that serves as a tether between the cytotoxic payload and scFv antibody [127]. Hydrophilic linkers with negatively charged sulfonate (such as PEG or pyrophosphate) groups are often used in ADC preparation instead of hydrophobic linkers because hydrophobicity has been linked to protein/ADC aggregation [211, 212]. The SNAP-tag ADC investigated in this study was conjugated to BG-linker-AURIF produced by the Hunter group, department of Chemistry, UCT. The cytotoxicity activities of H22(scFv)-SNAP-AURIF were evaluated towards IFN- γ stimulated and unstimulated U937 and HL60 cells. Before the evaluation, a comparative cytotoxicity study of BG-AURIF and AURIF on IFN-γ stimulated U937 was conducted to check for retentive cytotoxicity after BG-modification. Interestingly, a benzyl guanine modification of AURIF demonstrated retentive (and improved) cytotoxicity compared to unmodified AURIF (21.57 nM vs 53.85 nM) (Figure 3.19). Benzyl guanine (BG) can be used as a standalone or in combinational therapy as an anti-neoplastic agent [213, 214], hence modification with BG possibly improved the killing potential of Auristatin F.

Subsequently, H22(scFv)-SNAP-AURIF was evaluated towards IFN-γ stimulated and unstimulated CD64+ monocytic cells. The cytotoxic analysis showed that the ADC demonstrated killing to CD64+ monocytic cells but not CD64-(A2058) at nanomolar concentrations. Comparatively, the cytotoxicity on stimulated cells (IC_{50} = 14.54 nM; 125.0 nM) was higher than

.[106].

on unstimulated cells (617.0 nM; 255.2 nM) (Figure 3.21). This is expected as cytokine stimulation with IFN-γ is linked to upregulated CD64, hence increasing the internalization of AURIF and killing potential compared to unstimulated cells with low/baseline CD64 [55]. Furthermore, ADCs possess an advantage over protein-based therapeutics like immunotoxins (ITs) and cytolytic fusion proteins (hCFPs) because the drug moiety (AURIF) is non-protein and cannot be affected by endosomal protease activity which limits the efficacy of ITs and hCFPs by degrading them at lower concentrations. This also explains why ADCs are effective against unstimulated CD64 cells in comparison to protein-based therapeutics and hCFPs [206, 212].

Conclusively, previous studies have shown the efficacy of H22(scFv)-ETA` and H22(scFv)-GrB (granzyme B) against proliferating CD64+ monocytic cells (activated monocytes) as observed in AML [78, 93], however, the generated ADC investigated in this study could serve as a better therapeutic candidate for AML treatments in the future due to the above mentioned properties.

4.6 Photoimmunotherapeutic application of CD64-targeting SNAP PIC

Photoimmunotherapy (PIT) leverages on the combined clinical benefits of immunotherapy and photodynamic therapy to induce cell death on target diseased cells [139]. Usually, a photoimmunoconjugate (PIC) which contains a cell-specific antibody linked to a photosensitizer (PS) is used. Upon internalization in target cells, and massive bioaccumulation of PS, the exposure of the cells to light at a specific wavelenght, result in the generation of free radicals or reactive oxygen species (ROS) which causes oxidative damage, DNA disruption in target cells and activation of diverse immunogenic cell death mechanisms [139, 141, 142]. Based on low light absorbance and high penetration in human tissues, near-infrared (NIR) and water-soluble phthalocyanine PS, IR700 have been developed and used in conjugation with different monoclonal antibodies for PIT in cancers [215]. Currently, IR700 is used as a theranostic agent – a single molecule with a dual purpose including diagnostic or therapeutic potential [144].

In a comparative manner with SNAP-tag ADC, a SNAP-tag PIC; H22(scFv)-SNAP-IR700 was generated and investigated for selective phototoxicity against polarized *ex vivo* macrophages. The result documented shows that all PIC doses (500, 100, 20 nM) demonstrated phototoxicity on all polarized macrophages subtypes due to CD64 expression on all macrophages and subsequent bioaccumulation of PIC. However, more photokilling was observed in M1(LPS + IFN- γ) macrophages compared to both M2(IL-4) macrophages and resting M (0) macrophages even at the lowest doses (20nM) because of large biaoccumulation of PIC due to its elevated CD64 expression (Figure 3.23). This result highlight the importance of NIR-PIT in targted killing of dysfunctional macrophages or monocytes localized in chronic lesions and solid tumors without

.[107].

causing systemic toxicities. For example, this can applied to dysregulated proinflammatory (M1-type) macrophages present in cutaneous lesions and other chronic inflammatory diseases. Also, tumor-associated macrophages present in most solid cancers can be selectively eliminated after internalization of PIC, and NIR-irradiation. Aside the necrosis from the PIC induced cell death, the immune systems are activated after release of damage-associated molecular patterns (DAMPs), including calreticulin, heat shock proteins (HSPs) etc., which often results in recrutment of immune cells like circulating monocytes, dendritic cells and cytotoxic T lymphocytes (CTLs). Circulating monocytes upon entering are differentiated into M1-type antitumor macrophages and in collaboration with cytotoxic T-lymphocytes destroys residual tumor mass via immunogenic cell death [142, 150]. Over all, SNAP-tag PIC provides an effective (pre) clinical diagnostic/therapeutic tool towards localized diseased cells with least side effects especially systemic toxicities.

.[108].

|CHAPTER 5: CONCLUSION AND FUTURE PERSPECTIVES|

Dysfunctional macrophages and monocytes are major drivers of human pathologies specifically chronic inflammatory diseases and cancers [10]. Over the last two decades, there has been increasing interest in the development of curative clinical agents especially immunotherapeutics that selectively eliminate these dysfunctional cells, and overcome the limitations associated with conventional symptomatic therapies [20, 68, 103].

In this study, recombinant antibody formats targeting the CD64 receptor present abundantly on monocytes and macrophages were evaluated for their therapeutic potential using CD64+ monocytic cell lines and polarized *ex vivo* differentiated human macrophages as preclinical experimental models. The therapeutics evaluated include recombinant immunotoxin (rIT); its deimmunized variant, SNAP-tag-based ADC ; and PIC.

As shown above, the rIT, H22(scFv)-ETA` and its deimmunized version, H22(scFv)-dETA`(RG7787-MT2) demonstrated successful binding and selective cytotoxicity against CD64+ monocytic cell lines at nanomolar concentrations. Previous studies from our lab have also validated this outcome in which H22(scFv)-ETA` has been used in the treatment of chronic skin inflammation like unhealing wounds, atopic dermatitis [94, 104] and myeloid-derived leukemia xenograft models [93]. An interesting step towards addressing the negative immune response (immunogenicity) arising from rIT usage, led to the development of a next generation deimmunized variant, H22(scFv)-dETA`(RG7787-MT2) which was evaluated in this study. H22(scFv)-dETA's(RG7787-MT2) enzymatic and cytotoxic activities were confirmed in this thesis, however further in vivo research is needed to for immunogenicity testing. Also, an area of research interest, potentially during a PhD study to advance on the current findings will be to generate anti-CD64 specific recombinant nanobodies (VHH) genetically fused to ETA`/dETA`(RG7787-MT2). The hypothesis is that based on the relative small size of VHH (~15 kDa) compared to an scFv (~30 kDa), could help increase cell penetration, cytosolic accumulation, and faster systemic clearance [216, 217]. Lastly, a previous study has confirmed that an increase in valency also increases the efficacy of anti-CD64 recombinant immunotoxins [94]. This is because crosslinking the CD64 receptors by the bivalent antibody increases receptor crosslinking mediated internalization of the toxin and by so doing increases dose-dependent cytotoxicity and clinical efficacy. Hence, a bivalent anti-CD64 deimmunized immunotoxin variant, (H22(scFv))2 -dETA`(RG7787-MT2) can be generated and evaluated for improved efficacy like bivalent rIT, (H22(scFv))2 -ETA` - dual benefits of immunogenecity with bivalency in determination of cytotoxicity/clinical efficacy [50, 51].

.[109].

Aside from rITs, another class of CD64-targeting immunotherapeutics investigated in this study is the SNAP-tag fusion protein. The SNAP-tag is a self-labelling protein that allows auto-labelling of BG-modified substrates with a protein of interest. In this study, SNAP-tag-based ADC; H22(scFv)-SNAP-AURIF successfully induced apoptosis in activated CD64+ proliferating cells. Interestingly, auristatin F (AURIF) is an antimitotic agent that induces cell death by microtubule destruction upon internalization. Hence, H22(scFv)-SNAP-AURIF was effective both on stimulated and unstimulated CD64+ monocytic cells, although activation increased cytotoxicity based on CD64 upregulation. This could apply to normal acute inflamed cells in atopic dermatitis as well as myeloid-derived leukemia with CD64+ presentation.

In a previous study conducted in our lab, a bispecific antibody, bs-Ki4-H22 demonstrated Fc-γ mediated elimination of CD30+ Hodgkin lymphoma cells [218]. Based on this background, a recombinant bispecific antibody could be used to generate a novel ADC. For example, in leukemic blasts, high-expressing CD33 and CD64 could be used to generate a bispecific antibody and investigate for therapeutic potential on myeloid-derived cells. Another interesting area of research with SNAP-tag ADC would be to investigate fully the internalization and track its routing mechanisms. In this study, Alexa647-labelled H22(scFv)-SNAP-fusion protein was internalized by all macrophage sub-types as expected, however, the exact organelles of localization/staining were not investigated. In future studies, it will be interesting to investigate if fusion proteins are routed to the lysosomes, golgi network, nucleus etc. Such studies might help identify molecular adapters that could help direct the translocation of the therapeutic molecule to the part of the cell for exerting their biological activity.

Like SNAP-tag ADC, a recombinant PIC, H22(scFv)-SNAP-IR700 was generated and confirmed to have successfully induced photokilling in all polarized *ex vivo* differentiated human macrophages. An advantage of IR700 over other photosensitizers is that it is a theranostic with high penetration in tissues and minimally invasive [219]. Upon exposure of IR700 to near-infrared light, ROS is generated which often results in cell death due to membrane disruption, damage to organelles and DNA damage [219]. As reported in literature, photokilling is proportional to bioaccumulation of PIC in localized cell type [139], and as observed in this study, M1(LPS + IFN- γ) has the highest bioaccumulation and more photokilling at lowest dose compared to M2(IL-4) and M(0).

Potentially, this novel SNAP-tag PIC adds another level of targted protection to normal/healthy cells as targted photokilling of dysfunctional macrophages can be confined to a localized area or tissue by the activation of PIC by NIR light. This can be used for localized skin lesions in atopic dermatitis and localized solid tumors. Worthy of note, IR700 is a theranostic fluorophore i.e., a single molecule with dual diagnostic and therapeutic potential. In this study, the therapeutic

potential was evaluated, however, in a future study, the diagnostic potential of IR700 will be investigated first by tracking its bioactivity / bioaccumulation in vivo before activation of the PIC in target tissues with NIR light. As well, of importance is the antibody format used for generating PIC. In a previous (MSc) project in our lab, *Maryam Karaan* generated monovalent and bivalent anti-chondroitin sulphate proteoglycan 4 (CSPG-4) recombinant SNAP-tag fusion protein towards triple negative breast cancers (TNBCs) and concluded that monovalent proteins are more efficient as immunodiagnostic agents while bivalent proteins are more efficient as immunotherapeutic agents. In a future study, monovalent and bivalent CD64-targeting SNAP-tag IR700 could be investigated to validate their efficacy as either immunodiagnostic or immunotherapeutic agents on activated CD64+ monocytic cells compared to monovalent contructs documented in this research work.

In summary, this thesis documents the therapeutic potential of four CD64-targeting immunotherapeutics – H22(scFv)-ETA` , H22(scFv)-dETA`(RG7787-MT2), H22(scFv)-SNAP-AURIF, and H22(scFv)-SNAP-IR700 as a potential clinical agents for the treatment of diseases caused by macrophages and monocytes especially chronic inflammatory skin diseases, skin cancers, AML and solid tumors etc., and provides extensive areas to be explored for future (pre) clinical studies.

| CHAPTER 6: REFERENCES |

1. Gordon S: **Elie Metchnikoff: father of natural immunity**. *European journal of immunology* 2008, **38**(12):3257-3264.
2. Wynn TA, Chawla A, Pollard JW: **Macrophage biology in development, homeostasis and disease**. *Nature* 2013, **496**(7446):445-455.
3. Matin MA, Hossen MJ, Ahmed MS, Rahman M, Sikder MH: **The role of macrophages in inflammation**. In: *Recent Advancements in Microbial Diversity.* Elsevier; 2022: 53-71.
4. Pei Y, Yeo Y: **Drug delivery to macrophages: challenges and opportunities**. *Journal of Controlled Release* 2016, **240**:202-211.
5. Ginhoux F, Jung S: **Monocytes and macrophages: developmental pathways and tissue homeostasis**. *Nature Reviews Immunology* 2014, **14**(6):392-404.
6. Epelman S, Lavine KJ, Randolph GJ: **Origin and functions of tissue macrophages**. *Immunity* 2014, **41**(1):21-35.
7. Sreejit G, Fleetwood AJ, Murphy AJ, Nagareddy PR: **Origins and diversity of macrophages in health and disease**. *Clinical & Translational Immunology* 2020, **9**(12):e1222.
8. Mantovani A, Sica A, Sozzani S, Allavena P, Vecchi A, Locati M: **The chemokine system in diverse forms of macrophage activation and polarization**. *Trends in immunology* 2004, **25**(12):677-686.
9. Martinez FO, Sica A, Mantovani A, Locati M: **Macrophage activation and polarization**. *Frontiers in Bioscience-Landmark* 2008, **13**(2):453-461.
10. Sica A, Erreni M, Allavena P, Porta C: **Macrophage polarization in pathology**. *Cellular and molecular life sciences* 2015, **72**(21):4111-4126.
11. Lee KY: **M1 and M2 polarization of macrophages: a mini-review**. 2019.
12. Dey A, Allen J, Hankey-Giblin PA: **Ontogeny and polarization of macrophages in inflammation: blood monocytes versus tissue macrophages**. *Frontiers in immunology* 2015, **5**:683.
13. Martinez FO, Helming L, Gordon S: **Alternative activation of macrophages: an immunologic functional perspective**. *Annual review of immunology* 2009, **27**(1):451-483.
14. Mosser DM: **The many faces of macrophage activation**. *Journal of leukocyte biology* 2003, **73**(2):209-212.
15. Mantovani A, Biswas SK, Galdiero MR, Sica A, Locati M: **Macrophage plasticity and polarization in tissue repair and remodelling**. *The Journal of pathology* 2013, **229**(2):176-185.
16. Mantovani A, Sozzani S, Locati M, Allavena P, Sica A: **Macrophage polarization: tumor-associated macrophages as a paradigm for polarized M2 mononuclear phagocytes**. *Trends in immunology* 2002, **23**(11):549-555.
17. Chanmee T, Ontong P, Konno K, Itano N: **Tumor-associated macrophages as major players in the tumor microenvironment**. *Cancers* 2014, **6**(3):1670-1690.
18. Duluc D, Corvaisier M, Blanchard S, Catala L, Descamps P, Gamelin E, Ponsoda S, Delneste Y, Hebbar M, Jeannin P: **Interferon-γ reverses the immunosuppressive and protumoral properties and prevents the generation of human tumor-associated macrophages**. *International journal of cancer* 2009, **125**(2):367-373.
19. Labonte AC, Tosello-Trampont A-C, Hahn YS: **The role of macrophage polarization in infectious and inflammatory diseases**. *Molecules and cells* 2014, **37**(4):275.

20. Chen S, Saeed AF, Liu Q, Jiang Q, Xu H, Xiao GG, Rao L, Duo Y: **Macrophages in immunoregulation and therapeutics**. *Signal Transduction and Targeted Therapy* 2023, **8**(1):207.
21. Sica A, Mantovani A: **Macrophage plasticity and polarization: in vivo veritas**. *The Journal of clinical investigation* 2012, **122**(3):787-795.
22. Urban K, Chu S, Giesey RL, Mehrmal S, Uppal P, Nedley N, Delost GR: **The global, regional, and national burden of atopic dermatitis in 195 countries and territories: an ecological study from the Global Burden of Disease Study 2017**. *JAAD international* 2021, **2**:12-18.
23. Kiekens R, Thepen T, Bihari I, Knol E, Van De Winkel J, Bruijnzeel-Koomen C: **Expression of Fc receptors for IgG during acute and chronic cutaneous inflammation in atopic dermatitis**. *British Journal of Dermatology* 2000, **142**(6):1106-1113.
24. Ou L-S, Leung D: **Advances in atopic dermatitis**. *Chang Gung medical journal* 2005, **28**(1):1-8.
25. Kasraie S, Werfel T: **Role of macrophages in the pathogenesis of atopic dermatitis**. *Mediators of inflammation* 2013, **2013**.
26. Breuer K, Kapp A, Werfel T: **Bacterial infections and atopic dermatitis**. *Allergy* 2001, **56**(11):1034-1041.
27. Kiekens R, Thepen T, Oosting A, Bihari I, Van de Winkel J, Bruijnzeel-Koomen C, Knol E: **Heterogeneity within tissue-specific macrophage and dendritic cell populations during cutaneous inflammation in atopic dermatitis**. *British Journal of Dermatology* 2001, **145**(6):957-965.
28. Leung DY, Boguniewicz M, Howell MD, Nomura I, Hamid QA: **New insights into atopic dermatitis**. *The Journal of clinical investigation* 2004, **113**(5):651-657.
29. Yamanaka K-i, Mizutani H: **The role of cytokines/chemokines in the pathogenesis of atopic dermatitis**. *Pathogenesis and Management of Atopic Dermatitis* 2011, **41**:80-92.
30. Leung DY: **Atopic dermatitis: new insights and opportunities for therapeutic intervention**. *Journal of Allergy and Clinical Immunology* 2000, **105**(5):860-876.
31. Awad N, Abaas A, Altayeb N, Khalil H: **HEMATOLOGICAL PARAMETERS OF CHRONIC MYELOID LEUKEMIA PATIENTS IN SUDAN TREATED WITH IMATINIB**. *European Journal of Biomedical* 2021, **8**(7):01-04.
32. Stone RM, O'Donnell MR, Sekeres MA: **Acute myeloid leukemia**. *ASH Education Program Book* 2004, **2004**(1):98-117.
33. Watts J, Nimer S: **Recent advances in the understanding and treatment of acute myeloid leukemia**. *F1000Research* 2018, **7**.
34. Khan M, Din M, Naeem Z, Sajid Z, Dilawar Khan A, MD ZA, Anwar F, Akhtar M, Noreen S: **Insights Into Acute Myeloid Leukemia: Critical Analysis In Its Wide Aspects**. *Abasiyan journal of Life Sciences* 2020, **3**(2).
35. Bennett JM, Catovsky D, Daniel MT, Flandrin G, Galton DA, Gralnick HR, Sultan C: **Proposed revised criteria for the classification of acute myeloid leukemia: a report of the French-American-British Cooperative Group**. *Annals of internal medicine* 1985, **103**(4):620-625.
36. Thepen T, Huhn M, Melmer G, Tur M, Barth S: **Fcγ receptor 1 (CD64), a target beyond cancer**. *Current pharmaceutical design* 2009, **15**(23):2712-2718.
37. Tur MK, Huhn M, Thepen T, Stöcker M, Krohn R, Vogel S, Jost E, Osieka R, van de Winkel JG, Fischer R: **Recombinant CD64-specific single chain immunotoxin exhibits specific cytotoxicity against acute myeloid leukemia cells**. *Cancer research* 2003, **63**(23):8414-8419.

38. Al-Matary YS, Botezatu L, Opalka B, Hönes JM, Lams RF, Thivakaran A, Schütte J, Köster R, Lennartz K, Schroeder T: **Acute myeloid leukemia cells polarize macrophages towards a leukemia supporting state in a Growth factor independence 1 dependent manner**. *Haematologica* 2016, **101**(10):1216.
39. Yang X, Feng W, Wang R, Yang F, Wang L, Chen S, Ru Y, Cheng T, Zheng G: **Repolarizing heterogeneous leukemia-associated macrophages with more M1 characteristics eliminates their pro-leukemic effects**. *Oncoimmunology* 2018, **7**(4):e1412910.
40. Chen S-Y, Yang X, Feng W-L, Liao J-F, Wang L-N, Feng L, Lin Y-M, Ren Q, Zheng G-G: **Organ-specific microenvironment modifies diverse functional and phenotypic characteristics of leukemia-associated macrophages in mouse T cell acute lymphoblastic leukemia**. *The Journal of Immunology* 2015, **194**(6):2919-2929.
41. Fleischer DM, Udkoff J, Borok J, Friedman A, Nicol N, Bienstock J, Lio P, Tollefson M, Eichenfield LF: **Atopic dermatitis: skin care and topical therapies**. *Semin Cutan Med Surg* 2017, **36**(3):104-110.
42. Mansnérus J, Faduola P, Hakim A, Imai A, O'Neill R: **Acute myeloid leukaemia-therapy-past, present and future**. *Translational Biomedicine* 2013, **4**(2):18.
43. Daver N, Wei AH, Pollyea DA, Fathi AT, Vyas P, DiNardo CD: **New directions for emerging therapies in acute myeloid leukemia: The next chapter**. *Blood cancer journal* 2020, **10**(10):107.
44. Naran K, Nundalall T, Chetty S, Barth S: **Principles of immunotherapy: implications for treatment strategies in cancer and infectious diseases**. *Frontiers in microbiology* 2018, **9**:3158.
45. Kiyoshi M, Caaveiro JM, Kawai T, Tashiro S, Ide T, Asaoka Y, Hatayama K, Tsumoto K: **Structural basis for binding of human IgG1 to its high-affinity human receptor FcγRI**. *Nature communications* 2015, **6**(1):1-11.
46. Lu J, Chu J, Zou Z, Hamacher NB, Rixon MW, Sun PD: **Structure of FcγRI in complex with Fc reveals the importance of glycan recognition for high-affinity IgG binding**. *Proceedings of the National Academy of Sciences* 2015, **112**(3):833-838.
47. Bruhns P, Iannascoli B, England P, Mancardi DA, Fernandez N, Jorieux S, Daëron M: **Specificity and affinity of human Fcγ receptors and their polymorphic variants for human IgG subclasses**. *Blood, The Journal of the American Society of Hematology* 2009, **113**(16):3716-3725.
48. Harrison PT, Allen JM: **High affinity IgG binding by FcgammaRI (CD64) is modulated by two distinct IgSF domains and the transmembrane domain of the receptor**. *Protein engineering* 1998, **11**(3):225-232.
49. Lu J, Ellsworth JL, Hamacher N, Oak SW, Sun PD: **Crystal structure of Fcγ receptor I and its implication in high affinity γ-immunoglobulin binding**. *Journal of Biological Chemistry* 2011, **286**(47):40608-40613.
50. Lux A, Yu X, Scanlan CN, Nimmerjahn F: **Impact of immune complex size and glycosylation on IgG binding to human FcγRs**. *The Journal of Immunology* 2013, **190**(8):4315-4323.
51. Mancardi DA, Albanesi M, Jönsson F, Iannascoli B, Van Rooijen N, Kang X, England P, Daëron M, Bruhns P: **The high-affinity human IgG receptor FcγRI (CD64) promotes IgG-mediated inflammation, anaphylaxis, and antitumor immunotherapy**. *Blood, The Journal of the American Society of Hematology* 2013, **121**(9):1563-1573.
52. Holtrop T, Budding K, Brandsma AM, Leusen JH: **Targeting the high affinity receptor, FcγRI, in autoimmune disease, neuropathy, and cancer**. *Immunotherapy Advances* 2022, **2**(1):ltac011.

53. Groselj-Grenc M, Ihan A, Derganc M: **Neutrophil and monocyte CD64 and CD163 expression in critically ill neonates and children with sepsis: comparison of fluorescence intensities and calculated indexes**. *Mediators of inflammation* 2008, **2008**.
54. Harrison PT, Davis W, Norman JC, Hockaday AR, Allen JM: **Binding of monomeric immunoglobulin G triggers Fc gamma RI-mediated endocytosis**. *Journal of Biological Chemistry* 1994, **269**(39):24396-24402.
55. Van Der Poel CE, Karssemeijer RA, Boross P, Van Der Linden JA, Blokland M, Van De Winkel JG, Leusen JH: **Cytokine-induced immune complex binding to the high-affinity IgG receptor, FcγRI, in the presence of monomeric IgG**. *Blood, The Journal of the American Society of Hematology* 2010, **116**(24):5327-5333.
56. Fanger NA, Voigtlaender D, Liu C, Swink S, Wardwell K, Fisher J, Graziano RF, Pfefferkorn LC, Guyre PM: **Characterization of expression, cytokine regulation, and effector function of the high affinity IgG receptor Fc gamma RI (CD64) expressed on human blood dendritic cells**. *Journal of immunology (Baltimore, Md: 1950)* 1997, **158**(7):3090-3098.
57. Guyre P, Graziano R, Vance B, Morganelli P, Fanger M: **Monoclonal antibodies that bind to distinct epitopes on Fc gamma RI are able to trigger receptor function**. *Journal of immunology (Baltimore, Md: 1950)* 1989, **143**(5):1650-1655.
58. Guyre PM, Morganelli PM, Miller R: **Recombinant immune interferon increases immunoglobulin G Fc receptors on cultured human mononuclear phagocytes**. *The Journal of clinical investigation* 1983, **72**(1):393-397.
59. Mendoza-Coronel E, Ortega E: **Macrophage polarization modulates FcγR-and CD13-mediated phagocytosis and reactive oxygen species production, independently of receptor membrane expression**. *Frontiers in immunology* 2017, **8**:303.
60. Nimmerjahn F, Ravetch JV: **Fcγ receptors as regulators of immune responses**. *Nature Reviews Immunology* 2008, **8**(1):34-47.
61. Barnes N, Gavin AL, Tan PS, Mottram P, Koentgen F, Hogarth PM: **FcγRI-deficient mice show multiple alterations to inflammatory and immune responses**. *Immunity* 2002, **16**(3):379-389.
62. Getahun A, Cambier JC: **Of ITIM s, ITAM s, and ITAM is: revisiting immunoglobulin Fc receptor signaling**. *Immunological reviews* 2015, **268**(1):66-73.
63. Bournazos S, Gupta A, Ravetch JV: **The role of IgG Fc receptors in antibody-dependent enhancement**. *Nature Reviews Immunology* 2020, **20**(10):633-643.
64. Blank U, Launay P, Benhamou M, Monteiro RC: **Inhibitory ITAMs as novel regulators of immunity**. *Immunological reviews* 2009, **232**(1):59-71.
65. van Vugt MJ, Heijnen I, Capel P, Park SY, Ra C, Saito T, Verbeek JS, van De Winkel J: **FcR gamma-chain is essential for both surface expression and function of human Fc gamma RI (CD64) in vivo**. 1996.
66. Swisher JF, Feldman GM: **The many faces of FcγRI: implications for therapeutic antibody function**. *Immunological reviews* 2015, **268**(1):160-174.
67. Boekhoudt GH, Frazier-Jessen MR, Feldman GM: **Immune complexes suppress IFN-γ signaling by activation of the FcγRI pathway**. *Journal of Leucocyte Biology* 2007, **81**(4):1086-1092.
68. Superson M, Szymańska K, Walczak K, Wnorowski J, Zarębski Ł: **Clinical application of monoclonal antibodies in targeted therapy**. *European Journal of Clinical and Experimental Medicine* 2019(4):338-346.
69. Rodríguez-Nava C, Ortuño-Pineda C, Illades-Aguiar B, Flores-Alfaro E, Leyva-Vázquez MA, Parra-Rojas I, del Moral-Hernández O, Vences-Velázquez A, Cortés-

Sarabia K, Alarcón-Romero LdC: **Mechanisms of Action and Limitations of Monoclonal Antibodies and Single Chain Fragment Variable (scFv) in the Treatment of Cancer**. *Biomedicines* 2023, **11**(6):1610.
70. Maini RN, Feldmann M: **How does infliximab work in rheumatoid arthritis?** *Arthritis Research & Therapy* 2002, **4**(2):1-7.
71. Nelson A: **Antibody fragments: hope and hype. MAbs 2: 77–83**. In.: DOI; 2010.
72. Ericson S, Coleman K, Wardwell K, Baker S, Fanger M, Guyre P, Ely P: **Monoclonal antibody 197 (anti-FcγRI) infusion in a patient with immune thrombocytopenia purpura (ITP) results in down-modulation of FcγRI on circulating monocytes**. *British journal of haematology* 1996, **92**(3):718-724.
73. Wallace PK, Keler T, Coleman K, Fisher J, Vitale L, Graziano RF, Guyre PM, Fanger MW: **Humanized mAb H22 binds the human high affinity Fc receptor for IgG (FcγRI), blocks phagocytosis, and modulates receptor expression**. *Journal of leukocyte biology* 1997, **62**(4):469-479.
74. Graziano RF, Tempest PR, White P, Keler T, Deo Y, Ghebremariam H, Coleman K, Pfefferkorn LC, Fanger MW, Guyre PM: **Construction and characterization of a humanized anti-gamma-Ig receptor type I (Fc gamma RI) monoclonal antibody**. *Journal of immunology (Baltimore, Md: 1950)* 1995, **155**(10):4996-5002.
75. Heijnen I, Van Vugt MJ, Fanger NA, Graziano RF, De Wit T, Hofhuis F, Guyre PM, Capel P, Verbeek JS, Van De Winkel J: **Antigen targeting to myeloid-specific human Fc gamma RI/CD64 triggers enhanced antibody responses in transgenic mice**. *The Journal of clinical investigation* 1996, **97**(2):331-338.
76. van der Poel CE, Spaapen RM, van de Winkel JG, Leusen JH: **Functional characteristics of the high affinity IgG receptor, FcγRI**. *The Journal of Immunology* 2011, **186**(5):2699-2704.
77. de Kruif J, Tijmensen M, Goldsein J, Logtenberg T: **Recombinant lipid-tagged antibody fragments as functional cell-surface receptors**. *Nature Medicine* 2000, **6**(2):223-227.
78. Schiffer S, Rosinke R, Jost E, Hehmann-Titt G, Huhn M, Melmer G, Barth S, Thepen T: **Targeted ex vivo reduction of CD64-positive monocytes in chronic myelomonocytic leukemia and acute myelomonocytic leukemia using human granzyme B-based cytolytic fusion proteins**. *International journal of cancer* 2014, **135**(6):1497-1508.
79. Thepen T, Van Vuuren A, Kiekens R, Damen CA, Vooijs WC, van de Winkel JG: **Resolution of cutaneous inflammation after local elimination of macrophages**. *Nature biotechnology* 2000, **18**(1):48-51.
80. Barth S: **Editorial [Hot Topic: recombinant immunotoxins-The Next Generation (Executive Editor: Stefan Barth)]**. *Current Pharmaceutical Design* 2009, **15**(23):2650-2651.
81. Mungra N, Jordaan S, Hlongwane P, Naran K, Chetty S, Barth S: **Targeted human cytolytic fusion proteins at the cutting edge: harnessing the apoptosis-inducing properties of human enzymes for the selective elimination of tumor cells**. *Oncotarget* 2019, **10**(8):897.
82. Teicher BA, Chari RV: **Antibody conjugate therapeutics: challenges and potential**. *Clinical cancer research* 2011, **17**(20):6389-6397.
83. Onda M, Beers R, Xiang L, Lee B, Weldon JE, Kreitman RJ, Pastan I: **Recombinant immunotoxin against B-cell malignancies with no immunogenicity in mice by removal of B-cell epitopes**. *Proceedings of the National Academy of Sciences* 2011, **108**(14):5742-5747.

84. Onda M, Beers R, Xiang L, Nagata S, Wang Q-c, Pastan I: **An immunotoxin with greatly reduced immunogenicity by identification and removal of B cell epitopes**. *Proceedings of the National Academy of Sciences* 2008, **105**(32):11311-11316.
85. Stahnke B, Thepen T, Stöcker M, Rosinke R, Jost E, Fischer R, Tur MK, Barth S: **Granzyme B-H22 (scFv), a human immunotoxin targeting CD64 in acute myeloid leukemia of monocytic subtypes**. *Molecular cancer therapeutics* 2008, **7**(9):2924-2932.
86. Hristodorov D, Mladenov R, Pardo A, Pham A, Huhn M, Fischer R, Thepen T, Barth S: **Microtubule-associated protein tau facilitates the targeted killing of proliferating cancer cells in vitro and in a xenograft mouse tumour model in vivo**. *British journal of cancer* 2013, **109**(6):1570-1578.
87. Hristodorov D, Mladenov R, Fischer R, Barth S, Thepen T: **Fully human MAP-fusion protein selectively targets and eliminates proliferating CD64+ M1 macrophages**. *Immunology and cell biology* 2016, **94**(5):470-478.
88. Jordaan S, Akinrinmade OA, Nachreiner T, Cremer C, Naran K, Chetty S, Barth S: **Updates in the development of immunoRNases for the selective killing of tumor cells**. *Biomedicines* 2018, **6**(1):28.
89. Hoehnel S, Lutolf M: **Capturing cell–cell interactions via SNAP-tag and CLIP-tag technology**. *Bioconjugate chemistry* 2015, **26**(8):1678-1686.
90. Keppler A, Gendreizig S, Gronemeyer T, Pick H, Vogel H, Johnsson K: **A general method for the covalent labeling of fusion proteins with small molecules in vivo**. *Nature biotechnology* 2003, **21**(1):86-89.
91. Peters C, Brown S: **Antibody–drug conjugates as novel anti-cancer chemotherapeutics**. *Bioscience reports* 2015, **35**(4).
92. van Vuuren AJ, van Roon JA, Walraven V, Stuij I, Harmsen MC, McLaughlin PM, van de Winkel JG, Thepen T: **CD64-directed immunotoxin inhibits arthritis in a novel CD64 transgenic rat model**. *The Journal of Immunology* 2006, **176**(10):5833-5838.
93. Tur MK, Huhn M, Jost E, Thepen T, Brümmendorf TH, Barth S: **In vivo efficacy of the recombinant anti-CD64 immunotoxin H22 (scFv)-ETA′ in a human acute myeloid leukemia xenograft tumor model**. *International journal of cancer* 2011, **129**(5):1277-1282.
94. Ribbert T, Thepen T, Tur M, Fischer R, Huhn M, Barth S: **Recombinant, ETA′-based CD64 immunotoxins: improved efficacy by increased valency, both in vitro and in vivo in a chronic cutaneous inflammation model in human CD64 transgenic mice**. *British Journal of Dermatology* 2010, **163**(2):279-286.
95. Duranti C, Arcangeli A: **Ion channel targeting with antibodies and antibody fragments for cancer diagnosis**. *Antibodies* 2019, **8**(2):33.
96. Olsnes S: **The history of ricin, abrin and related toxins**. *Toxicon* 2004, **44**(4):361-370.
97. Jetzt AE, Li X-P, Tumer NE, Cohick WS: **Toxicity of ricin A chain is reduced in mammalian cells by inhibiting its interaction with the ribosome**. *Toxicology and applied pharmacology* 2016, **310**:120-128.
98. Sousa NL, Cabral GB, Vieira PM, Baldoni AB, Aragão FJ: **Bio-detoxification of ricin in castor bean (Ricinus communis L.) seeds**. *Scientific Reports* 2017, **7**(1):1-9.
99. Van Roon JA, Van Vuuren AJ, Wijngaarden S, Jacobs KM, Bijlsma JW, Lafeber FP, Thepen T, Van De Winkel JG: **Selective elimination of synovial inflammatory macrophages in rheumatoid arthritis by an Fcγ receptor I–directed immunotoxin**. *Arthritis & Rheumatism* 2003, **48**(5):1229-1238.
100. Wolf P, Elsässer-Beile U: **Pseudomonas exotoxin A: from virulence factor to anti-cancer agent**. *International Journal of Medical Microbiology* 2009, **299**(3):161-176.

101. Michalska M, Wolf P: **Pseudomonas exotoxin A: optimized by evolution for effective killing. Front Microbiol 6: 963**. In.; 2015.
102. Mahmoudi R, Dianat-Moghadam H, Poorebrahim M, Siapoush S, Poortahmasebi V, Salahlou R, Rahmati M: **Recombinant immunotoxins development for HER2-based targeted cancer therapies**. *Cancer cell international* 2021, **21**:1-17.
103. Hristodorov D, Mladenov R, Huhn M, Barth S, Thepen T: **Macrophage-targeted therapy: CD64-based immunotoxins for treatment of chronic inflammatory diseases**. *Toxins* 2012, **4**(9):676-694.
104. Hristodorov D, Mladenov R, von Felbert V, Huhn M, Fischer R, Barth S, Thepen T: **Targeting CD64 mediates elimination of M1 but not M2 macrophages in vitro and in cutaneous inflammation in mice and patient biopsies**. In: *MAbs: 2015*. Taylor & Francis: 853-862.
105. Griswold KE, Bailey-Kellogg C: **Design and engineering of deimmunized biotherapeutics**. *Current opinion in structural biology* 2016, **39**:79-88.
106. Mazor R, King EM, Pastan I: **Strategies to reduce the immunogenicity of recombinant immunotoxins**. *The American Journal of Pathology* 2018, **188**(8):1736-1743.
107. Gülsen A, Wedi B, Jappe U: **Hypersensitivity reactions to biologics (part II): classifications and current diagnostic and treatment approaches**. *Allergo Journal International* 2020, **29**(5):139-154.
108. Mathew M, Verma RS: **Humanized immunotoxins: a new generation of immunotoxins for targeted cancer therapy**. *Cancer science* 2009, **100**(8):1359-1365.
109. Safdari Y, Farajnia S, Asgharzadeh M, Khalili M: **Antibody humanization methods–a review and update**. *Biotechnology and Genetic Engineering Reviews* 2013, **29**(2):175-186.
110. Onda M, Nagata S, FitzGerald DJ, Beers R, Fisher RJ, Vincent JJ, Lee B, Nakamura M, Hwang J, Kreitman RJ: **Characterization of the B cell epitopes associated with a truncated form of Pseudomonas exotoxin (PE38) used to make immunotoxins for the treatment of cancer patients**. *The Journal of Immunology* 2006, **177**(12):8822-8834.
111. Filpula D, Yang K, Basu A, Hassan R, Xiang L, Zhang Z, Wang M, Wang Q-c, Ho M, Beers R: **Releasable PEGylation of mesothelin targeted immunotoxin SS1P achieves single dosage complete regression of a human carcinoma in mice**. *Bioconjugate chemistry* 2007, **18**(3):773-784.
112. Mazor R, Pastan I: **Immunogenicity of immunotoxins containing Pseudomonas exotoxin A: causes, consequences, and mitigation**. *Frontiers in Immunology* 2020, **11**:1261.
113. Liu W, Onda M, Lee B, Kreitman RJ, Hassan R, Xiang L, Pastan I: **Recombinant immunotoxin engineered for low immunogenicity and antigenicity by identifying and silencing human B-cell epitopes**. *Proceedings of the National Academy of Sciences* 2012, **109**(29):11782-11787.
114. Hollevoet K, Mason-Osann E, Liu X-f, Imhof-Jung S, Niederfellner G, Pastan I: **In vitro and in vivo activity of the low-immunogenic antimesothelin immunotoxin RG7787 in pancreatic cancer**. *Molecular cancer therapeutics* 2014, **13**(8):2040-2049.
115. Gautier A, Juillerat A, Heinis C, Corrêa Jr IR, Kindermann M, Beaufils F, Johnsson K: **An engineered protein tag for multiprotein labeling in living cells**. *Chemistry & biology* 2008, **15**(2):128-136.
116. Hughes PW: **Follow That Protein: SNAP-Tagging Permits High-Resolution Protein Localization**. In.: American Society of Plant Biologists; 2020.

117. Gautier A, Hinner MJ: **Preface. Site-specific protein labeling**. *Methods in Molecular Biology (Clifton, NJ)* 2015, **1266**:v-viii.
118. Hussain AF, Heppenstall PA, Kampmeier F, Meinhold-Heerlein I, Barth S: **One-step site-specific antibody fragment auto-conjugation using SNAP-tag technology**. *Nature Protocols* 2019, **14**(11):3101-3125.
119. Juillerat A, Gronemeyer T, Keppler A, Gendreizig S, Pick H, Vogel H, Johnsson K: **Directed evolution of O6-alkylguanine-DNA alkyltransferase for efficient labeling of fusion proteins with small molecules in vivo**. *Chemistry & biology* 2003, **10**(4):313-317.
120. Damoiseaux R, Schultz PG, Johnsson K: **Towards the Generation of Artificial O6-Alkylguanine-DNA Alkyltransferases: In Vitro Selection of Antibodies with Reactive Cysteine Residues**. *ChemBioChem* 2002, **3**(6):573-575.
121. Damoiseaux R, Keppler A, Johnsson K: **Synthesis and applications of chemical probes for human O6-alkylguanine-DNA alkyltransferase**. *ChemBioChem* 2001, **2**(4):285-287.
122. Padayachee ER, Biteghe FAN, Malindi Z, Bauerschlag D, Barth S: **Human antibody fusion proteins/antibody drug conjugates in breast and ovarian cancer**. *Transfusion Medicine and Hemotherapy* 2017, **44**(5):303-310.
123. Padayachee ER, Adeola HA, Van Wyk JC, Nsole Biteghe FA, Chetty S, Khumalo NP, Barth S: **Applications of SNAP-tag technology in skin cancer therapy**. *Health Science Reports* 2019, **2**(2):e103.
124. Amoury M, Bauerschlag D, Zeppernick F, von Felbert V, Berges N, Di Fiore S, Mintert I, Bleilevens A, Maass N, Bräutigam K: **Photoimmunotheranostic agents for triple-negative breast cancer diagnosis and therapy that can be activated on demand**. *Oncotarget* 2016, **7**(34):54925.
125. Fu Z, Li S, Han S, Shi C, Zhang Y: **Antibody drug conjugate: the "biological missile" for targeted cancer therapy**. *Signal Transduction and Targeted Therapy* 2022, **7**(1):1-25.
126. Khongorzul P, Ling CJ, Khan FU, Ihsan AU, Zhang J: **Antibody–Drug Conjugates: A Comprehensive ReviewAntibody–Drug Conjugates in Cancer Immunotherapy**. *Molecular Cancer Research* 2020, **18**(1):3-19.
127. Huysamen AM, Fadeyi OE, Mayuni G, Dogbey DM, Mungra N, Biteghe FA, Hardcastle N, Ramamurthy D, Akinrinmade OA, Naran K: **Click Chemistry-Generated Auristatin F–Linker–Benzylguanine for a SNAP-Tag-Based Recombinant Antibody–Drug Conjugate Demonstrating Selective Cytotoxicity toward EGFR-Overexpressing Tumor Cells**. *ACS omega* 2023, **8**(4):4026-4037.
128. Chalouni C, Doll S: **Fate of antibody-drug conjugates in cancer cells**. *Journal of Experimental & Clinical Cancer Research* 2018, **37**(1):1-12.
129. Peters C, Brown S: **Antibody–drug conjugates as novel anti-cancer chemotherapeutics**. *Bioscience reports* 2015, **35**(4):e00225.
130. Baron J, Wang ES: **Gemtuzumab ozogamicin for the treatment of acute myeloid leukemia**. *Expert review of clinical pharmacology* 2018, **11**(6):549-559.
131. Amiri-Kordestani L, Blumenthal GM, Xu QC, Zhang L, Tang SW, Ha L, Weinberg WC, Chi B, Candau-Chacon R, Hughes P: **FDA Approval: Ado-Trastuzumab Emtansine for the Treatment of Patients with HER2-Positive Metastatic Breast Cancer**. *Clinical Cancer Research* 2014, **20**(17):4436-4441.
132. Connors JM, Jurczak W, Straus DJ, Ansell SM, Kim WS, Gallamini A, Younes A, Alekseev S, Illés Á, Picardi M: **Brentuximab vedotin with chemotherapy for stage III or IV Hodgkin's lymphoma**. *New England Journal of Medicine* 2018, **378**(4):331-344.

133. Zhao P, Zhang Y, Li W, Jeanty C, Xiang G, Dong Y: **Recent advances of antibody drug conjugates for clinical applications**. *Acta Pharmaceutica Sinica B* 2020, **10**(9):1589-1600.
134. Doronina SO, Mendelsohn BA, Bovee TD, Cerveny CG, Alley SC, Meyer DL, Oflazoglu E, Toki BE, Sanderson RJ, Zabinski RF: **Enhanced activity of monomethylauristatin F through monoclonal antibody delivery: effects of linker technology on efficacy and toxicity**. *Bioconjugate chemistry* 2006, **17**(1):114-124.
135. Johansson MP, Maaheimo H, Ekholm FS: **New insight on the structural features of the cytotoxic auristatins MMAE and MMAF revealed by combined NMR spectroscopy and quantum chemical modelling**. *Scientific reports* 2017, **7**(1):1-10.
136. Park M-H, Lee BI, Byeon J-J, Shin S-H, Choi J, Park Y, Shin YG: **Pharmacokinetic and metabolism studies of monomethyl auristatin f via liquid chromatography-quadrupole-time-of-flight mass spectrometry**. *Molecules* 2019, **24**(15):2754.
137. Woitok M, Klose D, Niesen J, Richter W, Abbas M, Stein C, Fendel R, Bialon M, Püttmann C, Fischer R: **The efficient elimination of solid tumor cells by EGFR-specific and HER2-specific scFv-SNAP fusion proteins conjugated to benzylguanine-modified auristatin F**. *Cancer letters* 2016, **381**(2):323-330.
138. Woitok M, Klose D, Di Fiore S, Richter W, Stein C, Gresch G, Grieger E, Barth S, Fischer R, Kolberg K: **Comparison of a mouse and a novel human scFv-SNAP-auristatin F drug conjugate with potent activity against EGFR-overexpressing human solid tumor cells**. *OncoTargets and therapy* 2017, **10**:3313.
139. Mussini A, Uriati E, Bianchini P, Diaspro A, Cavanna L, Abbruzzetti S, Viappiani C: **Targeted photoimmunotherapy for cancer**. *Biomolecular Concepts* 2022, **13**(1):126-147.
140. Shirasu N, Nam SO, Kuroki M: **Tumor-targeted photodynamic therapy**. *Anticancer research* 2013, **33**(7):2823-2831.
141. Allison RR, Moghissi K: **Photodynamic therapy (PDT): PDT mechanisms**. *Clinical endoscopy* 2013, **46**(1):24-29.
142. Wei D, Qi J, Hamblin MR, Wen X, Jiang X, Yang H: **Near-infrared photoimmunotherapy: design and potential applications for cancer treatment and beyond**. *Theranostics* 2022, **12**(16):7108.
143. Ruggiero E, Alonso-de Castro S, Habtemariam A, Salassa L: **Upconverting nanoparticles for the near infrared photoactivation of transition metal complexes: new opportunities and challenges in medicinal inorganic photochemistry**. *Dalton Transactions* 2016, **45**(33):13012-13020.
144. Ito K, Mitsunaga M, Nishimura T, Kobayashi H, Tajiri H: **Combination photoimmunotherapy with monoclonal antibodies recognizing different epitopes of human epidermal growth factor receptor 2: an assessment of phototherapeutic effect based on fluorescence molecular imaging**. *Oncotarget* 2016, **7**(12):14143.
145. Wei D, Tao Z, Shi Q, Wang L, Liu L, She T, Yi Q, Wen X, Liu L, Li S: **Selective photokilling of colorectal tumors by near-infrared photoimmunotherapy with a GPA33-targeted single-chain antibody variable fragment conjugate**. *Molecular Pharmaceutics* 2020, **17**(7):2508-2517.
146. Cognetti DM, Johnson JM, Curry JM, Kochuparambil ST, McDonald D, Mott F, Fidler MJ, Stenson K, Vasan NR, Razaq MA: **Phase 1/2a, open-label, multicenter study of RM-1929 photoimmunotherapy in patients with locoregional, recurrent head and neck squamous cell carcinoma**. *Head & Neck* 2021, **43**(12):3875-3887.
147. Kim KS, Kim J, Kim DH, Hwang HS, Na K: **Multifunctional trastuzumab–chlorin e6 conjugate for the treatment of HER2-positive human breast cancer**. *Biomaterials science* 2018, **6**(5):1217-1226.

148. Son J, Yi G, Kwak M-H, Yang SM, Park JM, Lee B-I, Choi M-G, Koo H: **Gelatin–chlorin e6 conjugate for in vivo photodynamic therapy**. *Journal of nanobiotechnology* 2019, **17**(1):1-12.
149. Bhatti M, Yahioglu G, Milgrom LR, Garcia-Maya M, Chester KA, Deonarain MP: **Targeted photodynamic therapy with multiply-loaded recombinant antibody fragments**. *International journal of cancer* 2008, **122**(5):1155-1163.
150. von Felbert V, Bauerschlag D, Maass N, Bräutigam K, Meinhold-Heerlein I, Woitok M, Barth S, Hussain AF: **A specific photoimmunotheranostics agent to detect and eliminate skin cancer cells expressing EGFR**. *Journal of cancer research and clinical oncology* 2016, **142**(5):1003-1011.
151. Barth S, Huhn M, Matthey B, Klimka A, Galinski E, Engert A: **Compatible-solute-supported periplasmic expression of functional recombinant proteins under stress conditions**. *Applied and environmental microbiology* 2000, **66**(4):1572-1579.
152. Czarniecki D, Noel Jr RJ, Reznikoff WS: **The-45 region of the Escherichia coli lac promoter: CAP-dependent and CAP-independent transcription**. *Journal of bacteriology* 1997, **179**(2):423-429.
153. Clark D, Pazdernik N: **Chapter 7. Cloning Genes for Analysis**. *Molecular Biology, 2nd ed; Academic Cell Update Edition; Elsevier Inc: Waltham, MA, USA* 2013:194-226.
154. Zhao X, Li G, Liang S: **Several affinity tags commonly used in chromatographic purification**. *Journal of analytical methods in chemistry* 2013, **2013**.
155. Tabor S: **Expression using the T7 RNA polymerase/promoter system**. *Current protocols in molecular biology* 1990, **11**(1):16.12. 11-16.12. 11.
156. Makrides SC: **Components of vectors for gene transfer and expression in mammalian cells**. *Protein expression and purification* 1999, **17**(2):183-202.
157. PFARR DS, RIESER LA, WOYCHIK RP, ROTTMAN FM, ROSENBERG M, REFF ME: **Differential effects of polyadenylation regions on gene expression in mammalian cells**. *Dna* 1986, **5**(2):115-122.
158. Gong H, Kovar JL, Baker B, Zhang A, Cheung L, Draney DR, Corrêa Jr IR, Xu M-Q, Olive DM: **Near-infrared fluorescence imaging of mammalian cells and xenograft tumors with SNAP-tag**. *PloS one* 2012, **7**(3):e34003.
159. Smith R, Traul D, Schaack J, Clayton G, Staley K, Wilcox C: **Characterization of promoter function and cell-type-specific expression from viral vectors in the nervous system**. *Journal of virology* 2000, **74**(23):11254-11261.
160. Sutcliffe JG: **Nucleotide sequence of the ampicillin resistance gene of Escherichia coli plasmid pBR322**. *Proceedings of the National Academy of Sciences* 1978, **75**(8):3737-3741.
161. Sambrook J, Russell DW: **The condensed protocols from molecular cloning: a laboratory manual**: Cold Spring Harbor Laboratory Press; 2006.
162. Lee BS, Lee Y, Park J, Jeong BS, Jo M, Jung ST, Yoo TH: **Construction of an immunotoxin via site-specific conjugation of anti-Her2 IgG and engineered Pseudomonas exotoxin A**. *Journal of Biological Engineering* 2019, **13**:1-13.
163. Chen KC, Xie H, Cai Y: **Modes of action of ADP-ribosylated elongation factor 2 in inhibiting the polypeptide elongation cycle: a modeling study**. *PloS one* 2013, **8**(7):e66446.
164. Al Qaraghuli MM, Kubiak-Ossowska K, Ferro VA, Mulheran PA: **Antibody-protein binding and conformational changes: identifying allosteric signalling pathways to engineer a better effector response**. *Scientific reports* 2020, **10**(1):13696.

165. Ahmadzadeh K, Vanoppen M, Rose CD, Matthys P, Wouters CH: **Multinucleated Giant cells: current insights in phenotype, biological activities, and mechanism of formation**. *Frontiers in Cell and Developmental Biology* 2022, **10**:873226.
166. Bertani F, Mozetic P, Fioramonti M, Iuliani M, Ribelli G, Pantano F, Santini D, Tonini G, Trombetta M, Businaro L: **Classification of M1/M2-polarized human macrophages by label-free hyperspectral reflectance confocal microscopy and multivariate analysis. Sci Rep 7: 8965**. *Link: https://bit ly/3fkFeIi* 2017.
167. Akinrinmade OA, Chetty S, Daramola AK, Islam M-u, Thepen T, Barth S: **CD64: an attractive immunotherapeutic target for M1-type macrophage mediated chronic inflammatory diseases**. *Biomedicines* 2017, **5**(3):56.
168. Fawzi Hussain A, Amoury M, Barth S: **SNAP-tag technology: a powerful tool for site specific conjugation of therapeutic and imaging agents**. *Current pharmaceutical design* 2013, **19**(30):5437-5442.
169. Gomez S, Tsung A, Hu Z: **Current targets and bioconjugation strategies in photodynamic diagnosis and therapy of cancer**. *Molecules* 2020, **25**(21):4964.
170. Ponzoni M, Pastorino F, Di Paolo D, Perri P, Brignole C: **Targeting macrophages as a potential therapeutic intervention: impact on inflammatory diseases and cancer**. *International journal of molecular sciences* 2018, **19**(7):1953.
171. Lee W-H, Loo C-Y, Traini D, Young PM: **Nano-and micro-based inhaled drug delivery systems for targeting alveolar macrophages**. *Expert opinion on drug delivery* 2015, **12**(6):1009-1026.
172. Brignole C, Perri P, Piaggio F, Pastorino F, Di Paolo D, Emionite L, Daga A, Kondylis V, Pasparakis M, Ribatti D: **A novel liposomal Clodronate depletes tumor-associated macrophages in primary and metastatic melanoma: anti-angiogenic and anti-tumor effects**. *Cancer Research* 2016, **76**(14_Supplement):3844-3844.
173. Zanganeh S, Hutter G, Spitler R, Lenkov O, Mahmoudi M, Shaw A, Pajarinen JS, Nejadnik H, Goodman S, Moseley M: **Iron oxide nanoparticles inhibit tumour growth by inducing pro-inflammatory macrophage polarization in tumour tissues**. *Nature nanotechnology* 2016, **11**(11):986-994.
174. Bu L, Gao M, Qu S, Liu D: **Intraperitoneal injection of clodronate liposomes eliminates visceral adipose macrophages and blocks high-fat diet-induced weight gain and development of insulin resistance**. *The AAPS journal* 2013, **15**:1001-1011.
175. Barrera P, Blom A, Van Lent PL, Van Bloois L, Beijnen JH, Van Rooijen N, De Waal Malefijt MC, Van De Putte LB, Storm G, Van Den Berg WB: **Synovial macrophage depletion with clodronate-containing liposomes in rheumatoid arthritis**. *Arthritis & Rheumatism: Official Journal of the American College of Rheumatology* 2000, **43**(9):1951-1959.
176. Bacci M, Capobianco A, Monno A, Cottone L, Di Puppo F, Camisa B, Mariani M, Brignole C, Ponzoni M, Ferrari S: **Macrophages are alternatively activated in patients with endometriosis and required for growth and vascularization of lesions in a mouse model of disease**. *The American journal of pathology* 2009, **175**(2):547-556.
177. Ortega RA, Barham W, Sharman K, Tikhomirov O, Giorgio TD, Yull FE: **Manipulating the NF-κB pathway in macrophages using mannosylated, siRNA-delivering nanoparticles can induce immunostimulatory and tumor cytotoxic functions**. *International journal of nanomedicine* 2016:2163-2177.
178. Albanell J, Codony J, Rovira A, Mellado B, Gascón P: **Mechanism of action of anti-HER2 monoclonal antibodies: scientific update on trastuzumab and 2C4**. In: *New Trends in Cancer for the 21 st Century: Proceedings of the International Symposium*

on Cancer: New Trends in Cancer for the 21 st Century, held November 10–13, 2002, in Valencia, Spain: 2003. Springer: 253-268.
179. Giusti RM, Shastri KA, Cohen MH, Keegan P, Pazdur R: **FDA drug approval summary: Panitumumab (Vectibix™)**. *The oncologist* 2007, **12**(5):577-583.
180. Lee CJ, Savani BN, Mohty M, Gorin NC, Labopin M, Ruggeri A, Schmid C, Baron F, Esteve J, Giebel S: **Post-remission strategies for the prevention of relapse following allogeneic hematopoietic cell transplantation for high-risk acute myeloid leukemia: expert review from the Acute Leukemia Working Party of the European Society for Blood and Marrow Transplantation**. *Bone marrow transplantation* 2019, **54**(4):519-530.
181. Pelechas E, Voulgari PV, Drosos AA: **Golimumab for rheumatoid arthritis**. *Journal of Clinical Medicine* 2019, **8**(3):387.
182. Umeda M, Koga T, Ichinose K, Takatani A, Igawa T, Shimizu T, Fukui S, Nishino A, Horai Y, Hirai Y: **Efficacy of infliximab as a switched biologic in rheumatoid arthritis patients in daily clinical practice**. *Immunological Medicine* 2018, **41**(4):181-186.
183. Van Dyck CH: **Anti-amyloid-β monoclonal antibodies for Alzheimer's disease: pitfalls and promise**. *Biological psychiatry* 2018, **83**(4):311-319.
184. Muñoz-López P, Ribas-Aparicio RM, Becerra-Báez EI, Fraga-Pérez K, Flores-Martínez LF, Mateos-Chávez AA, Luria-Pérez R: **Single-chain fragment variable: recent Progress in cancer diagnosis and therapy**. *Cancers* 2022, **14**(17):4206.
185. Huleani S, Roberts MR, Beales L, Papaioannou EH: **Escherichia coli as an antibody expression host for the production of diagnostic proteins: significance and expression**. *Critical Reviews in Biotechnology* 2022, **42**(5):756-773.
186. Hunter M, Yuan P, Vavilala D, Fox M: **Optimization of protein expression in mammalian cells**. *Current protocols in protein science* 2019, **95**(1):e77.
187. Rosano GL, Ceccarelli EA: **Recombinant protein expression in Escherichia coli: advances and challenges**. *Frontiers in microbiology* 2014, **5**:172.
188. Daegelen P, Studier FW, Lenski RE, Cure S, Kim JF: **Tracing ancestors and relatives of Escherichia coli B, and the derivation of B strains REL606 and BL21 (DE3)**. *Journal of molecular biology* 2009, **394**(4):634-643.
189. Gottesman S: **Proteases and their targets in Escherichia coli**. *Annual review of genetics* 1996, **30**(1):465-506.
190. Sørensen HP, Mortensen KK: **Advanced genetic strategies for recombinant protein expression in Escherichia coli**. *Journal of biotechnology* 2005, **115**(2):113-128.
191. Buchner J, Pastan I, Brinkmann U: **A method for increasing the yield of properly folded recombinant fusion proteins: single-chain immunotoxins from renaturation of bacterial inclusion bodies**. *Analytical biochemistry* 1992, **205**(2):263-270.
192. Kotra SR, Peravali J, Yanamadala S, Kumar A, Rao K, Pulicherla K: **Large scale production of soluble recombinant staphylokinase variant from cold shock expression system using IPTG inducible E. coli BL21 (DE3)**. *Int J Bio-Sci Bio-Technol* 2013, **5**:107-116.
193. Saraswat M, Musante L, Ravidá A, Shortt B, Byrne B, Holthofer H: **Preparative purification of recombinant proteins: current status and future trends**. *BioMed research international* 2013, **2013**.
194. de los Milagros Bassani Molinas M, Beer C, Hesse F, Wirth M, Wagner R: **Optimizing the transient transfection process of HEK-293 suspension cells for protein production by nucleotide ratio monitoring**. *Cytotechnology* 2014, **66**:493-514.

195. Ryan BJ, Henehan GT: **Overview of approaches to preventing and avoiding proteolysis during expression and purification of proteins**. *Current protocols in protein science* 2013, **71**(1):5.25. 21-25.25. 27.
196. Schwarz H, Zhang Y, Zhan C, Malm M, Field R, Turner R, Sellick C, Varley P, Rockberg J, Chotteau V: **Small-scale bioreactor supports high density HEK293 cell perfusion culture for the production of recombinant Erythropoietin**. *Journal of Biotechnology* 2020, **309**:44-52.
197. Fox S, Rossi AG: **8 Macrophages**. *Fundamentals of Inflammation* 2010:96.
198. Heinrich F, Lehmbecker A, Raddatz BB, Kegler K, Tipold A, Stein VM, Kalkuhl A, Deschl U, Baumgärtner W, Ulrich R: **Morphologic, phenotypic, and transcriptomic characterization of classically and alternatively activated canine blood-derived macrophages in vitro**. *PloS one* 2017, **12**(8):e0183572.
199. Zanoni I, Granucci F: **Role of CD14 in host protection against infections and in metabolism regulation**. *Frontiers in cellular and infection microbiology* 2013, **3**:32.
200. Wright PB, McDonald E, Bravo-Blas A, Baer HM, Heawood A, Bain CC, Mowat AM, Clay SL, Robertson EV, Morton F: **The mannose receptor (CD206) identifies a population of colonic macrophages in health and inflammatory bowel disease**. *Scientific reports* 2021, **11**(1):19616.
201. Antignani A, FitzGerald D: **Immunotoxins: the role of the toxin**. *Toxins* 2013, **5**(8):1486-1502.
202. Zhao P, Wang P, Dong S, Zhou Z, Cao Y, Yagita H, He X, Zheng SG, Fisher SJ, Fujinami RS: **Depletion of PD-1-positive cells ameliorates autoimmune disease**. *Nature biomedical engineering* 2019, **3**(4):292-305.
203. Kreitman RJ, Wilson WH, White JD, Stetler-Stevenson M, Jaffe ES, Giardina S, Waldmann TA, Pastan I: **Phase I trial of recombinant immunotoxin anti-Tac (Fv)-PE38 (LMB-2) in patients with hematologic malignancies**. *Journal of Clinical Oncology* 2000, **18**(8):1622-1636.
204. Wayne AS, FitzGerald DJ, Kreitman RJ, Pastan I: **Immunotoxins for leukemia**. *Blood, The Journal of the American Society of Hematology* 2014, **123**(16):2470-2477.
205. Azemar M, Djahansouzi S, Jäger E, Solbach C, Schmidt M, Maurer AB, Mross K, Unger C, Minckwitz Gv, Dall P: **Regression of cutaneous tumor lesions in patients intratumorally injected with a recombinant single-chain antibody-toxin targeted to ErbB2/HER2**. *Breast cancer research and treatment* 2003, **82**:155-164.
206. Aggarwal D, Yang J, Salam MA, Sengupta S, Al-Amin MY, Mustafa S, Khan MA, Huang X, Pawar JS: **Antibody-drug conjugates: the paradigm shifts in the targeted cancer therapy**. *Frontiers in immunology* 2023, **14**.
207. Dean AQ, Luo S, Twomey JD, Zhang B: **Targeting cancer with antibody-drug conjugates: Promises and challenges**. In: *MAbs: 2021*. Taylor & Francis: 1951427.
208. Shastry M, Gupta A, Chandarlapaty S, Young M, Powles T, Hamilton E: **Rise of Antibody-Drug Conjugates: The Present and Future**. *American Society of Clinical Oncology Educational Book* 2023, **43**:e390094.
209. Ponziani S, Di Vittorio G, Pitari G, Cimini AM, Ardini M, Gentile R, Iacobelli S, Sala G, Capone E, Flavell DJ: **Antibody-drug conjugates: the new frontier of chemotherapy**. *International Journal of Molecular Sciences* 2020, **21**(15):5510.
210. Cole NB: **Site-Specific Protein Labeling with SNAP-Tags**. *Current protocols in protein science* 2013, **73**(1):30.31. 31-30.31. 16.
211. Zhao RY, Wilhelm SD, Audette C, Jones G, Leece BA, Lazar AC, Goldmacher VS, Singh R, Kovtun Y, Widdison WC: **Synthesis and evaluation of hydrophilic linkers for antibody–maytansinoid conjugates**. *Journal of medicinal chemistry* 2011, **54**(10):3606-3623.

212. Tsuchikama K, An Z: **Antibody-drug conjugates: recent advances in conjugation and linker chemistries**. *Protein & cell* 2018, **9**(1):33-46.
213. Meany HJ, Warren KE, Fox E, Cole DE, Aikin AA, Balis FM: **Pharmacokinetics of temozolomide administered in combination with O 6-benzylguanine in children and adolescents with refractory solid tumors**. *Cancer chemotherapy and pharmacology* 2009, **65**:137-142.
214. Ewesuedo RB, Dolan ME: **Pharmacokinetics of oral O 6-benzylguanine and evidence of interaction with oral ketoconazole in the rat**. *Cancer chemotherapy and pharmacology* 2000, **46**:150-155.
215. Van Straten D, Mashayekhi V, De Bruijn HS, Oliveira S, Robinson DJ: **Oncologic photodynamic therapy: basic principles, current clinical status and future directions**. *Cancers* 2017, **9**(2):19.
216. Yang EY, Shah K: **Nanobodies: next generation of cancer diagnostics and therapeutics**. *Frontiers in Oncology* 2020, **10**:1182.
217. Bannas P, Hambach J, Koch-Nolte F: **Nanobodies and nanobody-based human heavy chain antibodies as antitumor therapeutics**. *Frontiers in immunology* 2017, **8**:1603.
218. Ranft K, Thepen T, Fischer R, Barth S, Stöcker M: **Recombinant bispecific single chain antibody fragments induce Fcγ-receptor-mediated elimination of CD30+ lymphoma cells**. *Cancer letters* 2009, **282**(2):187-194.
219. Nakajima T, Sano K, Choyke PL, Kobayashi H: **Improving the efficacy of Photoimmunotherapy (PIT) using a cocktail of antibody conjugates in a multiple antigen tumor model**. *Theranostics* 2013, **3**(6):357.

|CHAPTER 7: APPENDIX|

7.1 ABBREVIATIONS

AD	Atopic dermatitis
ADC	Antibody-drug conjugate
AhD	Alzheimer's disease
AML	Acute myeloid leukemia
AURIF	Auristatin F
BG	Benzyl guanine
CCL	Chemokine (C-C motif) ligand
CCSN	Cell culture supernatant
CD	Cluster of differentiation
CDR	Complementary determining region
CR	Complete remission
CV	Column volume
CXCL	Chemokine (C-X-C motif) ligand
DC	Dendritic cells
dETA`	deimmunized Exotoxin A
DNA	Deoxyribose nucleic acid
dPBS	Dulbecco Phosphate Buffer Saline
d-rITs	Deimmunized rITs
EC	Extracellular domain
EGFR	Epidermal growth factor receptor
FACS	Fluorescent associated cell sorting
Fc	Fragment crystalline
FCS	Furin cleavage site
FDA	Food and Drug Administration
GC	Glucocorticoid
G-CSF	Granulocyte colony stimulating factor
GM-CSF	Granulocyte macrophages colony stimulating factor
hAGT	O^6-Alkylguanine-DNA alkyl transferase
hCFPs	Human cytolytic FPs

hMDMs	Human monocyte-derived macrophages
HPA	Hypothalamic-pituitary-adrenal (HPA) axis
HSCs	Hematopoietic stem cells
HSCT	Hematopoietic stem cell transplantation
IC	Immune complex
IFN-γ	Interferon Gamma,
IgG	Gamma Immunoglobulins
IL	Interleukins
IL-1ra	Interleukin-1 receptor antagonist
IMAC	Immobilized metal-ion affinity chromatography
IPTG	Isopropyl β- d-1-thiogalactopyranoside
ITAM	Immunoreceptor tyrosine activating motif
ITIM	Immunoreceptor tyrosine inhibitory motif
LAMs	leukemia-associated macrophages
LB	Lysogenic broth
LPS	Lipopolysaccharide
mAb	Monoclonal antibody
MDMs	Monocyte- derived macrophages
MDSC	Myeloid-derived suppressor cells
MHC	Major histocompatibility complex
MMAE	Monomethyl auristatin E
MMAF	Monomethyl auristatin F
MR	Mannose receptor
ORF	Open reading frame
PAGE	Polyacrylamide gel electrophoresis
PBMCs	Peripheral blood mononuclear cells
PBS	Phosphate buffer saline
PCR	Polymerase chain reaction
PE	*Pseudomonas aeruginosa* Exotoxin A
PI	Protease inhibitor
PIC	PIC
PKC	Protein kinase C
POI	Protein of interest

PVDF	Polyvinylidene difluoride
RA	Rheumatoid arthritis
RAP-MAPK	Rap- Mitogen-activated protein kinase
rITs	RITs
RNA	Ribose nucleic acid
ROS	Reactive oxygen species
RT	Room temperature
scFv	Single-chain fragment variable
SDS	Sodium dodecyl sulphate
SEC	Size Exclusion Chromatography
SR	Scavenger receptor
TAAs	Tumor-associated antigens
TAMs	Tumor-associated macrophages
TB	Terrific broth
TCI	Topical calcineurin inhibitors
TCS	Topical corticosteroids
TLR	Toll-like receptor
TNF-α	Tumor necrosis factor alpha
TRM	Tissue-resident macrophages
TSPC	Target specific photoimmunoconjugate
VEGF	Vascular endothelial growth factor
VH	Variable heavy chain
VL	Variable light chain
WB	WB

7.2 Plasmid vector maps

7.2.1 pCB-H22(scFv)-SNAP

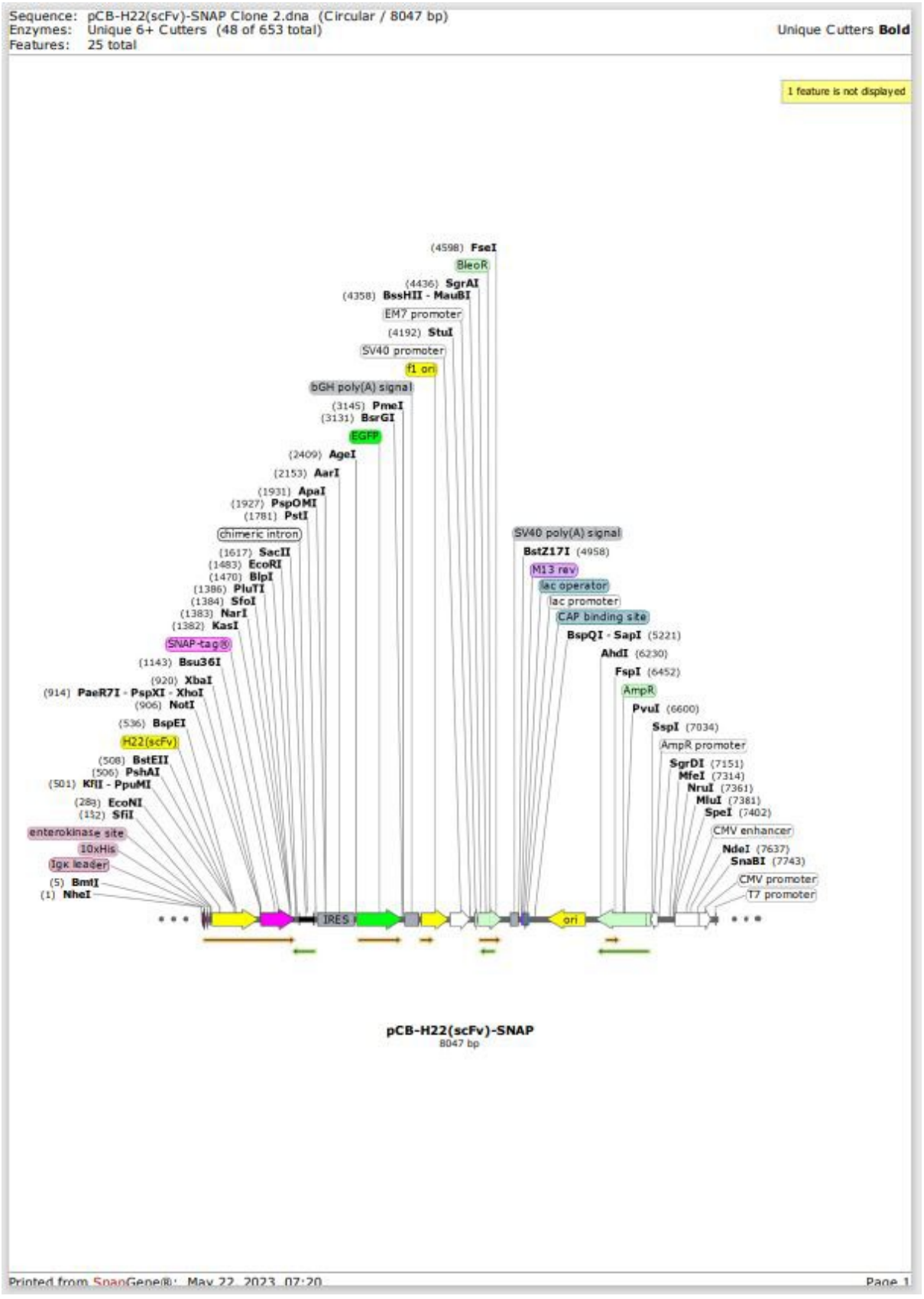

7.2.2 pMT-H22(scFv)-ETA`

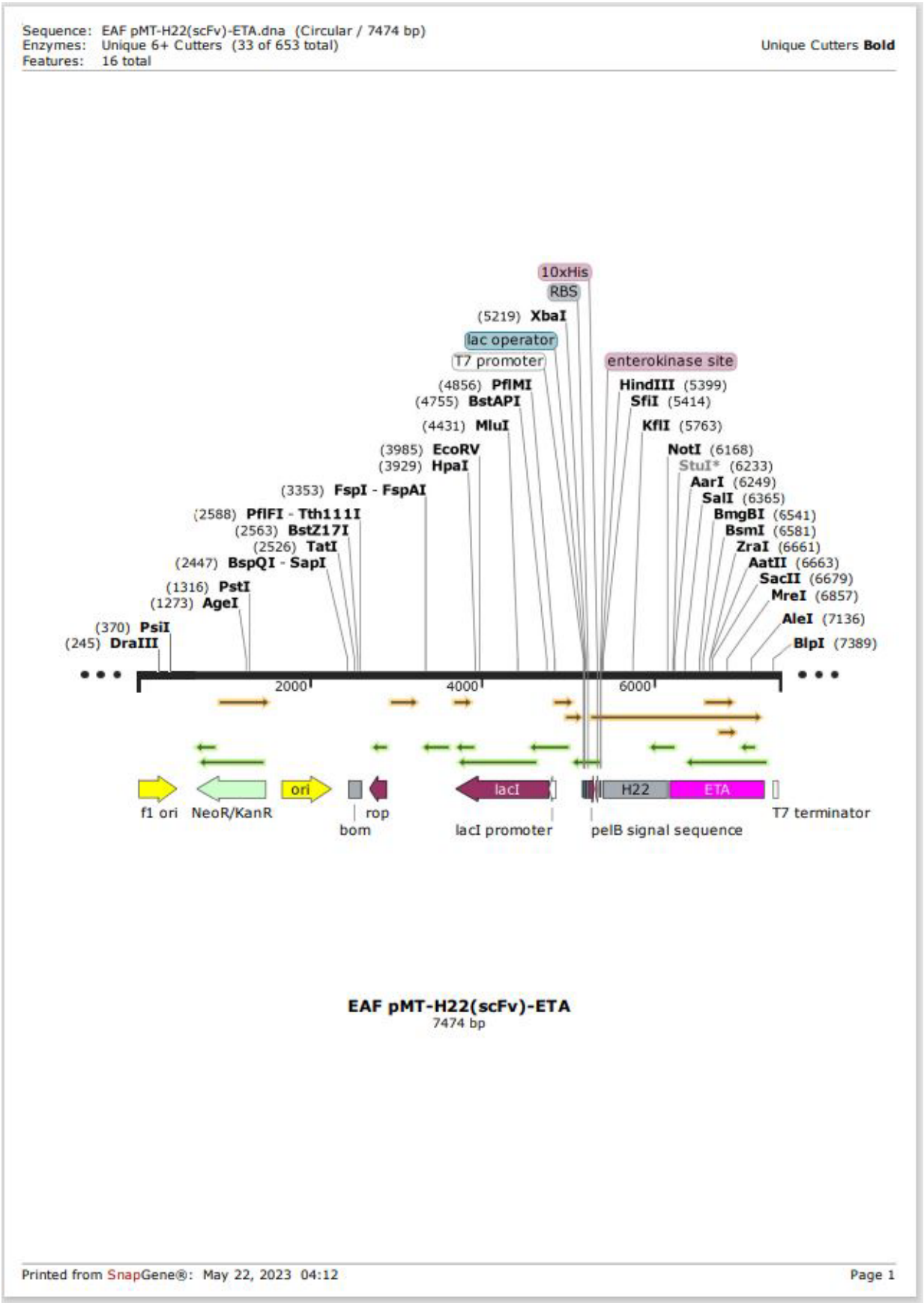

7.2.3 pMT-H22(scFv)-dETA`(RG7787-MT2)/(RG7787 (R456T)-R490A)